Facile Synthesis of Activated Carbon from Cellulose in the Presence of Air for Ammonia Recovery in Resource-Constrained Settings

by

Mohit Nahata

A dissertation submitted in partial fulfillment
of the requirements for the degree of
Doctor of Philosophy
(Chemical Engineering)
in the University of Michigan
2018

Doctoral Committee:

Professor Johannes W. Schwank, Chair
Professor Mark A. Barteau
Adjunct Professor Galen B. Fisher
Professor Lutgarde M. Raskin
Assistant Research Scientist Andrew R. Tadd

Mohit Nahata

mnahata@umich.edu

ORCID id: 0000-0002-2164-0280

Acknowledgments

The research carried out as expressed in this thesis was a part of the larger effort at U-M called REFRESCH, aimed to address Food-Energy-Water issues in resource-constrained settings. The project funded my entire research and was quite a unique opportunity in terms of the nature of the work and breadth of opportunities posed. I am most thankful to my advisor Prof. Johannes Schwank for giving me an opportunity to work on this project and learn some amazing things along the way. He has great enthusiasm to experiment with new ideas and has been very encouraging in challenging times.

I thank my committee members Prof. Mark Barteau and Prof. Galen Fisher for their insights and valuable suggestions during the course of my research. I thank Dr. Andrew Tadd for his patience and guidance, especially during the initial phase as a graduate student when I was learning new tools and skills. His clarity of thought and approach is something I admire and wish to inculcate. I thank Prof. Lutgarde Raskin for her valuable input on carrying out experiments on-site in Gabon and suggestions to incorporate my thoughts on practical applicability of the proposed activated carbon synthesis process.

I am grateful to Prof. Nancy Love and Zerihun Getaneh for their collaboration and ideas along the way. Dr. Chang Yup Seo has been a constant friend and guide throughout; we started our PhD's together. I can't thank him enough. I thank Dr. Xiaoyin Chen for all his training on the equipment in the Schwank lab. He is always there to help you out. All the other Schwank lab

members: Yasser Shalabi, Dr. Lei Ma, Pradeep Krishnakumar, Ping Li, Maithri Venkat, Anna Hayden and Adarsh Bhat have been instrumental in this journey in one way or the other.

Living away from home is not easy and friends are family away from home. This list is a long one and I cannot possibly elaborate everyone's role in my life, as this section would become an essay. I am really grateful to have wonderful friends: Animesh Jain, Tanvi Gujarati, Siva Aduri, Vimal Rathee, Neha Agarwal, Ankit Sethia, Divya Golchha, Priyamvada Goyal, Daya S. Khudia, Nischit Bharadwaj, Ajit Aluri, Pushkar Arora, Stacy Ramcharan, Amin Reihani, Matthew Vedrin, Claudio Vilas Boas Favero, Ramya Kumar. The list goes on. All have had a profound influence on my life and this journey wouldn't have been possible without them.

I am blessed to have a wonderful family and would like to take this opportunity to especially thank my parents, Mr. Rajkumar Nahata and Mrs. Sarika Nahata for all their sacrifice and making sure that I have a strong foundation to build upon. A special note of thanks to Shri Bhate Chandji Lunia (maternal grandfather) for his financial help during my Master's and my aunt Mrs. Sarita Dugar for her constant encouragement to pursue a PhD. I would like to convey immense gratitude to my entire family, especially cousins for being my pillar of strength. Lastly I would like to thank God for the infinite grace, manifesting itself in ways that can only be experienced, not measured.

Table of Contents

List of Tables

List of Figures

List of Abbreviations

REFRESCH	Researching Fresh Solutions to the Food Energy Water Problem in Resource Constrained Settings
FEW	Food Energy Water
IUPAC	International Union of Pure and Applied Chemists
XRD	X-Ray Diffraction
DRIFTS	Diffuse Reflectance Infra-Red Fourier Transform Spectroscopy
XPS	X-Ray Photoelectron Spectroscopy
TPD	Temperature Programmed Desorption
SEM	Scanning Electron Microscopy
EDS	Energy Dispersive Spectroscopy
TEM	Transmission Electron Microscopy
AC	Activated Carbon
NAE	Nitrogen Accumulation Efficiency
NUE	Nitrogen Utilization Efficiency
BS	Broido Shafizadeh
HTC	Hydrothermal Carbonization
DAP	Diammonium hydrogenphosphate
MAP	Monoammonium phosphate
MCC	Microcrystalline cellulose
TGA	Thermogravimetric Analysis
DTG	Differential Thermogravimetry

TG-MS	Thermogravimetry Mass Spectroscopy
TG-IR	Thermogravimetry Infra-Red Spectroscopy
POX	Partial Oxidation
BET	Brunauer Emmett Teller
DR	Dubinin Radushkevich
DA	Dubinin Astakhov
BJH	Barrett Joyner Halenda
HK	Horvath Kawazoe
PZC	Point of Zero Charge
IEP	Isoelectric Point
NIST	National Institute of Standards and Technology
NREL	National Renewable Energy Laboratory
HTT	Heat Treatment Temperature
BAC	Beaded Activated Carbon
VOC	Volatile Organic Compounds
PSD	Pore Size Distribution
DI water	Deionized water
USTM	Masuku University of Science & Technology
ICP-MS	Inductively Coupled Plasma-Mass Spectroscopy
EPA	Environment Protection Agency
WHO	World Health Organization
WASH	Water and Sanitation Hygiene
/	This symbol is used in figures and tables to denote : “in units of”

Abstract

As efforts to provide sanitation services in low-resource rural settings of the world proliferate, nutrient recovery via source separation of urine becomes important for economic and environmental implications in these regions of challenging socio-economic constraints. Substantial N (in some cases > 50%) is lost from urine via off-gassed ammonia which can be captured and utilized more efficiently by the use of sorbents such as activated carbon synthesized locally in resource-constrained settings.

My work is focused on developing a simple method to synthesize functionalized-activated carbon from locally available biomass at moderate temperatures (400-450)°C in the presence of air. Using cellulose as a model biomass and diammonium hydrogenphosphate (DAP) as the activating agent, the production of activated carbon is explored in a simple semi-batch Partial Oxidation (POX) reactor setup. DAP helps to facilitate low temperature pyrolysis of cellulose by the action of phosphoric acid which helps in depolymerization and the breakdown of glycosidic linkages present in lignocellulosic biomass. Further, the film of condensed phosphates prevents carbon oxidation at high temperature in the presence of air. This study provides insight into the interaction between DAP and biomass, as well as the char forming mechanism. Various characterization techniques such as N_2 physisorption, XPS, DRIFTS, SEM, TEM, surface charge measurements and Raman spectroscopy are utilized to compare the properties between activated carbon formed under nitrogen and partial oxidative conditions.

The interaction of DAP with cellulose is investigated and the nature of bonding of the heteroatoms to the carbonaceous matrix is elucidated. Our results indicate that the quality of activated carbon prepared under partial oxidation condition is comparable to carbon prepared under nitrogen, leading to the possibility of an activated biochar production scheme on a small scale.

The prepared activated carbon is utilized to recover ammonia off-gassed from urine providing multiple benefits including odor removal and nutrient recovery since ammonia augmented biochar can serve as a soil amendment. The hygroscopic nature of the prepared activated biochar is useful for holding soil moisture during the dry season and is envisioned to provide better soil health for round the year crop production. The efficacy of the synthesized activated biochar as an ammonia adsorbent is evaluated from adsorption isotherms by studying equilibrium capacity and elucidating the nature of the interaction by Temperature Programmed Desorption (TPD) and DRIFTS measurements. Our results show promising capacities for ammonia adsorption from the gas phase. The total dry ammonia adsorption capacity of the synthesized activated carbons was found to be ~ (24-28) mg/g at 50°C, comparable in magnitude to zeolites. It was observed that > 90% of the adsorbed ammonia could be easily recovered by simple water washing at room temperature, facilitating facile regeneration.

Chapter 1

Introduction

In the words of Bernard Amadei, the founder for Engineering without Borders: "The engineering community has largely focused on the needs of 10% of the world's population; what about the remaining 90%?" This proposed research project emerged from a larger endeavor called REFRESCH which aims to address issues at the food-water-energy nexus in resource-constrained, off-grid environments. Technologies are designed and developed for a particular situation, scale, and context. Generally, there are no 'one-size fits all' solutions. Developed countries rely on large-scale centralized systems for material production and application, because of the cost advantage associated with the increased output of a product. Centralized solutions are expensive and often infeasible to be implemented in most resource-constrained settings. Implementation of decentralized resource management has advanced in emerging economies in the recent past and research on the dimensions of natural resources related to the nexus of water and arable land has expanded dramatically. The element carbon is central to life and the Food-Energy-Water (FEW) nexus in many ways. Trends in global sustainability push towards the development of eco-friendly processes which can stimulate recycling and provide cleaner air and water. This has culminated in an effort to synthesize activated carbon, a sorbent widely used in the chemical industry. Activated carbon is a unique material with high adsorption capacity. The adsorption behavior is intimately linked to its structure and surface functionality which is

inextricably linked to the method of synthesis. In this thesis, using cellulose as a model biomass, an attempt has been made to synthesize activated carbon, understand the proposed chemical activation process and use it to recycle ammonia off-gassed from urine.

The element carbon and activated carbon

Carbon is central to life on planet earth and is the basis for organic chemistry. It is the fourth most abundant element by mass in the universe and the second most abundant element in the human body [1]. It is uniquely placed in the periodic table with an atomic number of 6 (Electronic configuration: $1s^2 2s^2 2p^2$), which provides it an uncanny ability to form substances ranging from simple molecules to complex polymers. Atoms of carbon can bond in different ways known as allotropes of carbon. The best known are graphite and diamond. Graphite is thermodynamically the more stable phase where each carbon atom is sp^2 hybridized. Its density is ~ 2.25 g/cm^3 and the distance between the individual graphene layers is 0.335 nm [2]. Other than diamond, all known forms of carbon (including activated carbon) are considered forms of diminished order relative to the single crystal graphite. Because the term activated carbon has been introduced, it is necessary to define it. Generally speaking, carbonaceous matter with high 'porosity' is activated carbon. Structurally it is an assembly of defective sheets of graphene. What we mean by 'porosity' is central to its meaning, and the work done in this thesis. The aspect of porosity is covered in detail later. Referring to structural disorder, it becomes important to introduce two broad families of carbons, namely graphitizable and non-graphitizable. These terms were coined by the British chemist Rosalind Franklin, an expert in the domain of coals and carbon compounds. From the definitions of IUPAC (International Union of Pure and Applied Chemists), graphitic carbons are all varieties of substances consisting of the element carbon in

the allotropic form of graphite irrespective of the presence of structural defects. The use of the term graphitic is justified if a 3D hexagonal crystalline long-range order can be detected in the material via X-Ray Diffraction (XRD) measurements. Carbons which are graphitic or become graphitic upon heat treatment are called graphitizable carbons. Here the graphene layers are considerably planar and stacked. On the contrary, non-graphitizable carbon is one which cannot be transformed into graphitic carbon by heat treatment up to 3300 K under atmospheric or lower pressure [3]. All the porous carbons fall in this category. A cartoon diagram inspired by the works of Dr. Franklin is shown below in Figure 1.1 to visualize graphitizable and non-graphitizable carbons.

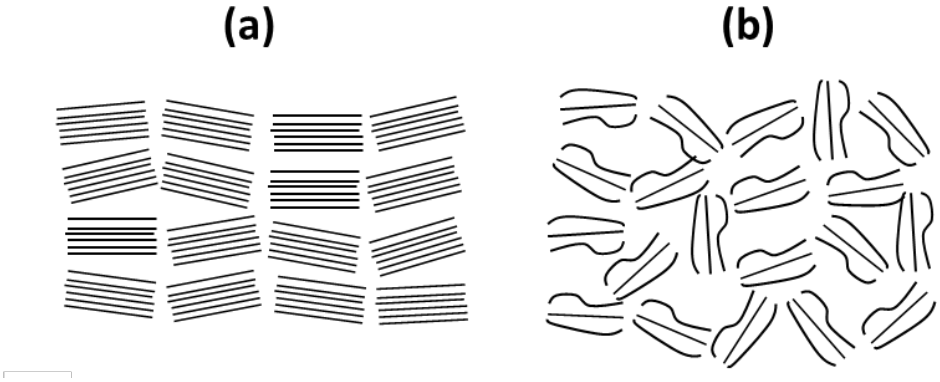

Figure 1.1: Representation of (a) graphitizable and (b) non-graphitizable carbons

Porosity is defined based on the size of the pores, which dictate how materials adsorb a given adsorptive. Pores smaller than 2 nm are called micropores, the ones between 2 and 50 nm are called mesopores. Porosity is the space between defective sheets of graphene layers [4]. As suggested by previous research, activated carbons have a networked pore-structure where macropores > 50 nm are generally just access pathways to the eventual meso and microporosity. Besides the void space, the nature of the graphene wall surrounding the porosity is critically important. That is essentially determined by the presence of functional groups, which largely

governs their behavior in a specific environment. Characterization of the pore space and its enclosing surface is central to understand activated carbon. These aspects which are key to understanding of activated carbons are discussed in detail in chapters 2 and 3. An overview of their physical properties and associated characterization methods are listed below in Table 1.1.

Table 1.1: Characterization techniques prevalent for activated carbon

Information provided	**Technique**
Pore volume, surface area, pore size distribution	Gas adsorption
Surface functional groups	DRIFTS, XPS and TPD
Particle morphology	SEM (Scanning Electron Microscopy)
Surface elemental composition	XPS (X-Ray Photoelectron Spectroscopy)
Total elemental analysis	Element specific technique
Molecular scale structure	TEM (Transmission Electron Microscopy)
Surface charge and amphoteric nature	Zeta potential and titrations
Defects in graphene	Raman microspectroscopy
Acidity probe in micropores	NH_3 adsorption and breakthrough

Applications of activated carbon

Activated Carbon (AC) in general is synthesized and optimized for a particular application though it may end up fitting multiple uses. It is important to have information about the total pore volume, nature of adsorption isotherm, functional groups, fraction of heteroatoms, acidity, etc. Carbons are amphoteric, i.e., they may exhibit acidic or basic properties depending on the environment. These factors govern a specific application and are discussed in detail in chapter 3. For now, a brief overview is presented, with a particular emphasis on the role of biochar in soil.

Gas separation and purification

In the chemical industry, high purity gases are often desired for various applications. The semiconductor industry demands gases ranging from single digit ppb to double-digit ppt sensitivity [5]. The process used by each company is a trade secret, but it often involves the use of adsorbents. Microporous carbons, zeolites, etc. can be manufactured with specific chemistries

and pore-size distributions to aid such separations. They can be used to reduce pollutant gases to a very low concentration. The technology is matured and well optimized for different applications. A recent emerging frontier is the use of activated carbons to clean up biogas from a digester [6]–[8]. The composition of biogas is mainly CO_2 and CH_4, but it is associated with H_2S, NH_3, and siloxanes which are desired to be removed to minimize damage to combustion equipment and ensure emission targets. Some operations involve removal of CO_2 as well to increase the energy density of the gas stream as per gas purity specifications. Synthesis of high surface area carbons impregnated with NaOH or KOH have been popular to control H_2S in wastewater treatment plants [9]. Although this process results in high capacities, it is associated with a risk of self-ignition of the carbon bed due to the evolution of a substantial amount of heat in the process. Efforts these days tend to focus on designing carbon materials which can function without an external alkali and sustain a balance between capacity, kinetics and exothermic heats. Boudou *et al*. for instance used NH_3 and steam pretreatment at 800°C to N-dope the carbons for H_2S and SO_2 removal by leveraging acid-base interactions [10]. Apart from gas separations, AC's are well known to aid adsorption of volatile organic compounds, especially in the petrochemical and paint industry [11]–[13].

Liquid phase applications

There is a vast literature describing adsorption from aqueous solutions, focusing mainly on water-treatment applications [14]–[17], the broad areas of which they cater to are mentioned below:

1. Treatment of drinking water for color, taste, and removal of chlorinated compounds
2. Removal of heavy metal ions and excess flotation agents associated with mining processes

3. Industrial and municipal wastewater treatment

4. Decolorization agent in sugar and sweetener industry

5. Face-cleansing components in soaps, face-wash in the consumer goods sector

6. Purification of process water in pharmaceutical, food and beverage industry

7. Cleaning of solvents in the paint and dry-cleaning sector

Many authors, however, fail to give due consideration to studies about regeneration post adsorption. Liquid phase applications are more complex than gas phase applications because of the presence of charged species, competitive adsorption, etc. One of the major gaps which still exists is an understanding of the mechanism by which ionic species are attached to a carbon surface. Solutes in liquid phase and ionic species, in general, are hydrated with water molecules, which increases their effective size. Thus, liquid phase applications prefer to use mesoporous carbons with broader pore size distribution for rapid diffusion of the liquid to the interior of the carbon particle as opposed to microporous carbons which are generally more suitable for gas phase applications.

Biochar and the soil nitrogen cycle

Generally speaking, char or charcoal is the solid matter synthesized upon pyrolysis of biomass. Depending upon the extents of carbonization, percentage of carbon, physical properties and end-use various terms such as char, charcoal, biochar may be used. If the origin of the carbonaceous material is biological in its recent history of evolution, and the end application pertains that of a soil amendment the term biochar is often used in the scientific jargon [18]. Since the desired application is that of a soil amendment in this thesis, the terms activated carbon and activated biochar have been used interchangeably.

The ancient people in the Amazon are known to have added substantial quantities of biochar to wet-desert soil to render it fertile [19], [20]. The discovery of terra-preta in the Amazon belt provides evidence to its long-term stability and efficacy. Learning from the past, modern scientists have encouraged its use, helping in sequestering carbon. The N-cycle in soil is one area where biochar is proposed to have a significant impact. Intensively managed soil fortified with inorganic fertilizers, urea or bovine urine are generally hot-spots for NH_3 formation and its subsequent loss by volatilization. In open urine patches, almost 40 % of the nitrogen can be lost as off-gassed ammonia [21]. The leaching away of excess nutrients has been known to cause eutrophication. In this context, the role of biochar as a soil-amendment has been investigated by several researchers focusing on the retention, stability, loss prevention and bioavailability of the useful N. Spokas, for instance, suggested that biochar has a very important role to play in the soil-N cycle. Using ^{15}N markers, it was found that NH_3 was stably but not irreversibly bound to the biochar, and the longevity of the trapped NH_3 was postulated to beneficially aid plant growth [22]. Toosi *et al*. synthesized low-temperature biochar from woody biomass with an aim to reduce NH_3 volatilization from remnant urine decomposition. Using ^{15}N markers again, it was found that, following the application of biochar, NH_3 volatilization was reduced by 45% along with the simultaneous increase in uptake of ^{15}N by plant tissues [23]. Zheng *et al*. carried out a comprehensive study where they established NO_3^- and NH_4^+ leaching was significantly reduced by addition of biochar to soil. They attributed this result to the enhanced water holding capacity of soil and NH_4^+ adsorption, upon addition of biochar. The positive effects were reflected in stimulated maize growth indicating that the N was bioavailable. The bioavailability was measured as NAE (Nitrogen Accumulation Efficiency) and NUE (Nitrogen Utilization Efficiency) as the amount of biomass produced per unit of N [24]. Johannes Lehmann in his

review paper elucidated the effects of biochar on the soil microbial community. In general, it was found that the application of biochar increased the population density of soil micro-organisms with substantial changes in their community composition and enzymatic activity [25]. However, the mechanism by which biochar affected microbial abundance was not well understood. Anderson *et al*. in their large-scale study investigated seasonal bacterial community changes on a silt-loam pastoral soil in Canterbury, New Zealand by the application of 0.15 or 0.30 t/ha of biochar synthesized at 450°C. Their observation was that biochar addition did not have a significant impact on the microbial community structure in pastoral soil over two years but the relative proportions of nitrifiers and denitrifiers increased in biochar amended soils [26]. In all these studies, there has been a lack of understanding of the mechanisms at work because of the insufficient characterization of the biochar and an understanding of its true structure. Biochars not synthesized under properly controlled conditions, exhibit large variability in performance, have low porosity and lack a well-defined structure. This along with the lack of necessary characterization hinders understanding and comparisons between different types of materials and is an aspect of work which has been unequivocally suggested for pursuit by the authors.

Thermochemical conversion of biomass

Millions of years ago coal and petroleum were formed when a significant fraction of the earth's flora and fauna got buried deep under the earth due to natural calamities. Under the high temperature and pressure beneath the crust, aided by microbial activity the slow transformation to coal, petroleum, and natural gas occurred. In the laboratory today, efforts are being made to optimize process conditions to enhance the yield and quality of charcoals, biocrude, or combustible gas by the thermochemical conversion of biomass. It is important to remember that

a particular set of conditions are required to favor the biomass decomposition pathway to a particular product. Biomass is an oxygen-rich, highly functionalized complex substance consisting primarily of cellulose, hemicellulose, and lignin in addition to some organic extractives and inorganic ash. The relative proportions of these constituents with their associated interactions end up controlling decomposition behavior of the aggregate biomass. Numerous studies have been dedicated in the past to explore the mechanism of cellulose pyrolysis, the various pathways of which are well illustrated by the Broido-Shafizadeh (B-S) mechanism [27]. Various options exist for the thermochemical conversion of biomass to fuels such as pyrolysis, gasification, liquefaction, and reforming. Chheda *et al*. [28] provide the operating regime for each of the above-mentioned processes. Considering applications in low-resource settings, it is imperative that the process operates under moderate temperature and near atmospheric pressure conditions. Pyrolysis is traditionally carried out between 400-600ºC, and yields solid char or liquid oils as its primary product depending upon the heating rate and other process conditions employed. Charcoal production by slow pyrolysis via the low-temperature route is a known technology pioneered by the labs of Fred Shafizadeh and Michael Jerry Antal Jr. [29]. However, it did not fuel much research after the 1990's in the quest for liquid fuels to serve the transportation sector. Bridgewater in his seminal work reviewed the multifaceted design considerations and catalysts for successfully upgrading and implementing fast pyrolysis for making bio-oils [30]. Gasification of biomass to fuel-gas by carefully controlling the amount of oxygen fed to the system occurs at much higher temperatures (>800ºC) and is usually carried out under continuous flow conditions. Although gasification is a mature technology and known to produce high yields of syngas, it has associated problems of tar generation, the elimination of which has been extensively investigated [31]–[33]. Another option for the synthesis of these

materials is the hydrothermal route, where biomass is processed under elevated pressure in high-temperature water, and process variables are tuned to optimize the yield and properties of a desired product. Hydrothermal carbonization, liquefaction, and gasification have been extensively researched in the Savage research group at the University of Michigan [34], [35].

Low temperature pyrolysis

Acids (both Brønsted and Lewis type), and inorganic salts are known to lower the temperature of active pyrolysis and favor different pathways. Acids (such as H_3PO_4) in trace amounts favor the low temperature pathway and catalyze transglycosylation reactions for the conversion of cellulose to levoglucosan. In larger amounts they cause dehydration of the anhydrosugar [36]. Salts like Diammonium hydrogenphosphate (DAP) which produce H_3PO_4 upon heating are also known to be effective in facilitating the low temperature pathway. Studies pertaining to the pyrolysis of cellulose-DAP mixtures were carried out in the past to examine its effectiveness as a fire retardant. Condensed phosphates in carbon restrict the access of oxygen to carbon thereby preventing spontaneous ignition. Di Blasi for instance investigated the catalytic effects of DAP on wood pyrolysis at 800 K in a fixed-bed reactor over a range of salt concentrations (0-20) wt.%. The main focus of the work was to understand the effect of DAP loading on product distribution [37]. Statheropoulos and Kyriakou [38] examined the effects of two fire retardants ammonium sulfate and DAP, on cellulose pyrolysis, and analyzed gases by TG-MS (Thermogravimetry-Mass Spectrometry) in order to gain insights about the mechanism. A common conclusion was that DAP lowered the temperature of pyrolysis initiation and increased char yield at the expense of liquids and tars. However, it also increased the fraction of non-combustible gases like CO_2 and H_2O. With DAP, the focus has been largely restricted to using

relatively low concentration of the salt with wood for fire retardancy. Inorganic salts such as NaCl, $FeSO_4$ and $MgCl_2$ are known to be weak fire-retardants. Some work had been carried out in the past to investigate the thermal decomposition behavior of cellulose in presence of these salts along with a simultaneous gas phase analysis [39], [40]. These inorganic salts were found to lower the temperature of active pyrolysis and the temperature of maximum decomposition. They also catalyzed depolymerization reactions of macromolecules and its subsequent decomposition to smaller compounds making the gas phase rich in H_2O, CO and CO_2. The naturally obtained charcoal without activation is largely non-porous and devoid of useful surface functionality. Charcoal is a lightweight energy dense fuel (30-33) MJ/kg having a fixed carbon content of 75%, a volatile matter content between 21 and 23% and an ash content of (1-3)%, which eliminates problems due to smoke and particulate matter arising out of burning raw wood. According to most standards it is deemed to be of reasonably good quality for cooking and heating applications [41]. In the history of humankind, charcoal has been used in many applications: fuel, soil amendment, water filter, and many more. As the understanding of charcoal advanced, researchers realized that the porosity and functional groups present in charcoal were very important characteristics. Hence, a class of charcoal with high porosity has been classified as 'activated' to emphasize its properties of high surface area and well-defined pore size distributions, which made the charcoal much more valuable than just a better source of fuel.

Activated carbon synthesis

Making charcoal has been commonplace knowledge since times immemorial. However, making charcoal from lignocellulosic biomass with desired properties is an art and an evolving science despite decades of research. Its applications vary widely from its use in artistic work to being the

most valued reductant in the metallurgical industry (free of Hg, virtually free of S) [29]. Despite having ‘known' charcoal for centuries, there is still no consensus on its definition. The reason being its definition changes with end use. For instance, Foley indicates that metallurgical (industrial grade) charcoal should have a fixed carbon content of (85-90) %, whereas charcoal intended for domestic purposes should have a volatile matter content in between (20-40) %, fixed carbon being (60-80)% [42]. However, these standards evolve with time as we continue to better our technology. Yields of char reported in literature can be often confusing because it is highly specific to the process under consideration. One good way of comparison is to contrast the fixed carbon content. Biochar (char derived from biomass) is largely an aromatic polycyclic structure whose formation is generally favored by intra and intermolecular rearrangement reactions of the precursor (raw biomass), which results in higher thermal stability of the residue. All these rearrangement reactions are generally accompanied by the release of water and incondensable gas (CO, CO_2) [43]. In the absence of external additives, at temperatures > 200ºC, depolymerization reactions begin and volatiles are evolved. At this temperature, biomass slowly carbonizes into a dark-brown solid, corresponding to the breakdown of mainly hemicellulose. Cellulose and lignin, which are fairly stable thermally, start to decompose quite rapidly at temperatures higher than 300ºC. More volatile vapors and incondensable gases are evolved in the process. At T > 300°C, the solid substrate changes its color to black as more and more oxygen is removed from the matrix. Depolymerization to volatiles is maximum around 350ºC and fragmentation reactions to form smaller molecules dominate at temperatures in excess of 500ºC. When the released volatile compounds are not stable under the conditions of reactor temperature, they can undergo secondary reactions such as cracking or recombination [44]. Both of these reactions usually occur at long residence/holding times. Cracking reactions involve the breaking

of chemical bonds within the volatile compounds, which result in the formation of lower molecular weight molecules. Recombination (or recondensation) reactions are the combination of volatile compounds to give higher molecular weight molecules, which sometimes are no longer volatile in the reactor. Such reactions can lead to the formation of a secondary char. Secondary mechanisms can be catalyzed at the surface of primary char (formed by the rearrangement of the original biomass matrix) or on the surface of externally added catalysts, as demonstrated in the literature [45].

Activation is essentially about enhancing the pore structure of carbonaceous matter to make it more amenable for adsorption processes. Activated carbon must possess a large volume of pores with an appropriate pore size distribution to adsorb molecules of different sizes. The precursors for activated carbons range from conventional fossil fuels (coal and petroleum) to lignocellulosic biomass and synthetic polymeric resins. To form activated carbon, the precursor is converted to a carbon-rich residue. For instance, a typical lignocellulose has 49 wt. % C, 45 wt. % O, and 6 wt. % H, which needs to be carbonized to ~ (70-90) % fixed carbon. This carbon-rich matter is then activated by either of the two mechanisms namely: thermal activation or chemical activation.

Thermal activation: The carbonized sample is gasified by either carbon dioxide or steam (refer to equations 1.1 and 1. 2) at 800-1000ºC. Oxygen is not used as the activating agent because its reaction with carbon is highly exothermic and quite impossible to control unless used at very low partial pressure. The gasifying agents 'pluck' a carbon atom from the surface of solid carbon. Not all carbons are equally reactive and a selection process of some sensitivity occurs by the use of CO_2 or steam [46]. Making activated carbon by thermal gasification is a two-step process involving 1. carbonization and 2. activation

$$C + CO_2 \rightarrow 2CO \qquad (1.1)$$

$$C + H_2O \rightarrow CO + H_2 \qquad (1.2)$$

Chemical activation process: In this process, the precursor is carbonized in the presence of relatively strong dehydrating chemicals called activating agents. The most popular ones used industrially are $ZnCl_2$, H_3PO_4, and KOH. Other proposed chemicals include $AlCl_3$, $MgCl_2$, and K_2CO_3. The precursor is first soaked in an aqueous solution of the salt/acid to impregnate it with the additive of a desired concentration. The mixture is dried by evaporation. The precursor is then carbonized at a given temperature for a few hours in a flow-through setup where the volatiles are swept off by a purging gas. The carbonized residue is then leached with an appropriate reagent to recover the additive and then dried to obtain activated carbon.

Activation by zinc chloride: Zinc chloride is impregnated into the biomass precursor via solution. This facilitates hydration and enhances contact of the salt with the substrate. After impregnation and drying, carbonization is carried out at ~500ºC under N_2 flow. During carbonization, it is believed that the salt acts as a template for the creation of pores, which is then washed to eliminate the remaining chemical and produce activated carbon. Usually, very high loadings of zinc chloride are used: (0.2-1.2) g Zn/g raw material. Zinc chloride in water is known to impart Brønsted acidity (6M solution of Zinc chloride has pH =1) [47] to the solution via the formation of chloro-aqua complexes and at high concentration can dissolve cellulose. Bringing cellulose in solution makes it more amenable to reactions. Cellulose being the bulk component of biomass can be chosen as a model compound to understand reaction pathways.

The maximum yield of carbon from cellulose is obtained as per equation 1.3

$$C_6H_{10}O_5 \rightarrow 6C + 5H_2O \quad (1.3)$$

The above equation plainly suggests that dehydrating agents should be beneficial for increasing the yield of char, although their effect on the pore structure and chemistry of activated carbon remains unknown. Sabio and Reinoso [48] published a comprehensive paper explaining the role of chemical activation on carbon porosity. The increase in porosity with increasing strength of activation suggested that the porosity created, was due to the spaces left by zinc chloride after washing. The pore size distribution (PSD) of the generated activated carbon was fairly uniform, even though it is generally dependent on the mass loading of zinc-chloride.

Activation by phosphoric acid: The synthesis procedure for phosphoric acid is very similar to that of zinc chloride. The nature and amount of the porosity are dependent strongly on the mass loading of phosphoric acid used for activation. Acid loadings greater than 0.3 g P/g raw material have produced commercially attractive activated carbons and mass loadings of H_3PO_4 as much as twice that of the raw material have been used [49]. Phosphoric acid was found to play an important role below 500ºC leading to highly activated carbons. An important feature of the carbon synthesized from phosphoric acid is a relatively broad distribution in pore sizes. This is because H_3PO_4, when heated up, generates a mix of molecules from $H_4P_2O_7$ to $H_7P_5O_{16}$ in different proportions as predicted by the vapor-liquid phase diagram of P_2O_5-H_2O mixtures [50] which aid in creation of the porosity. The distribution of pore sizes is an important factor which drives a specific application. Carbons activated from $ZnCl_2$, on the other hand, have a more uniform PSD and require a strong acid to re-extract the activant, however with H_3PO_4 the extraction of the activant can be accomplished by water.

KOH activation: Chemical activations offer an advantage of lower temperature activations relative to thermal activations and substantial recovery of the initial activating agent. However, the mechanism of KOH is quite different compared to H_3PO_4 and $ZnCl_2$. KOH acts effectively under vigorous conditions above 700ºC and the porosity is a function of the concentration of KOH loaded initially, as true with other activating agents. As KOH does not act as a dehydrating agent to biomass, it does not react at low temperature during pyrolysis. Under vigorous conditions (>700ºC), it is believed that during activation, a redox reaction occurs where C is oxidized to CO and CO_2 and KOH is reduced to metallic K [51]. At such high temperatures, K is intercalated between the graphene layers and the larger particles breakdown and disintegrates to powder. With KOH the advantage of low-temperature activation is lost. However, it produces narrow micropores and other features that may be useful for specific applications such as combustible gas storage [52].

Apart from the methods mentioned above, several facile low-temperature routes to synthesize porous and functionalized carbonaceous materials with controllable morphology via HTC (Hydrothermal carbonization) have also been elucidated in the literature [53], [54]. Depending upon the end-use and other desirable properties, one may choose to adopt one or more of the above-mentioned approaches for activation.

Analysis and direction

Activated carbon synthesis has been successful in flow-through setups like tube furnaces connected to inert gas flows, where evolved volatiles can be swept off by the gas flow. This type of reactor system works well in places with modern infrastructure, but in resource-constrained environments, other factors may become limiting. Flow-through setups requiring sophisticated

mechanisms like an inert gas purge, numerous moving parts, and condensation mechanisms are difficult to conceive of being operative in off-grid settings. Such reactors typically operate in a fixed or fluidized bed configuration. Plugging of transfer lines by condensable volatiles called tars is a problem most often experienced in such configurations. Strategies to counter them have been researched extensively in the literature as discussed previously. Unlike conventional flow systems for gasification designed to operate at large scales, not much has been investigated in the past about small-scale batch pyrolysis The natural design of a batch reactor does not allow volatiles to escape, so they can react amongst themselves to make more char via recombination reactions. Under pressure, these vapors get more time to interact, resulting in higher total char yields. Also smaller specific volumes in such environments favorably enhance the rate of reaction due to increased activity (concentration). Batch systems have reported higher yields of char as compared to flow-through systems at the same temperature.

Also, from a study of the literature, it was clear that the global heat of biomass pyrolysis is not a constant, but rather a function of the process conditions: temperature, pressure, environment (air, inert) moisture content, extent of decomposition [55]. Stoichiometric calculations show that for all practical loadings one would operate in oxygen-starved environments in a batch setup. Secondary decomposition reactions and tar cracking reactions are known to be catalyzed by alkali and alkaline earth metal salts. Mok, in his seminal work at Princeton, explained the dependence of the global heat of reaction on such secondary reactions. Simply put, as the holding times are increased, vapors undergo these secondary reactions to produce more char. He also described the magnitude of the heat changes as a function of the mass-loadings inside the reactor [41]. Although a closed batch system would have advantages associated with higher yields, it would be at the cost of separating the char from the tar. The re-condensed volatiles

could adversely affect the porosity of the obtained carbon material and would require the additional step of an organic solvent separation. A modification in design is required. For leveraging benefits associated with no moving parts (helpful in resource-constrained environments), we envision a ‘one-pot', portable semi-batch reactor containing biomass in a simple vessel. The details will be described in chapter 2. Flow-through setups requiring sophisticated mechanisms like an inert gas purge, numerous moving parts, and condensation mechanisms are difficult to conceive of being operative unhindered in off-grid settings. This leads to the natural next question of the synthesis approach. High-temperature thermal activation was not considered because of the difficulty of attaining and maintaining such temperatures. Instead, we focused our effort towards lower temperature chemical activation. The rationale behind the choice of the proposed activant, its mechanism of activation followed by characterization and application of the activated carbon are discussed in the subsequent chapters of this work.

Thesis Layout

Given the context mentioned in Chapter 1 (Introduction), a plan of study was implemented to achieve the synthesis of activated biochar in a semi-batch setup in the presence of ambient air. This was followed by an elaborate characterization and a study elucidating the effect of process variables on the yield and porosity of biochar. An assessment of the interaction of NH_3 with activated carbon followed to understand the mechanism and to justify the validity of the proposed application. Finally, key findings based on preliminary water testing at Lambaréné, Gabon are reported, and avenues for future directions are elucidated.

Chapter 2 elaborates upon the synthesis methodology and tracks chemical transformations during synthesis by a host of techniques. There is a focus on understanding the activation process and computing porosity as a function of DAP loading in environments of pure nitrogen and ambient air. The chapter also attempts to shed light on the microstructure of activated carbon from electron microscopy and Raman spectroscopy.

Chapter 3 goes into details of assessing the surface functional groups by XPS, DRIFTS, elemental analysis and surface charge measurements A systematic study of the effect of process variables on the porosity and yield of activated biochar provides interesting insights about trade-offs associated by tuning various parameters during the synthesis. The bulk of the data presented in chapters 2 and 3 are published in Frontiers of Chemical Science and Engineering.

Chapter 4 explores a potential application of the synthesized activated biochar as an adsorbent to recycle ammonia off-gassed from urine for soil amendment applications. The efficacy of the synthesized activated carbon as an ammonia adsorbent is evaluated by studying equilibrium capacity via Thermogravimetric analysis. The nature of NH_3 bonding on carbon surface is elucidated by by TPD and DRIFTS measurements. Practical insights into ammonia desorption and N mass balance is provided. The data presented in chapter 4 is a manuscript currently under preparation.

Chapter 5 describes two natural pathways that emerge for future work, one in the context of plant growth studies and the other on water treatment applications. Preliminary data on water quality testing in rural Gabon is provided and avenues for more long-term studies are discussed.

References

[1] J. Reece, L. Urry, M. Cain, S. Wasserman, P. Minorsky, and J. Robert, *Campbell Biology*. Pearson, 2013.

[2] H. Marsh and F. Rodríguez-Reinoso, *Activated carbon*. Elsevier, 2006.

[3] A. D. McNaught and A. Wilkinson, *IUPAC:Compendium of Chemical Terminology, 2nd ed. (the "Gold Book")*. Oxford, 1997.

[4] J. Byrne and H. Marsh, *Porosity in carbons: characterization and applications*. London: Edward Arnold, 1995.

[5] J. L. Briesacher, M. Nakamura, and T. Ohmi, "Gas Purification and Measurement at the PPT Level," *J. Electrochem. Soc.*, vol. 138, pp. 3717–3723, 1991.

[6] N. Abatzoglou and S. Boivin, "A review of biogas purification processes," *Biofuels, Bioprod. Biorefining*, vol. 3, no. 1, pp. 42–71, 2009.

[7] E. Ryckebosch, M. Drouillon, and H. Veruaeren, "Techniques for transformation of biogas to biomethane," *Biomass and Bioenergy*, vol. 35, no. 5, pp. 1633–1645, May 2011.

[8] M. Farooq, M. N. Almustapha, M. Imran, M. A. Saeed, and J. M. Andresen, "In-situ regeneration of activated carbon with electric potential swing desorption (EPSD) for the H_2S removal from biogas," *Bioresour. Technol.*, vol. 249, no. Supplement C, pp. 125–131, 2018.

[9] A. Bagreev and T. J. Bandosz, "A Role of Sodium Hydroxide in the Process of Hydrogen Sulfide Adsorption/Oxidation on Caustic-Impregnated Activated Carbons," *Ind. Eng. Chem. Res.*, vol. 41, no. 4, pp. 672–679, Feb. 2002.

[10] J. P. Boudou, M. Chehimi, E. Broniek, T. Siemieniewska, and J. Bimer, "Adsorption of H_2S or SO_2 on an activated carbon cloth modified by ammonia treatment," *Carbon N. Y.*, vol. 41, no. 10, pp. 1999–2007, 2003.

[11] L. Li, S. Liu, and J. Liu, "Surface modification of coconut shell based activated carbon for the improvement of hydrophobic VOC removal," *J. Hazard. Mater.*, vol. 192, no. 2, pp. 683–690, 2011.

[12] X. S. Zhao, Q. Ma, and G. Q. (Max) Lu, "VOC Removal: Comparison of MCM-41 with Hydrophobic Zeolites and Activated Carbon," *Energy & Fuels*, vol. 12, no. 6, pp. 1051–1054, Nov. 1998.

[13] D. Das, V. Gaur, and N. Verma, "Removal of volatile organic compound by activated carbon fiber," *Carbon N. Y.*, vol. 42, no. 14, pp. 2949–2962, 2004.

[14] D. Mohan and C. U. Pittman, "Activated carbons and low cost adsorbents for remediation of tri- and hexavalent chromium from water," *J. Hazard. Mater.*, vol. 137, no. 2, pp. 762–811, 2006.

[15] T. M. Huggins, A. Haeger, J. C. Biffinger, and Z. J. Ren, "Granular biochar compared with activated carbon for wastewater treatment and resource recovery," *Water Res.*, vol. 94, pp. 225–232, 2016.

[16] J. P. Kearns, L. S. Wellborn, R. S. Summers, and D. R. U. Knappe, "2,4-D adsorption to biochars: Effect of preparation conditions on equilibrium adsorption capacity and comparison with commercial activated carbon literature data," *Water Res.*, vol. 62, pp. 20–28, 2014.

[17] L. Kovalova, D. R. U. Knappe, K. Lehnberg, C. Kazner, and J. Hollender, "Removal of highly polar micropollutants from wastewater by powdered activated carbon," *Environ. Sci. Pollut. Res.*, vol. 20, no. 6, pp. 3607–3615, 2013.

[18] S. P. Sohi, E. Krull, E. Lopez-Capel, and R. B. T.-A. in A. Bol, "Chapter 2 - A Review of Biochar and Its Use and Function in Soil," in *Advances in Agronomy*, vol. 105, no. Supplement C, Academic Press, 2010, pp. 47–82.

[19] B. Glaser, L. Haumaier, G. Guggenberger, and W. Zech, "The 'Terra Preta' phenomenon: a model for sustainable agriculture in the humid tropics," *Naturwissenschaften*, vol. 88, no. 1, pp. 37–41, 2001.

[20] B. Glaser, J. Lehmann, and W. Zech, "Ameliorating physical and chemical properties of highly weathered soils in the tropics with charcoal – a review," *Biol. Fertil. Soils*, vol. 35, no. 4, pp. 219–230, 2002.

[21] D. W. Bussink and O. Oenema, "Ammonia volatilization from dairy farming systems in temperate areas: a review," *Nutr. Cycl. Agroecosystems*, vol. 51, no. 1, pp. 19–33, 1998.

[22] K. A. Spokas, J. M. Novak, and R. T. Venterea, "Biochar's role as an alternative N-fertilizer: ammonia capture," *Plant Soil*, vol. 350, no. 1–2, pp. 35–42, 2012.

[23] A. Taghizadeh-Toosi, T. J. Clough, R. R. Sherlock, and L. M. Condron, "A wood based low-temperature biochar captures NH3-N generated from ruminant urine-N, retaining its bioavailability," *Plant Soil*, vol. 353, no. 1–2, pp. 73–84, 2012.

[24] H. Zheng, Z. Wang, X. Deng, S. Herbert, and B. Xing, "Impacts of adding biochar on nitrogen retention and bioavailability in agricultural soil," *Geoderma*, vol. 206, pp. 32–39, 2013.

[25] J. Lehmann, M. C. Rillig, J. Thies, C. A. Masiello, W. C. Hockaday, and D. Crowley, "Biochar effects on soil biota – A review," *Soil Biol. Biochem.*, vol. 43, no. 9, pp. 1812–1836, 2011.

[26] C. R. Anderson, K. Hamonts, T. J. Clough, and L. M. Condron, "Biochar does not affect soil N-transformations or microbial community structure under ruminant urine patches but does alter relative proportions of nitrogen cycling bacteria," *Agric. Ecosyst. Environ.*, vol. 191, no. Supplement C, pp. 63–72, 2014.

[27] M. J. J. Antal and G. Varhegyi, "Cellulose Pyrolysis Kinetics: The Current State of Knowledge," *Ind. Eng. Chem. Res.*, vol. 34, no. 3, pp. 703–717, Mar. 1995.

[28] J. N. Chheda, G. W. Huber, and J. A. Dumesic, "Liquid-Phase Catalytic Processing of Biomass-Derived Oxygenated Hydrocarbons to Fuels and Chemicals," *Angew. Chemie Int. Ed.*, vol. 46, no. 38, pp. 7164–7183, Sep. 2007.

[29] M. J. Antal and M. Grønli, "The Art, Science, and Technology of Charcoal Production," *Ind. Eng. Chem. Res.*, vol. 42, no. 8, pp. 1619–1640, Apr. 2003.

[30] S. Czernik and A. V Bridgwater, "Overview of Applications of Biomass Fast Pyrolysis Oil," *Energy & Fuels*, vol. 18, no. 2, pp. 590–598, Mar. 2004.

[31] L. Devi, K. J. Ptasinski, and F. J. J. . Janssen, "A review of the primary measures for tar elimination in biomass gasification processes," *Biomass and Bioenergy*, vol. 24, no. 2, pp. 125–140, 2003.

[32] J. Delgado, M. P. Aznar, and J. Corella, "Biomass Gasification with Steam in Fluidized Bed: Effectiveness of CaO, MgO, and CaO−MgO for Hot Raw Gas Cleaning," *Ind. Eng. Chem. Res.*, vol. 36, no. 5, pp. 1535–1543, May 1997.

[33] M. Asadullah, S. Ito, K. Kunimori, M. Yamada, and K. Tomishige, "Energy Efficient Production of Hydrogen and Syngas from Biomass: Development of Low-Temperature Catalytic Process for Cellulose Gasification," *Environ. Sci. Technol.*, vol. 36, no. 20, pp. 4476–4481, Oct. 2002.

[34] P. J. Valdez, M. C. Nelson, H. Y. Wang, X. N. Lin, and P. E. Savage, "Hydrothermal liquefaction of Nannochloropsis sp.: Systematic study of process variables and analysis of the product fractions," *Biomass and Bioenergy*, vol. 46, no. Supplement C, pp. 317–331, 2012.

[35] C. M. Huelsman and P. E. Savage, "Intermediates and kinetics for phenol gasification in supercritical water," *Phys. Chem. Chem. Phys.*, vol. 14, no. 8, pp. 2900–2910, 2012.

[36] R. P. Overend, T. A. Milne, and L. K. Mudge, *Fundamentals of thermochemical conversion of biomass*. 1985.

[37] C. Di Blasi, C. Branca, and A. Galgano, "Effects of Diammonium Phosphate on the Yields and Composition of Products from Wood Pyrolysis," *Ind. Eng. Chem. Res.*, vol. 46, no. 2, pp. 430–438, Jan. 2007.

[38] M. Statheropoulos and S. A. Kyriakou, “Quantitative thermogravimetric-mass spectrometric analysis for monitoring the effects of fire retardants on cellulose pyrolysis,” *Anal. Chim. Acta*, vol. 409, no. 1, pp. 203–214, 2000.

[39] G. Varhegyi, M. J. Antal, T. Szekely, F. Till, and E. Jakab, “Simultaneous thermogravimetric-mass spectrometric studies of the thermal decomposition of biopolymers. 1. Avicel cellulose in the presence and absence of catalysts,” *Energy & Fuels*, vol. 2, no. 3, pp. 267–272, May 1988.

[40] P. R. Patwardhan, D. L. Dalluge, B. H. Shanks, and R. C. Brown, “Distinguishing primary and secondary reactions of cellulose pyrolysis,” *Bioresour. Technol.*, vol. 102, no. 8, pp. 5265–5269, 2011.

[41] W. S. L. Mok, M. J. Antal, P. Szabo, G. Varhegyi, and B. Zelei, “Formation of charcoal from biomass in a sealed reactor,” *Ind. Eng. Chem. Res.*, vol. 31, no. 4, pp. 1162–1166, Apr. 1992.

[42] M. J. Antal, W. S. L. Mok, G. Varhegyi, and T. Szekely, “Review of methods for improving the yield of charcoal from biomass,” *Energy & Fuels*, vol. 4, no. 3, pp. 221–225, May 1990.

[43] F.-X. Collard and J. Blin, “A review on pyrolysis of biomass constituents: Mechanisms and composition of the products obtained from the conversion of cellulose, hemicelluloses and lignin,” *Renew. Sustain. Energy Rev.*, vol. 38, pp. 594–608, 2014.

[44] P. Morf, P. Hasler, and T. Nussbaumer, “Mechanisms and kinetics of homogeneous secondary reactions of tar from continuous pyrolysis of wood chips,” *Fuel*, vol. 81, no. 7, pp. 843–853, 2002.

[45] M. J. Antal Jr, “Biomass pyrolysis: a review of the literature. II: lignocellulose pyrolysis,” *Adv. Sol. energy*, vol. 2, pp. 175–255, 1985.

[46] F. Rodríguez-Reinoso, M. Molina-Sabio, and M. T. González, “The use of steam and CO2 as activating agents in the preparation of activated carbons,” *Carbon N. Y.*, vol. 33, no. 1, pp. 15–23, 1995.

[47] A. F. Holleman and E. Wiberg, *Inorganic Chemistry*. Academic Press, 2001.

[48] M. Molina-Sabio and F. Rodríguez-Reinoso, “Role of chemical activation in the development of carbon porosity,” *Colloids Surfaces A Physicochem. Eng. Asp.*, vol. 241, no. 1, pp. 15–25, 2004.

[49] M. Jagtoyen and F. Derbyshire, “Activated carbons from yellow poplar and white oak by H_3PO_4 activation,” *Carbon N. Y.*, vol. 36, no. 7, pp. 1085–1097, 1998.

[50] R. F. Jameson, “151. The composition of the ‘strong’ phosphoric acids,” *J*. *Chem*. *Soc*., no. 0, pp. 752–759, 1959.

[51] M. A. Lillo-Ródenas, D. Cazorla-Amorós, and A. Linares-Solano, “Understanding chemical reactions between carbons and NaOH and KOH: An insight into the chemical activation mechanism,” *Carbon N*. *Y*., vol. 41, no. 2, pp. 267–275, 2003.

[52] G. Sethia and A. Sayari, “Activated carbon with optimum pore size distribution for hydrogen storage,” *Carbon N*. *Y*., vol. 99, pp. 289–294, 2016.

[53] B. Hu, S.-H. Yu, K. Wang, L. Liu, and X.-W. Xu, “Functional carbonaceous materials from hydrothermal carbonization of biomass: an effective chemical process,” *Dalt*. *Trans*., no. 40, pp. 5414–5423, 2008.

[54] B. Hu, K. Wang, L. Wu, S. Yu, M. Antonietti, and M. Titirici, “Engineering carbon materials from the hydrothermal carbonization process of biomass,” *Adv*. *Mater*., vol. 22, no. 7, pp. 813–828, 2010.

[55] W. C. Park, A. Atreya, and H. R. Baum, “Experimental and theoretical investigation of heat and mass transfer processes during wood pyrolysis,” *Combust*. *Flame*, vol. 157, no. 3, pp. 481–494, 2010.

Chapter 2

Synthesis of activated carbon from cellulose by chemical activation using DAP and the characterization of the porosity

Introduction

Biochar derived from biomass is largely a polycyclic aromatic structure whose formation is favored by intra and intermolecular rearrangement reactions of the precursor (raw biomass), resulting in a better thermal stability of the residue [1]. In the history of humankind, biochar has been used in many applications: fuel, soil amendment, water filter, and many more [2]–[4]. As the understanding of biochar advanced, researchers realized that the porosity and functional groups present in biochar were very important characteristics. Hence, a class of biochar with high porosity has been classified as 'activated' to emphasize its properties of high surface area and well-defined pore size distributions, which made the biochar much more valuable than just a better source of fuel. For instance, activated carbon has widespread application in the field of water purification at different stages of the treatment process. So there may exist a need to synthesize activated carbon locally in resource-constrained communities using systems that are fairly easy to construct and operate. Traditionally, activated biochar has been synthesized by thermal gasification using CO_2 or H_2O at high temperatures generally > 800°C or by chemical activation using activants such as zinc chloride ($ZnCl_2$), phosphoric acid (H_3PO_4), and potassium

hydroxide (KOH) [5]–[8]. Among the activants, phosphoric acid activation of woody biomass has been well studied and explained by the pioneering works of Jagtoyen & Derbyshire, Molina-Sabio & Reinoso and many others [9], [10]. During the activation process, phosphoric acid acts as an acid catalyst and promotes bond cleavage reactions by cyclization and condensation. By reacting with organic species, it helps to crosslink biopolymer fragments via phosphate and polyphosphate bridges [9]. Pore size distributions of the carbons activated with phosphoric acid have shown a strong dependence on the mass of H_3PO_4 loaded per unit mass of the substrate and the final heat treatment temperature [9]. Besides activation, during the process of pyrolysis, heteroatoms like P and O are incorporated into the carbonaceous matrix. The concentration of these heteroatoms can impart interesting properties and govern the surface chemistry and cationic exchange properties of the resulting activated carbons [11], [12]. Several facile low temperature routes to synthesize porous and functionalized carbonaceous materials with controllable morphology via HTC (Hydrothermal carbonization) have also been elucidated in the literature [13], [14].

Unfortunately, activating agents like zinc chloride and phosphoric acid are strongly dehydrating and ought to be handled with care, which increases the difficulty of biochar production. One way to counter this would be to use a salt that forms an activant during the activation process while remaining benign at the storage condition. For instance, diammonium hydrogenphosphate (DAP) is a commonly available fertilizer which liberates phosphoric acid (H_3PO_4) and ammonia upon heating. In principle, it should be able to activate carbon as well because of the H_3PO_4 being formed during the process. In fact, Benaddi *et al*. studied the activation of wood flour with H_3PO_4 and DAP at low temperatures (300°C-500°C) in environments of nitrogen and steam [15].They were able to show that by changing process parameters such as the temperature, the

nature of the phosphorous activating agent, and the reaction environment, one could obtain activated carbons with significantly different properties. However, this study did not elaborate on the nature of bonding between different heteroatoms in the carbonaceous matrix. Therefore, it is worthwhile to further explore the activation process by DAP to gain a deeper understanding of the process, as DAP could be a safer alternative to phosphoric acid in such contexts. One outcome of understanding the DAP activation process is that it may allow preparation of activated char on a smaller scale outside an activated carbon production facility, where proper infrastructure and complex controls are required to ensure safe handling and recovery of the activant. This possible outcome may show a way to meeting the needs for activated biochar in a resource constrained environment, where purchasing pre-made biochar may not be favored due to socio-economic reasons.

Currently, most commonly used methods for biochar activation use flow-through systems where the evolved vapors during pyrolysis are swept off by an inert gas purge. The swept volatiles are then condensed to bio-crude, which is an oxygen-rich corrosive liquid. The biochar which is left as residue in the reactor is eventually recovered. This type of flow reactor system works well in places with modern infrastructure, but in resource constrained environments other factors may become limiting. Flow-through setups requiring sophisticated mechanisms like an inert gas purge, numerous moving parts, and condensation mechanisms are difficult to conceive of being operative in off-grid settings. Instead, need-based, batch production of biochar is more likely to occur in a resource constrained environment. Hence, demonstrating the possibility of activated biochar production on a small scale without access to a sophisticated system and characterizing the porosity of the produced biochar are the primary goals of this chapter.

Experimental

Preparation of the precursor

Microcrystalline cellulose (MCC) ($\geq$ 99.9%) and diammonium hydrogenphosphate (DAP) (≥99%) were purchased from Sigma-Aldrich (St. Louis, MO) and used as received. Aqueous DAP solutions of known concentrations were prepared as listed in Table 2.1 (which links the definition of concentration basis to the nomenclature of the substrates). A requisite volume of the solution was added to a fixed mass of cellulose to facilitate wetting of the sample and impregnate a desired concentration of DAP. The mixture was stirred well and then soaked for 3 hours at room temperature. It was then allowed to dry at 80°C for 48 hours to obtain a precursor which would then be used for subsequent pyrolysis. The precursor thus obtained is denoted as MCC-X-DAP, where 'X' is defined as the strength of activation (X = g DAP/100 g cellulose).

Table 2.1: Explanation of concentration basis and nomenclature of the biochar precursors

Precursor	Mass of cellulose /mg	Concentration of DAP solution /(mg·ml^{-1})	Volume of DAP solution /ml	DAP loading /(g DAP per 100 g cellulose)
MCC-11-DAP *	1000	10	11.1	11.1
MCC-50-DAP	1000	50	10	50
MCC-75-DAP	1000	100	7.5	75
MCC-100-DAP	1000	100	10	100

*Note: The precursor MCC-11-DAP is actually MCC-11.1-DAP. It has been written as MCC-11-DAP for notational simplicity.

Activated biochar preparation

In order to form activated biochar from the prepared cellulose-DAP complex listed above under conventional settings, approximately 900 mg of the DAP impregnated cellulosic precursor was loaded to a quartz boat which was then placed inside a Thermolyne 21100 tube furnace (flow-through system for pyrolysis). The precursor was purged under nitrogen gas at room temperature for two hours and then heated to 450°C at a ramp rate of 5°C/min. The N_2 flow rate was

maintained at 100 ml/min. When the desired temperature of 450°C was reached, the samples were held at that temperature for one hour and then cooled down to room temperature. The tube furnace setup is represented in Figure 2.1(a).

For facilitating experiments where the precursor has access to ambient air during heat treatment, a setup very closely approaching a batch reactor was constructed. The reactor, named as Partial Oxidation (POX) reactor, was essentially a cylindrical vessel assembled out of Swagelok® stainless steel (SS-316) fittings and had a small 1/8 inch opening in a 3/4 inch cap to allow access of air into the system and also the release of some of the vapors and gases (Figure 2.1b). The DAP impregnated precursor was loaded to cylindrical quartz inserts which fitted into the reactor. The reactor was heated in a Barnstead Thermolyne 48000 muffle furnace to 450°C at a rate of 5°C/min and held for one hour at that temperature before cooling down.

After heat treatment, the excess activating agent was extracted by washing it thoroughly with deionized water and the samples were dried at 110°C in a Thermo-Fisher sample oven for 24 hours. The dried samples, cooled down to room temperature were then stored for subsequent analysis. The activated biochar samples thus synthesized were denoted as AC-X-Y, where X denotes the strength of activation as defined earlier and Y denotes the environment under which the samples were formed. For instance, if the activated carbon sample was formed by using MCC-50-DAP as the precursor in a tube furnace with N_2 flow it will be denoted as AC-50-N_2. Similarly, a sample synthesized from MCC-50-DAP precursor under POX conditions will be denoted as AC-50-POX. The nomenclature defined above will be extensively used throughout the dissertation.

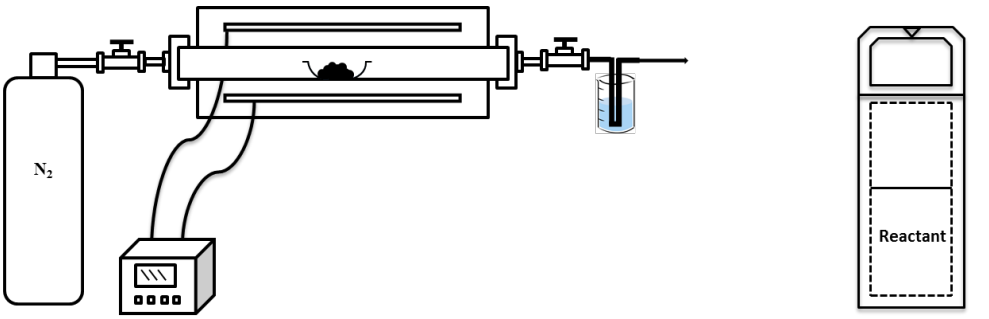

Figure 2.1: Reactor setups used for experiments (a) Flow-through type reactor and (b) POX reactor in an environment of ambient air with a small opening at its top. The dotted line shows the quartz insert containing the reactant

In-situ thermochemical decomposition studies

A TA Q500 Thermogravimetric Analyzer (TGA) was used for the experiments described here. Samples of cellulose and cellulose-DAP complexes approximately between 7 mg-12 mg were heated at a ramp rate of 5°C/min in different atmospheres (pure N_2, air) to a final temperature of 750°C, under a total gas flow rate of 100 ml/min. It should be noted that the air flow in the TGA system gets diluted by some balance N_2 gas, lowering the actual O_2 concentration to 16 %. Therefore, any future mention of 'air flow' in TGA studies implies a 16 % oxygen concentration, balance being N_2. A heating rate of 5°C/min was chosen to facilitate a slow pyrolysis. The vapors and gases released in the TGA were swept immediately to a transfer line, connected to a Nicolet 380 FTIR (Fourier Transform Infrared) spectrometer for qualitative analysis. The transfer line was heated to an internal temperature of 150°C, to avoid condensation of semi-volatile products. The gas phase IR spectrum was obtained for every 1°C rise in temperature and the scanning range was from 4000 to 500 cm^{-1}. The IR resolution was 4 cm^{-1}.

Characterization

The textural properties of the synthesized biochar were determined by nitrogen physisorption and desorption at 77 K using a Micromeritics ASAP 2020 apparatus. Before analysis, the samples were degassed for 24 hours under vacuum ($\sim 10^{-3}$ mm Hg) at a temperature of 300°C to eliminate any adsorbed moisture. The surface area was calculated by applying the BET equation to the isotherm data in the relative pressure (P/P_o) range from 0.05 to 0.20. The micropore volume was determined from the Dubinin-Radushkevich (DR) as well as the Dubinin-Astakhov (DA) equations. The mesopore volume was calculated from the Barrett-Joyner-Halenda (BJH) method. The micropore size distribution was obtained from the Horvath-Kawazoe (HK) model using slit pore geometry. CO_2 adsorption was carried out at 273 K to compute the volume in the ultra-micropores (< 0.7 nm). DRIFTS (Diffuse Reflectance Infrared Fourier Transform Spectroscopy) analysis was performed on a finely ground sample on a Bruker Tensor 27 FTIR using a Harrick Praying Mantis diffuse collection system and OPUS data collection program. The carbonized samples were diluted with KBr and finely ground in mortar-pestle. Pure KBr was used as a background and FTIR spectra were recorded. The resolution was set to 4 cm^{-1}, and the number of scans was set to 256. The IR scanning range was from 4000 to 600 cm^{-1}. For Transmission Electron Microscopy (TEM) analysis, the sample was ground in a mortar-pestle and suspended in ethanol. A small volume of this suspension was dried over holey carbon film supported on a molybdenum grid allowing direct access of the electron beam. The samples were then viewed and analyzed on a JEOL-2010F TEM. The sample morphology was examined under the Scanning Electron Microscope (SEM) using a Phillips XL30FEG scanning electron microscope. Raman spectra were obtained with a Renishaw inVia Raman microscope using a 532 nm laser as the excitation source. Samples were scanned within a range of 1000 to 1800 cm^{-1} and to get a

better signal to noise resolution, 30 scans were averaged for each sample. X-Ray Diffraction (XRD) characterization was carried out with a Rigaku Rotating Anode X-Ray Diffractometer with CuKα radiation from 2θ =10° to 60° at a step size of 0.02°.

Results and Discussion

Chemical transformations during the synthesis procedure

Lignocellulosic biomass most commonly found in our surroundings is composed of cellulose, hemicellulose, and lignin in addition to some organic extractives and inorganic ash. Cellulose $(C_6H_{1O}O_5)_n$ is the primary component which constitutes about 40-50 wt. % of dry wood [16]. It is a high molecular-weight linear polymer of glucopyranose units and is extensively hydrogen-bonded which imparts it some degree of crystallinity [16]. Because of its well-defined structure, it becomes a convenient and informative tool to study the chemistry of biomass pyrolysis to biochar systematically. For example, white oakwood contains approximately 53.2% cellulose, 24.7% hemicellulose and 24.6% lignin by weight [9]. Apart from being the major component and the advantages listed above; since cellulose also incorporates the bulk of thermal recalcitrance exhibited by a typical lignocellulosic biomass, it was chosen as a model compound to study its interaction with DAP during pyrolysis. To understand how DAP interacts with cellulose, it is essential to understand the decomposition of pure DAP which was laid out by Di Blasi [17]. The temperatures reported here are the peak temperatures obtained by Thermogravimetric-Mass Spectrometric studies (TG-MS). The reactions are listed as Equations (2.1) to (2.5). DAP upon decomposition forms ammonia and phosphoric acid at lower temperatures and the process further continues to give P_2O_5 and H_2O as final products.

$$(NH_4)_2HPO_4(s) \xrightarrow{159°C} NH_3(g)+(NH_4)H_2PO_4(s) \quad \text{Eq. (2.1)}$$

$$(NH_4)_2HPO_4(s) \xrightarrow{159°C} 2NH_3(g)+H_3PO_4(l) \quad \text{Eq. (2.2)}$$

$$(NH_4)H_2PO_4(s) \xrightarrow{209°C} NH_3(g)+H_3PO_4(l) \quad \text{Eq. (2.3)}$$

$$4H_3PO_4(l) \xrightarrow{159°C\ ,209°C} 2H_2O(g)+2H_4P_2O_7(l) \quad \text{Eq. (2.4)}$$

$$H_4P_2O_7(l) \xrightarrow{>209°C} 2H_2O(g)+ P_2O_5(s) \quad \text{Eq. (2.5)}$$

As laid out in the synthesis procedure, post soaking at room temperature to facilitate close contact of the activating agent with cellulose, the mixture was dried at 80°C for 2 days. Post drying chemical transformations occurs in DAP as well as cellulose. DAP can break down to Monoammonium phosphate (MAP), phosphoric acid and ammonia per equations 2.1 and 2.2. The decomposition of DAP is known to occur as early as 70°C. Thus, post drying at 80°C for 48 hours, DAP gets transformed to MAP as evidenced from XRD data (Ref # 01-078-2280) in Fig. 2.2. MAP crystals became larger as DAP loading increased (indicated by peak sharpness).

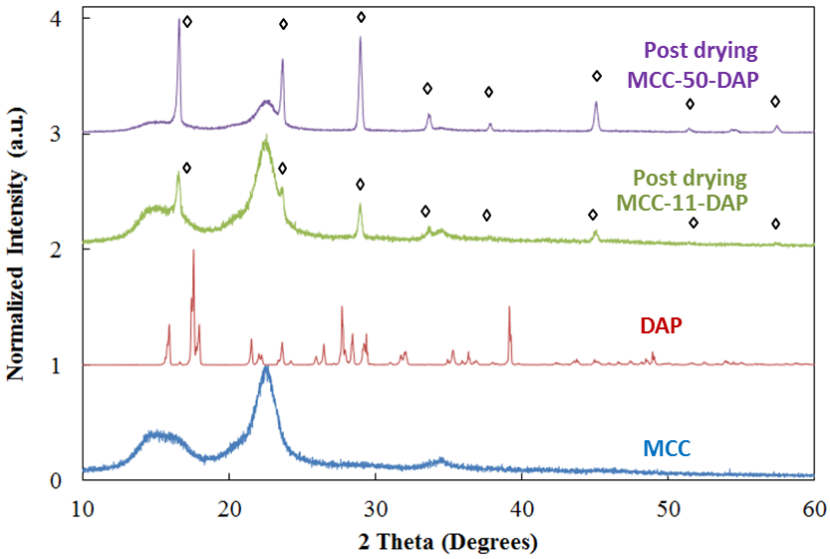

Figure 2.2: XRD spectra for MCC, DAP and the precursors MCC-11-DAP and MCC-50-DAP post the drying step. The diamond symbol is the peak identifier corresponding to MAP

Microcrystalline cellulose (MCC) itself is a white solid, but when loaded with different concentrations of DAP, the dried precursor shows a change in color. The precursor changes from white to yellow and then brown with increasing DAP loadings, indicating that chemical changes begin within the structure of cellulose as studied by DRIFTS in Figure 2.3. Microcrystalline cellulose has a well-defined structure with prominent peaks that have been identified and studied in the literature [18], [19]. Table 2.2 shows a comparison of the band assignment for the DRIFT spectra of MCC, based on the comprehensive work of Ilharco *et al*. [18].

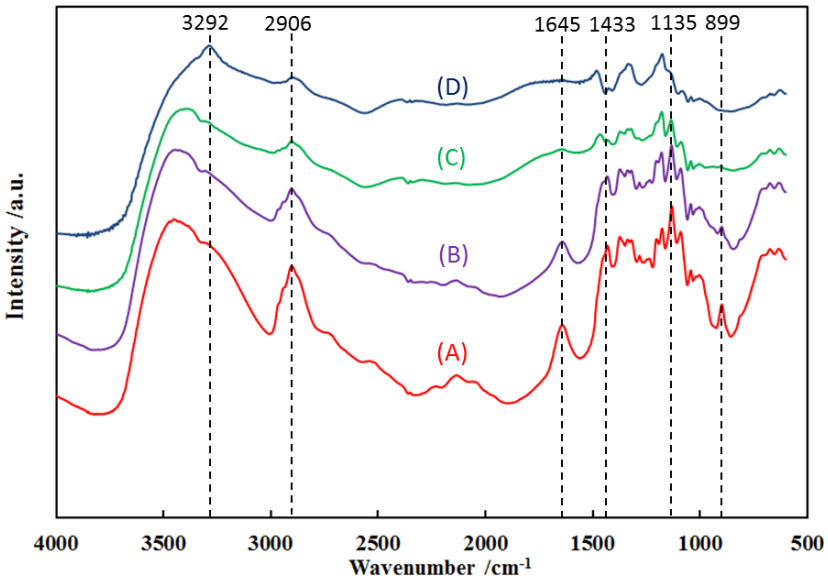

Figure 2.3: DRIFTS absorbance spectra of various precursors of biochar (A) MCC (B) MCC-11-DAP (C) MCC-50-DAP (D) MCC-100-DAP.

Table 2.2: Band assignment for cellulose in the DRIFT spectrum

MCC (Literature) ν /cm^{-1}	MCC (sample used in this work) ν /cm^{-1}	Band assignment
898	899	ν_{as} (ring)(out of phase) or δCH (wag)
1158	1135	ν_{as} C-O-C (bridge)
1429	1433	$\delta_s CH_2$
1634	1645	δOH (adsorbed water)
2900	2906	νCH

Increasing DAP loading on cellulose shows a progressive decay and disappearance of numerous peaks of cellulose. The decay of the peak at 1135 cm^{-1} indicates depolymerization of cellulose

due to a breakdown of the C-O-C bridge bonds. The dwindling of the bands related to CH and CH_2 (899, 1433, 2906) cm^{-1} indicate an increase in the degree of oxidation due to the action of H_3PO_4 obtained from DAP decomposition. The gradual loss of the OH vibration (1645 cm^{-1}) from adsorbed moisture concurs well with the dehydrating nature of the acid. Finally, when the DAP loading is increased significantly enough in MCC-100-DAP, the peak at 3292 cm^{-1} may suggest an O-H stretch from H_3PO_4 or the formation of amines, due to an interaction of ammonia with the depolymerizing cellulose. Our observations are in agreement with those of Jagtoyen and Derbyshire, who suggested that the primary effect of H_3PO_4 at low temperatures was to hydrolyze the glycosidic linkages in cellulose [9].

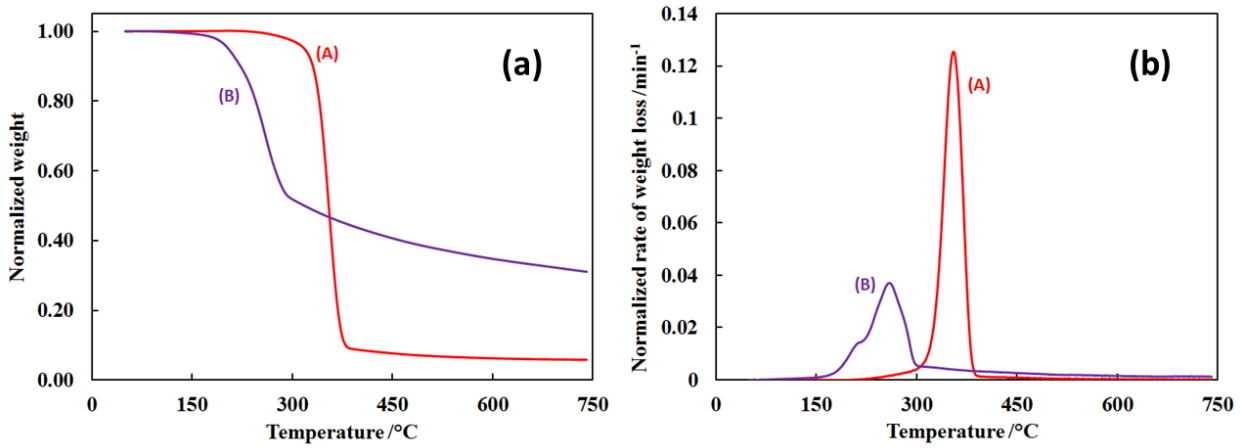

Figure 2.4: (a) Thermogravimetric and (b) Differential thermogravimetric analysis of (A) MCC and (B) MCC-11-DAP under N_2 flow of 100 ml/min

From Figure 2.4(a), the catalytic effect of phosphoric acid is apparent, as it helps to initiate cellulose pyrolysis at a lower temperature by aiding its dehydration and depolymerization. The differential thermogravimetry (DTG) curve (Figure 2.4b) shows that the temperature of peak decomposition is significantly lowered by ~ 90°C. Another effect is a reduction in volatiles. Volatiles and tars are undesirable when the desired product is char as they condense around the walls of the reactor and cause problems of clogging that necessitate frequent cleaning.

Levoglucosan which is a precursor to the formation of volatiles is an intermediate product of cellulose pyrolysis. Di Blasi observed that the ratio of noncombustible to combustible volatile products increased from 0.5 to 5.5 when wood impregnated with 10 wt. % DAP was pyrolyzed [17]. H_3PO_4 treatment inhibits the formation of levoglucosan and so does DAP given that H_3PO_4 is its primary decomposition product. Besides, the resultant char has increased aromaticity with a more cross-linked and thermally stable polycyclic structure [17]. The insertion of phosphate groups dilates the structure, and when the acid is washed out, the matrix remains in an expanded state with an accessible pore structure [9]. Because of these benefits associated with the use of DAP, a systematic experimental protocol was designed to activate cellulosic biochar first under conventional system with inert gas and subsequently under POX conditions.

Evolution of biochar structure with heat treatment and activation under nitrogen flow

The evolution of the structure of activated biochar (washed samples) from MCC-50-DAP precursor is shown in Figure 2.5. A summary of the vibrations and the associated references are given in Table 2.3. At temperatures > 150ºC, cross-linking reactions dominate. The reaction of cellulose with H_3PO_4 gives rise to phosphate esters. The existing hydrogen bonds between cellulosic chains are disrupted and formation of phosphate esters dilates the structure. This change points to the catalytic effect of phosphoric acid. Two small shoulders visible at 1125 and 1160 cm^{-1} in the 160^{o}C sample, are attributed to the C-O-C stretching vibrations of the glyosidic linkages. These tend to disappear by 200°C. The sample at 160^{o}C also contains a single broad band at 1660 cm^{-1} that can be attributed to aromatic C=C stretching. This peak actually shifts to a lower frequency (1580 cm^{-1}) with increasing HTT, perhaps due to aromatic ring condensation. Thus, as the temperature is increased, aromatic ring condensation and cyclization occur which enhances the aromaticity and size of the polyatomic units. The sample at 200^{o}C begins to form a

new peak at ~1700 cm^{-1}, which is well developed around 300°C and higher. This peak can be attributed to C=O stretching in carbonyl compounds and carboxylic acids. H_3PO_4 promotes bond cleavage reactions, which can be seen through the breaking of C-O bonds within the glucose rings present in MCC, subsequently forming surface carbonyls. The peak at 1440 cm^{-1} (visible at 160°C) which is due to -CH_2 bending vibrations in carbon chains diminishes greatly with increasing temperature and completely vanishes at 300°C due to phosphoric acid bond cleavage reactions. The defective graphene layers largely acquire their eventual form by 300°C, post evaporation of a significant fraction of the higher molecular weight volatiles.

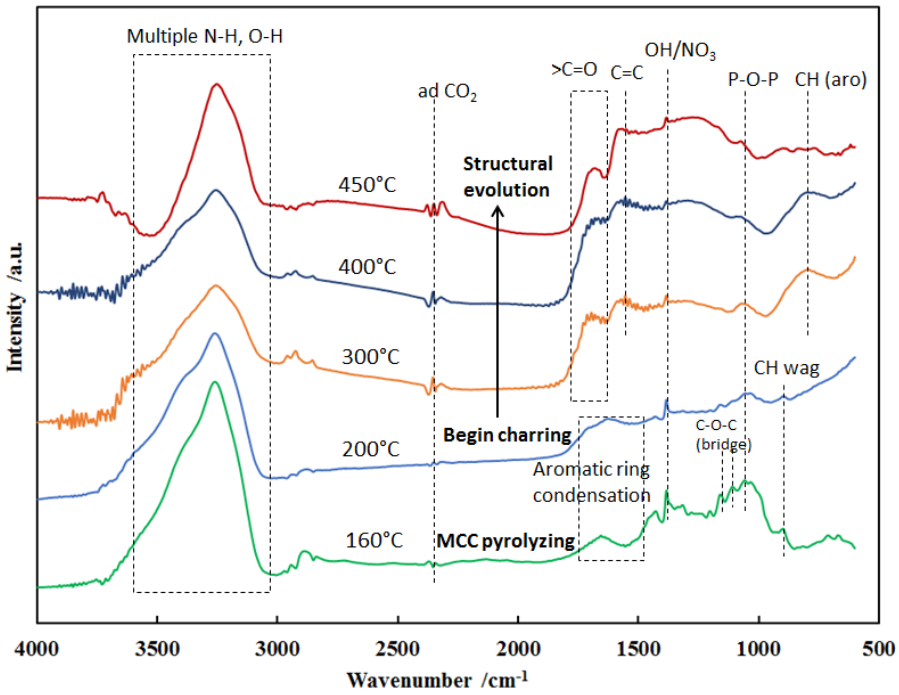

Figure 2.5: DRIFTS absorbance spectra showing the structural evolution of activated carbon during pyrolysis at various heat treatment temperatures

The broad peak (3100-3500) cm^{-1}, centered roughly at 3250 cm^{-1} is present at all temperatures and can be attributed to various types of O-H and N-H vibrations. The N-H vibrations stem from the interaction of NH_3 with the pyrolyzing cellulose. The peak at 2350 cm^{-1} is due to CO_2 adsorbed on the samples from the atmosphere. The region of interest in these spectra is from

1750-990 cm^{-1} because this is where the majority of changes occur. All samples contain a peak at ~1070 cm^{-1} which is due to P-O-P stretching vibrations in phosphate and polyphosphate bridges. The peaks at 2900 cm^{-1} are due to aliphatic C-H stretching modes, and seem to disappear at 450^{o}C, perhaps due to the thermal degradation of these linear C-H chains, forming methane. From a structural point of view, although most changes are accomplished by 300°C, but the volatile matter content is still significant at this temperature and the degree of carbonization (fixed carbon content) is low. Also, from previous work on H_3PO_4 activation it was known that its effect on porosity is maximum at 450°C, this thus work examined the synthesis first at 450°C.

Table 2.3: Compilation of DRIFT spectra bond vibrations at different temperatures

Literature wavenumber /cm^{-1}	Wavenumber /cm^{-1}	Band assignment	HTT /^{o}C
3319.2 [20]	3250	O-H, N-H (various)	160,200,300,400,450
2921,2855 [21]	2900	C-H aliphatic stretching	160,200,300,400
2380-2270 [22]	2350	adsorbed CO_2	160,200,300,400,450
1714 [23]	1710	C=O carbonyls	300,400,450
1580 [12]	1650(160^{o}C) 1575(>200^{o}C)	aromatic C=C	160,200,300,400,450
1450 [24]	1440	-CH_2 bending	160,200
1400 [12]	1385	O-H / N-O (nitrates)	200,300,400,450
1319 [24]	1320	-CH_3 bending	160
1135 [25]	1125,1160	C-O-C bridge	160, 200
1070 [26]	1060-1070	P-O-P stretch	160, 200,300,400,450
999 [26]	990-995	P-O-C asymmetrical stretch	450
885,840,775 [21]	800	C-H out-of-plane (aromatic)	160,200,300,400,450

In accordance with the nature of decomposition of DAP, H_3PO_4 was hypothesized to be the primary activating agent. Analogous to what is expected with H_3PO_4 upon heat treatment (Eq. 2.1-2.5); it was assumed that P_2O_5 would act as a template for porosity generation. The washing away of P_2O_5 provides access to the porosity in carbon [10]. In order to further confirm this hypothesis for DAP activation, biochar was synthesized following the procedure listed in the

synthesis section. Figure 2.6 shows the solid phase DRIFTS spectrum of AC-50-N_2 (unwashed and washed) .The unwashed samples clearly exhibits a strong peak of PO_2 , PO_3 and P=O vibrations associated with P_2O_5; but the washed samples do not as P_2O_5 is extracted by water forming H_3PO_4. The washing away of P_2O_5 provides access to the generated porosity. This fact is also reflected in the yield data of the washed and unwashed samples in chapter 3, Figure 3.6.

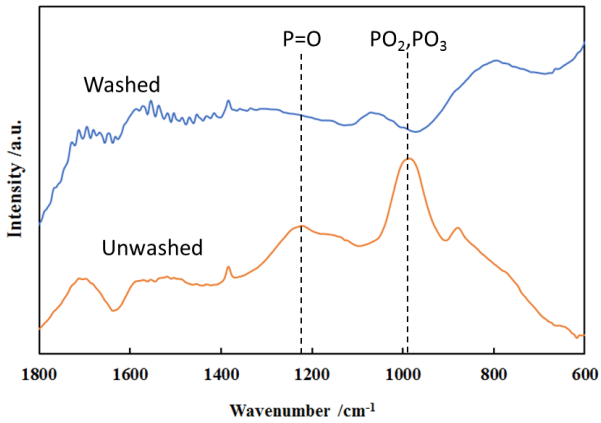

Figure 2.6: DRIFTS absorbance spectra of the unwashed and washed samples of AC-50-N_2, showing the absence of the P=O vibrations due to P_2O_5 in the washed sample

To assess the effect of DAP activation, isolating effects of O_2 synthesis was first carried out under inert N_2 flow in a tube furnace. The control biochar sample without DAP pretreatment had a BET surface area (370-410) m^2/g. As seen from Figure 2.7, we were successful in synthesizing microporous activated biochar (IUPAC- Type 1). The steep gradient of the initial part of the isotherm at low relative pressure suggests that the samples have narrow micropores. The micropore volume, BET surface area, pore size distributions and other properties are laid out in Table 2.4. These values increase almost linearly with the increase in the DAP loading. Traditional synthesis via chemical activation of H_3PO_4 uses much higher loading of the acid to substrate (upto 2:1 mass ratio, acid to wood) and the pore volumes are a strong function of this loading. We have used lower concentration of DAP in this study given the emphasis on efficient

resource utilization and relatively milder operating conditions. Although microporous, the pore size distribution is fairly broad, as seen in the inset of Figure 2.7. The spread of the pore size distribution is probably a result of the mix of polyphosphoric acids (from $H_4P_2O_7$ to $H_7P_5O_{16}$ in different proportions predicted by P_2O_5-H_2O phase diagram) generated during heat treatment. More validation to the role of P_2O_5 in the activation process is provided later in Chapter 3.

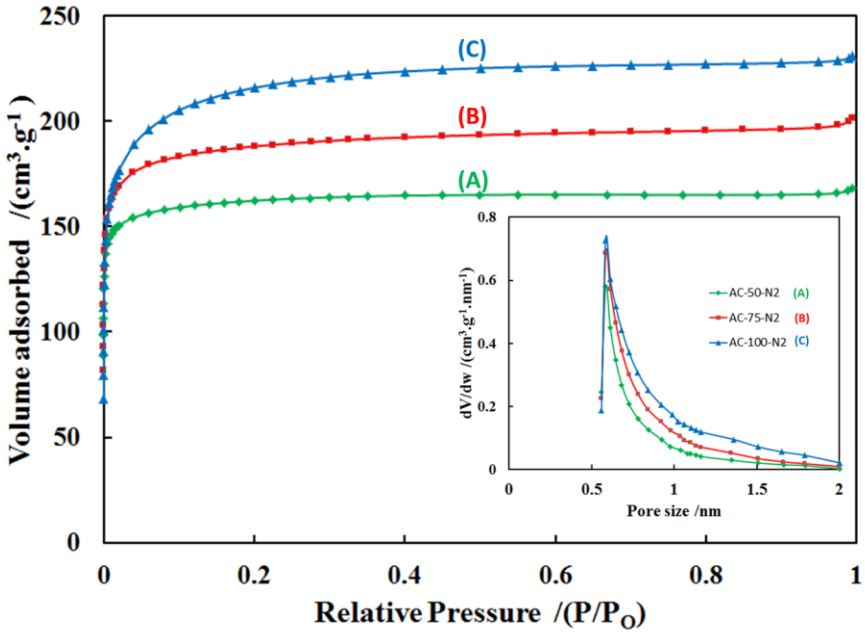

Figure 2.7: Nitrogen adsorption isotherms at 77 K for (A) AC-50-N_2 (B) AC-75-N_2 and (C) AC-100-N_2 along with their associated pore size distribution

Table 2.4: Textural properties of the activated biochar samples synthesized under nitrogen flow

Biochar sample	BET S.A. /($m^2 \cdot g^{-1}$)	DR-Micropore volume /($cm^3 \cdot g^{-1}$)	DA-Micropore volume /($cm^3 \cdot g^{-1}$)	Micropore size /nm	Mesopore volume /($cm^3 \cdot g^{-1}$)
AC-50-N_2	545	0.249	0.251	0.560	0.009
AC-75-N_2	635	0.288	0.297	0.583	0.015
AC-100-N_2	740	0.311	0.345	0.649	0.012

Effect of oxygen on thermochemical conversion of cellulose impregnated with DAP

The proof of concept of DAP activation in the tube furnace (N_2 flow) propelled further studies in the presence of air. Fundamental decomposition reactions of MCC and MCC-11-DAP were thus

carried out under air flow in a TGA-IR setup to assess what changes the presence of O_2 might bring to the system. Figure 2.8 illustrates the decomposition profile in air flow. DAP upon decomposition forms a film of condensed phosphoric acids and phosphates which prevents the access of atmospheric oxygen [27] and has thus found useful application as a fire retardant when mixed with cellulosic substrates. This can be seen from Figure 2.8(a) where around 450°C cellulosic char would have almost entirely burnt away but char impregnated with DAP seems resistant to oxidation. Although resistance to oxidation by air was observed, it became clear that a flow-through system with air flow cannot be used and the degree of exposure of char to oxygen needs to be limited. The catalytic temperature lowering effect of H_3PO_4 was still observed independent of the presence of oxygen. Figure 2.8(c) is a FTIR spectral snapshot of the gas phase at the peak temperature of decomposition corresponding to the DTG curve in Figure 2.8(b). One significant observation is that volatiles evolved during cellulose gasification in air (primarily carbonyl compounds, indicated by peaks around ~ 1760 cm^{-1} and 1500 cm^{-1}) are minimized when DAP is impregnated into the matrix (Figure 2.8c). This could be due to a new pathway induced by DAP (inhibiting levoglucosan formation) and/or the simultaneous facilitation of oxidation of the evolved volatiles to CO_2. These observations propelled the design of a POX reactor which very closely approaches a batch reactor whose details have been described previously in the experimental section. The design of the reactor allows ambient air in the muffle furnace to get into the system and volatiles to get oxidized and escape simultaneously by a natural pressure-driven flow. Analogous to the biochar synthesized in the tube-furnace under N_2 flow, biochar synthesized in the POX reactor could be directly washed with deionized water without the requirement of additional organic solvents. The porosity of the biochar samples synthesized with MCC-11-DAP were quite low and higher concentration of DAP

(MCC-50-DAP onwards) was necessary to obtain activated carbon with substantially high porosity comparable to commercially used activated carbon samples.

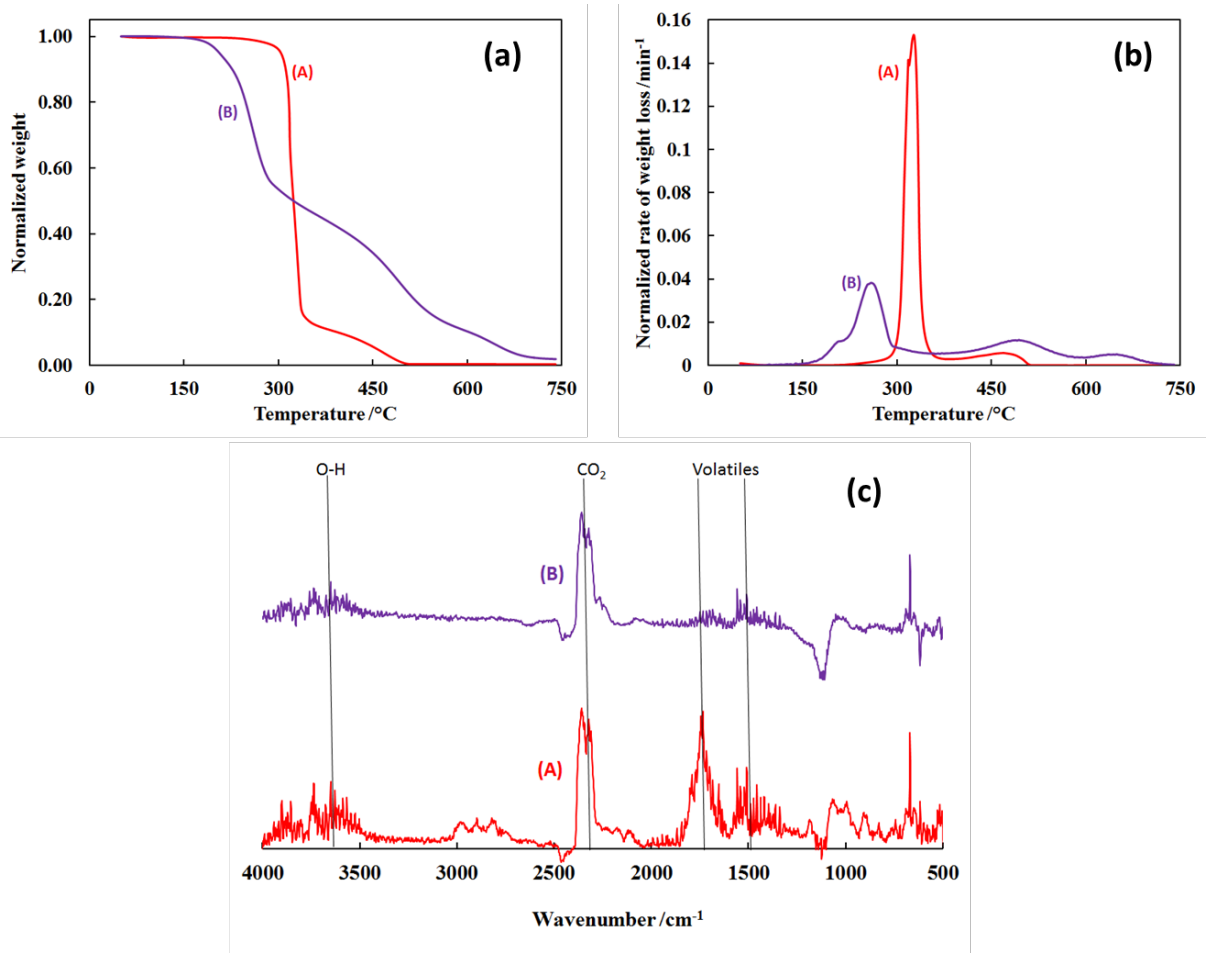

Figure 2.8: (a) Decomposition of (A) MCC, (B) MCC-11-DAP in air flow, (b) Differential thermogravimetric (DTG) curves corresponding to Figure 2.8(a) and (c) Gas phase FTIR spectral snapshot of the decomposition of MCC and MCC-11-DAP at their respective peak temperatures of decomposition identified from the DTG curve

The textural properties of the activated biochar after washing and drying were determined by N_2 physisorption. Figure 2.9 shows the isotherm at 77 K and Table 2.5 compiles the porosity features. (The inter batch variability in pore volumes and BET surface area was ± 5%). During characterization, samples (AC-50-POX and AC-75-POX) were found to be completely

microporous exhibiting an IUPAC-Type 1 isotherm [28]. The BET surface areas were fairly large and typical of activated carbons with significant micropore volume.

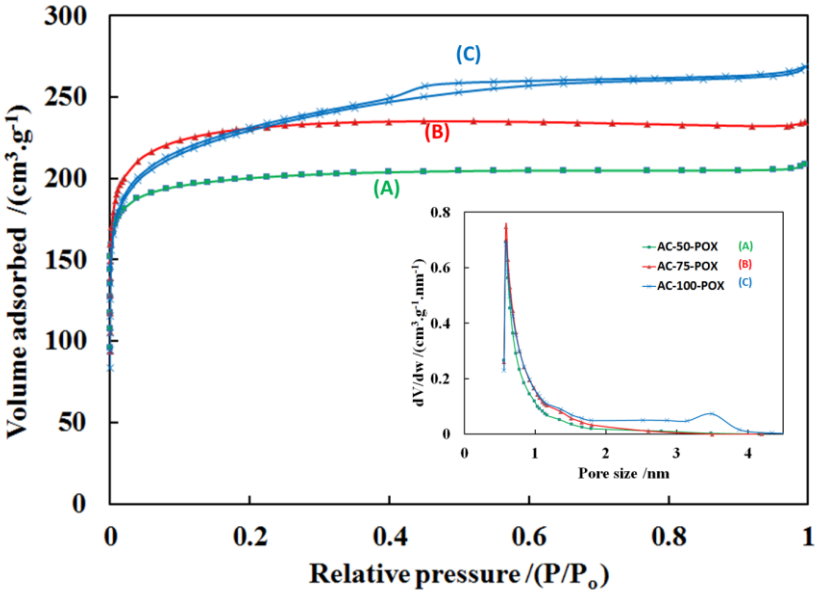

Figure 2.9: Nitrogen adsorption-desorption isotherms at 77 K and associated pore size distributions for samples (A) AC-50-POX (B) AC-75-POX and (C) AC-100-POX

This observation is consistent with more activation observed with higher H_3PO_4 loading within the range of equivalent concentrations studied [29]. Even the biochar (AC-100-POX) was still predominantly microporous, but hysteresis in desorption isotherm clearly demonstrated the beginnings of some perceivable mesoporosity which was also confirmed by an increased mesopore volume. The BET surface areas of AC-75-POX and AC-100-POX are similar as they are computed in the relative pressure range of 0.05 to 0.20, but the micropore volume for AC-75-POX is higher which can be explained from the magnitude of adsorption in the lower relative pressure range of the isotherm. A change in the porosity and surface of AC-100-POX is evident from the nature of its isotherm. With an equivalent loading of H_3PO_4 only, one would expect purely microporous samples as demonstrated by the work of Molina-Sabio and Reinoso [29]. This suggests that the presence of atmospheric oxygen may have a role to play along with H_3PO_4

in the activation process. Presently it is believed that under high DAP loadings, oxygen preferentially gasifies some of the carbon atoms around the existing microporosity, resulting in larger pore sizes and the beginning of mesoporosity. This explains the reduction in micropore volume at the expense of an increased mesopore volume for AC-100-POX. The total pore volume is still higher for AC-100-POX as compared to AC-75-POX because the nature of adsorption changes at higher relative pressure and more N_2 can be adsorbed as a consequence. The micropore width is seen to increase with increasing DAP loading but not significantly. The distribution of pore-size is again reflective of the nature of activation by phosphoric acid.

Table 2.5: Textural properties of the activated biochar samples from the POX reactor

Biochar sample	BET S.A. /($m^2 \cdot g^{-1}$)	DR-Micropore volume /($cm^3 \cdot g^{-1}$)	DA-Micropore volume /($cm^3 \cdot g^{-1}$)	Micropore size /nm	Mesopore volume /($cm^3 \cdot g^{-1}$)	Mesopore size /nm
AC-50-POX	675	0.305	0.316	0.564	0.024	N/A
AC-75-POX	783	0.344	0.371	0.600	0.019	N/A
AC-100-POX	788	0.324	0.358	0.622	0.094	3.5

To overcome diffusional limitations of N_2 into the finest of micropores at low temperature (77 K) at low relative pressures and further characterize the activated carbons, the conventional approach of CO_2 adsorption at 273 K was carried out to compute the volume in the ultramicropores (< 0.7 nm). The value of the saturation pressure of CO_2 at 273 K (~26100 mm Hg) restricts the range of the isotherm to a relative pressure of 0.03, such that the volume of the narrow micropores may be computed. The CO_2 adsorption isotherm and the associated volume in the ultramicropores is provided in Figure 2.10 and a comparison of the micropore volumes by CO_2 and N_2 adsorption is provided in Table 2.6. With CO_2 adsorption, we observe a similar trend in ultramicropore volume across the samples of activated carbons as observed with N_2 physisorption, suggesting that most of the microporosity is accessible by nitrogen. Lower concentrations of the activating agent result in larger fraction of the micropores as

ultramicropores. AC-50-POX and AC-75-POX have ~80-88 % of the micropore volume as ultramicropores, whereas AC-100-POX has roughly 75% of the volume in the finer micropores (broader pore size distribution). This suggests one would get broader pore size distributions with higher loading of the activating agent, consistent with our observation.

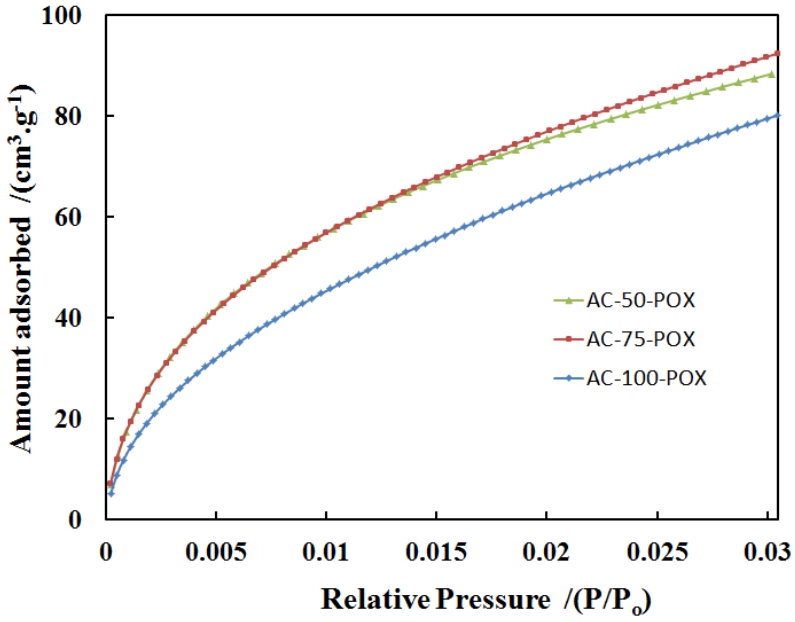

Figure 2.10: CO_2 adsorption isotherms at 273 K for the synthesized activated carbons

Table 2.6: Micropore volumes deduced by N_2 and CO_2 adsorption

Sample	V_{mi} (N_2) /$cm^3.g^{-1}$	V_{mi} (CO_2) /$cm^3.g^{-1}$	Fraction of ultramicropore
AC-50-POX	0.305	0.268	0.878
AC-75-POX	0.344	0.275	0.800
AC-100-POX	0.324	0.245	0.756

A comparison of the values of the textural properties of the pore with existing data in the literature is provided in Table 2.7. With respect to DAP activated biochar, the maximum phosphoric acid equivalent has been mentioned in parenthesis under the loading column in Table 2.7. It is to be noted that different authors use different notations to define the mass loading of the activating agent. Appropriate conversions are made where necessary to bring the data under a consistent set of units. The mass loading has been defined considering H_3PO_4, $ZnCl_2$ or KOH as

the activating agents. Some values have been estimated from graphs and plots of the referenced papers and may not be exactly precise. The measurements of the pore volume in certain cases have used different adsorptive gas (n-Butane) for instance. Besides, there are differences in initial particle size of the raw material, synthesis method and impregnation technique. Thus, conclusions from a simple direct comparison should be avoided. The reader may refer to the actual paper for more information.

Table 2.7: Compilation of pore properties of activated carbons from the literature

Activating agent	Raw material	Temp /°C	Hold time /hr	Loading /(g activant per g raw material)	Micropore volume /($cm^3.g^{-1}$)	Mesopore volume /($cm^3.g^{-1}$)	Total pore vol. /($cm^3.g^{-1}$)	BET S.A /$m^2.g^{-1}$	Ref
DAP	Cellulose (This work)	450	1	0.50 (0.37)	0.32	0.02	0.34	675	[25]
				0.75 (0.56)	0.37	0.02	0.39	781	
				1.00 (0.74)	0.36	0.09	0.45	788	
H_3PO_4	Wood (Ser. A)	500	3	0.20	0.22	0.00	0.22		[9]
				0.50	0.40	0.03	0.43		
				1.00	0.65	0.13	0.78		
				1.45	0.62	0.55	1.14		
H_3PO_4	Wood	450	4	0.79	NA	NA	0.40	891	[10]
				0.85	NA	NA	0.45	1147	
H_3PO_4	Olive stone	450	2	0.63	0.25	0.00	0.25		[7]
				0.85	0.31	0.00	0.31		
				1.11	0.70	0.10	0.80		
$ZnCl_2$	Peach stone	500	NA	0.40	0.45		0.45	850	[6]
				0.96				1600	
KOH	Organic chemical mix	550	2	1.50	0.16		0.26	526	[30]
		600		1.50	0.43		0.64	1317	
		650		1.50	0.50		0.65	1342	
$ZnCl_2$	Wood	400	1	1.50				1825	[31]
		500		1.50				1678	
		700		1.50				1313	

Electron Microscopy

The morphology of activated biochars obtained in typical flow-through N_2 and POX setups can be visualized from Figure 2.11 and Figure 2.12. The samples appear to be significantly attacked with much more pronounced porous/fracture sites than the parent material, cellulose (see appendix, Fig. A2). These fracture sites may be due to shrinkage cracks as a consequence of heat

treatment or because of the attack of H_3PO_4 during carbonization or both. From the point of view of morphology as seen under the SEM at low and high magnification (Figure 2.11 and Figure 2.12 respectively), no significant differences could be observed between the activated carbon samples prepared under flow-through N_2 and POX setups. The literature describes a networked pore structure in activated carbons where transport macropores (>50 nm pore size) and mesopores (pore size between 2 nm and 50 nm) may have 'entrances' to the eventual microporosity [32]. Figure 2.12(c) shows a fractured porous site which may provide access to a smaller pore (~100 nm), bringing out some possible evidence to what has already been described in the literature. Since the action of P_2O_5 has been hypothesized to be the major source of activation, it was necessary to understand the distribution of phosphorus in the samples. From an EDS mapping we found that phosphorus was uniformly distributed throughout the sample, which would suggest that the sample was uniformly porous (see appendix, Fig. A3) .

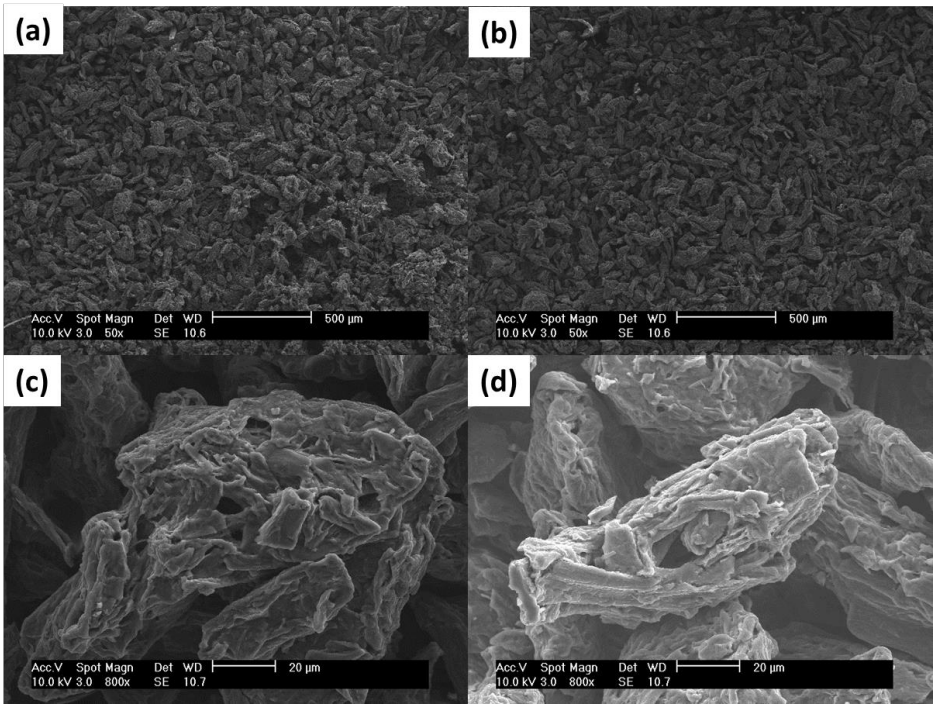

Figure 2.11: Low magnification SEM micrographs of (a) AC-50-N_2, (b) AC-50-POX, (c) AC-50-N_2 and (d) AC-50-POX showing the morphology of the samples

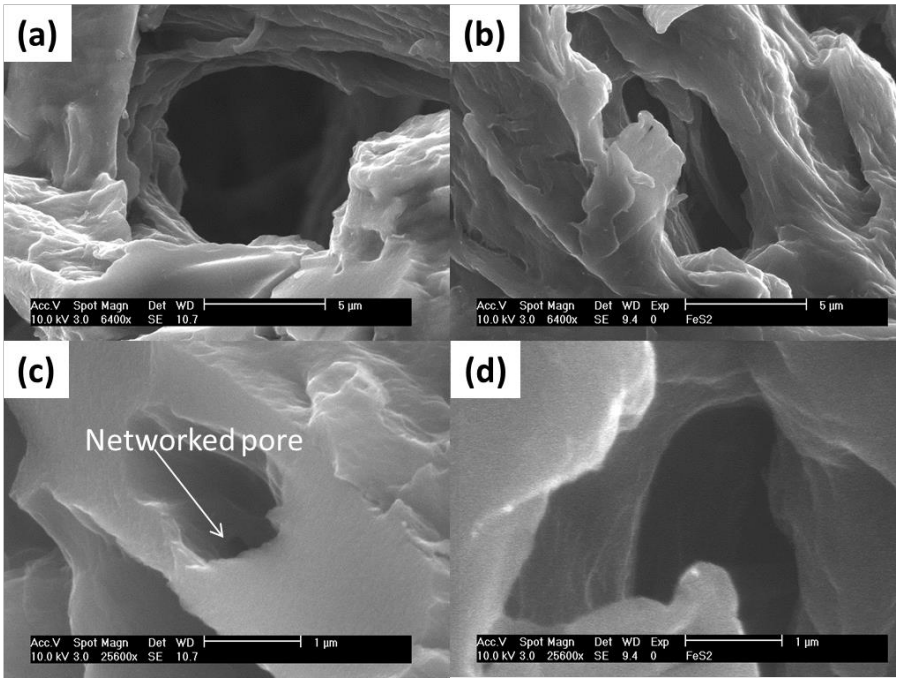

Figure 2.12: High magnification SEM micrographs of (a) AC-50-N_2, (b) AC-50-POX, (c) AC-50-N_2 and (d) AC-50-POX showing the morphology of the samples

By High-Resolution Transmission Electron Microscopy (HRTEM), an attempt has been made to bring out qualitatively the structural features of the synthesized activated carbons. An analysis of these images clearly brings out the complexity in structure. From the images, the different defective-graphene sheets are visible from the varying contrast. Their shape, size and relative positions can be visualized. The structure is akin to a 3D labyrinth or maze. Further characterization by TEM confirms that the activated biochar prepared under nitrogen flow has a similar microstructure to the one prepared under POX environments. The microporosity in activated carbons in the literature has been defined as the space between defective sheets of graphene [32]. Figure 2.13, for instance, shows high-resolution TEM images for activated biochars obtained from MCC-50-DAP in a typical setup and in the POX reactor. Because the sheets are of different dimensions and shapes and are in such close proximity to one-another, no conclusive remarks about the pore size can be made from the TEM images. However, these

micrographs do provide good detail for modeling efforts of the microporosity and help us to visualize the intricacy of structure in activated carbons.

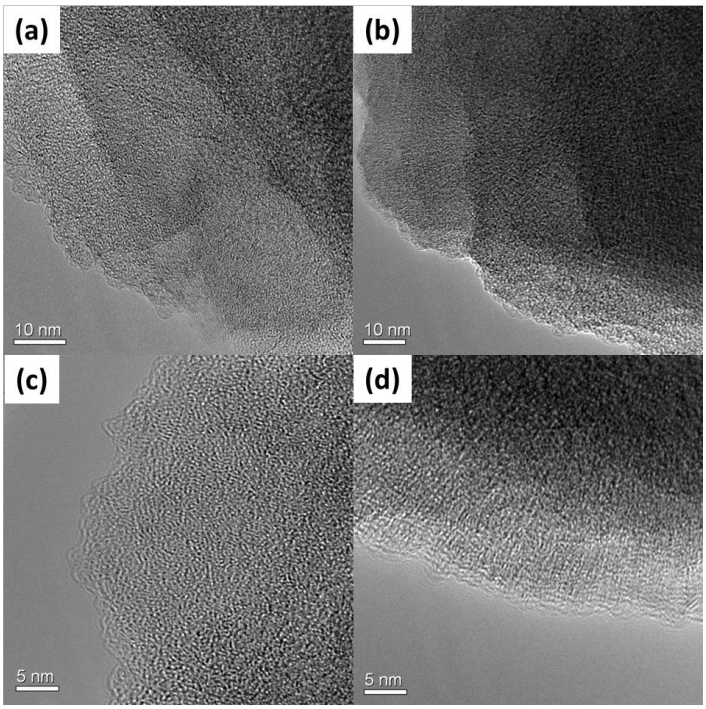

Figure 2.13: High-resolution TEM micrographs of (a) AC-50-N_2, (b) AC-50-POX, (c) AC-50-N_2 and (d) AC-50-POX

Raman spectroscopy

Raman spectra of carbonaceous materials contain two major bands, the D band occurring at ~1350 cm^{-1} and the G band around 1590 cm^{-1}. The D band is associated with the defects within the carbon material whereas the G band is identified with graphitic carbons. Additionally, other bands such as D″ at ~ 1500 cm^{-1} and the I band around 1180-1290 $cm^{-1}$are also present. The I band is observed in polyenes and is often associated with defects within the graphitic lattice and sp^2-sp^3 bonds [33]. The D″ band reveals its presence in amorphous carbon materials [34]. They together give clues about the structure of the material. An intensity ratio of the D and G bands is suggestive of the degree of graphitization. Samples with a higher value of I(D)/I(G) are postulated to have a lower degree of graphitization.

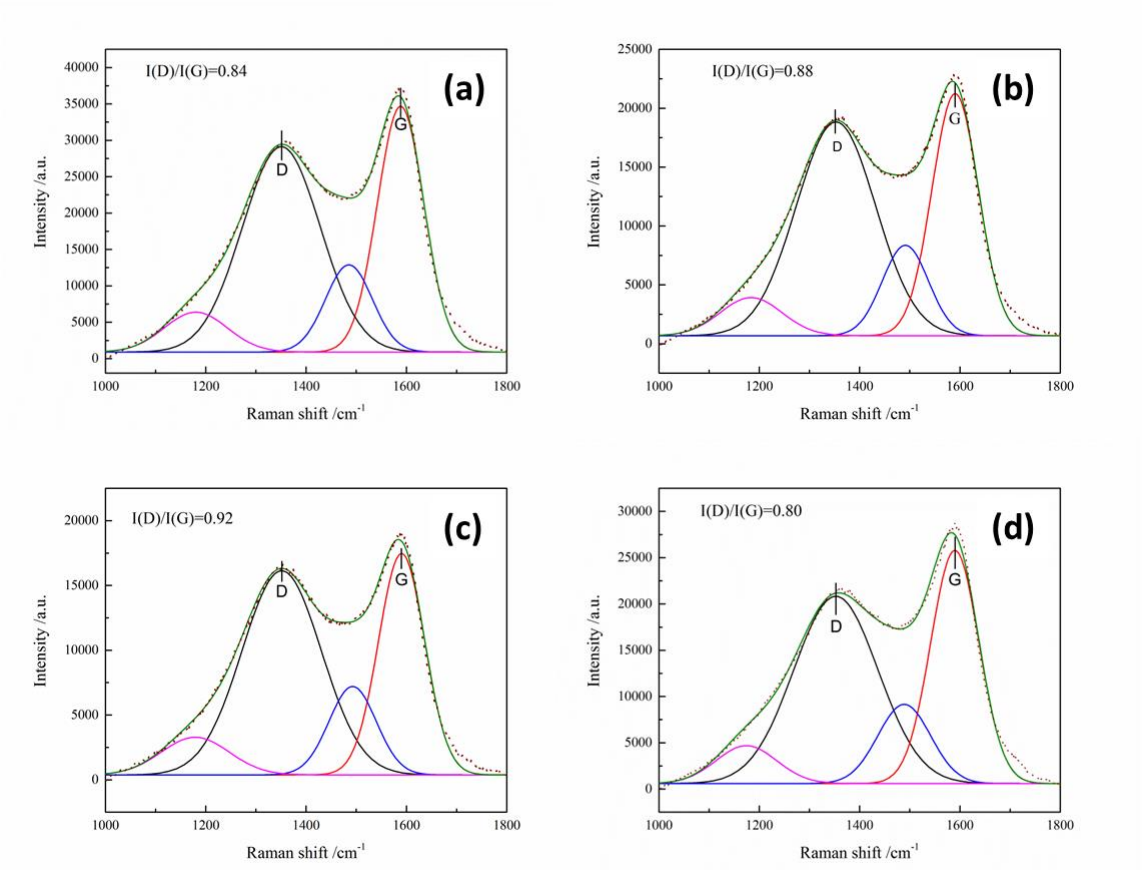

Figure 2.14: Deconvoluted Raman spectra of (a) AC-50-N_2, (b) AC-50-POX, (c) AC-75-POX and (d) AC-100-POX showing the D, G bands and the values of I(D)/I(G)

Due to an overlap of the bands, the obtained Raman spectra were deconvoluted using four Gaussians over a linear background. As evident from Figure 2.14, the samples with higher porosity generally exhibited a higher value of the intensity ratio I(D)/I(G). Since activated carbons are assemblies of defective graphene sheets, one may expect diminished graphitization with enhanced activation. The value of the intensity ratios increases from 0.84 for AC-50-N_2 to 0.88 for AC-50-POX and up to 0.92 for AC-75-POX seemingly correlating a decreasing degree of graphitization to increased porosity. The trend concurs well with purely microporous samples (AC-50-N_2, AC-50-POX, AC-75-POX) but does not extrapolate to AC-100-POX (with incipient mesoporosity) where the intensity ratio falls despite having the maximum total pore volume

among the samples synthesized. Shimodaira and Masui [35] in their comprehensive study of the Raman spectra of activated carbons found a similar pattern in the process of chemical activation with KOH, where the intensity ratio first increased and then decreased with increasing BET surface areas. Although activated carbons are arrays of defective graphene sheets, a description of the porosity requires an elucidation of the space enclosed between them. The intensity ratio may be suggestive of the degree of graphitization but it does not necessarily substantiate the enclosed porosity, thus no general trends are likely to be consistent between the BET surface area or total pore volume and the degree of graphitization. This suggests that the mode of activation and the concentration of the chemical activant contribute to the formation of unique microstructures.

Conclusion

DAP helps to facilitate low-temperature pyrolysis of cellulose by the action of phosphoric acid which helps in depolymerization and the breakdown of the glycosidic linkages of cellulose. It was possible to prepare activated carbons in typical flow-through setups of N_2 as well as under environments containing ambient air. The maximum mass ratio of DAP to cellulose used in this study was (1:1) corresponding to a strength of activation of 100 as defined earlier. Although this ratio may appear to be large at face-value, it has to be appreciated that the phosphoric acid generated from it is recoverable and can be used again for activation. The ratio of 1:1 is modest given that in the literature, ratios up to 2:1 of activant to raw material are often used. Higher ratios generally translate to higher porosities for chemical activation. Keeping in mind the needs of resource-constrained rural settings, the idea was to use an activant which would be more likely

to be accessible and safer to store. Thus an attempt was made to use DAP, a commercially available fertilizer. A detailed evaluation of the trade-offs and the economics of production will be very context specific and would require more detailed studies and on the ground data. The activated biochar samples synthesized were predominantly microporous with high surface areas and pore volume, which increased with the strength of activation. AC-50-POX and AC-75-POX were entirely microporous exhibiting IUPAC Type-1 isotherms. When the strength of activation was increased to 100 under POX conditions, the shape of the isotherm indicated the onset of mesoporosity at an expense of decreased micropore volume. Heteroatoms like nitrogen, oxygen and phosphorus were incorporated into the carbonaceous matrix due to the reaction of ammonia and phosphoric acid with cellulose. P_2O_5 appears to act as a template for the porosity, the washing away of which provides access to the micropores. Finally, SEM and TEM micrographs conveyed that the macrostructure and microstructure of the samples prepared under N_2 and POX environments were similar. Activated biochar preparation on a small scale, batch type system in the presence of ambient air without the need of a sophisticated flow-through reactor and organic solvents was demonstrated. The ability to produce high-quality activated biochar in relatively simple reactor systems may address various needs in resource-constrained settings. One such application is explored in depth in chapter 4.

Acknowledgments: The contribution of Dr. Xiaoyin Chen for providing training on the characterization tools and Dr. Chang Yup Seo with electron microscopy experiments is gratefully acknowledged. I would also like to thank Yasser Shalabi for helping me out with some of the experiments during the course of this research.

References

[1] F.-X. Collard and J. Blin, "A review on pyrolysis of biomass constituents: Mechanisms and composition of the products obtained from the conversion of cellulose, hemicelluloses and lignin," *Renew. Sustain. Energy Rev.*, vol. 38, pp. 594–608, 2014.

[2] M. J. Antal and M. Grønli, "The Art, Science, and Technology of Charcoal Production," *Ind. Eng. Chem. Res.*, vol. 42, no. 8, pp. 1619–1640, Apr. 2003.

[3] A. E. Downie, L. Van Zwieten, R. J. Smernik, S. Morris, and P. R. Munroe, "Terra Preta Australis: Reassessing the carbon storage capacity of temperate soils," *Agric. Ecosyst. Environ.*, vol. 140, no. 1, pp. 137–147, 2011.

[4] T. M. Huggins, A. Haeger, J. C. Biffinger, and Z. J. Ren, "Granular biochar compared with activated carbon for wastewater treatment and resource recovery," *Water Res.*, vol. 94, pp. 225–232, 2016.

[5] F. Rodríguez-Reinoso, M. Molina-Sabio, and M. T. González, "The use of steam and CO_2 as activating agents in the preparation of activated carbons," *Carbon N. Y.*, vol. 33, no. 1, pp. 15–23, 1995.

[6] F. Caturla, M. Molina-Sabio, and F. Rodríguez-Reinoso, "Preparation of activated carbon by chemical activation with $ZnCl_2$," *Carbon N. Y.*, vol. 29, no. 7, pp. 999–1007, 1991.

[7] M. Molina-Sabio, C. Almansa, and F. Rodríguez-Reinoso, "Phosphoric acid activated carbon discs for methane adsorption," *Carbon N. Y.*, vol. 41, no. 11, pp. 2113–2119, 2003.

[8] S.H. Yoon, S. Lim, Y. Song, Y. Ota, W. Qiao, A. Tanaka, and I. Mochida, "KOH activation of carbon nanofibers," *Carbon N. Y.*, vol. 42, no. 8, pp. 1723–1729, 2004.

[9] M. Jagtoyen and F. Derbyshire, "Activated carbons from yellow poplar and white oak by H_3PO_4 activation," *Carbon N. Y.*, vol. 36, no. 7, pp. 1085–1097, 1998.

[10] M. Molina-Sabio, F. Rodríguez-Reinoso, F. Caturla, and M. J. Sellés, "Porosity in granular carbons activated with phosphoric acid," *Carbon N. Y.*, vol. 33, no. 8, pp. 1105–1113, 1995.

[11] E. Fitzer, K.H. Geigl, W. Hüttner, and R. Weiss, "Chemical interactions between the carbon fibre surface and epoxy resins," *Carbon N. Y.*, vol. 18, no. 6, pp. 389–393, 1980.

[12] A. Puziy, O. Poddubnaya, A. Martínez-Alonso, F. Suárez-García, and J. M. Tascón, "Synthetic carbons activated with phosphoric acid: I. Surface chemistry and ion binding properties," *Carbon N. Y.*, vol. 40, no. 9, pp. 1493–1505, 2002.

[13] B. Hu, K. Wang, L. Wu, S. Yu, M. Antonietti, and M. Titirici, "Engineering carbon materials from the hydrothermal carbonization process of biomass," *Adv. Mater.*, vol. 22, no. 7, pp. 813–828, 2010.

[14] B. Hu, S.H. Yu, K. Wang, L. Liu, and X.-W. Xu, "Functional carbonaceous materials from hydrothermal carbonization of biomass: an effective chemical process," *Dalt. Trans.*, no. 40, pp. 5414–5423, 2008.

[15] H. Benaddi, T. Bandosz, J. Jagiello, J. Schwarz, J. Rouzaud, D. Legras, and F. Béguin, "Surface functionality and porosity of activated carbons obtained from chemical activation of wood," *Carbon N. Y.*, vol. 38, no. 5, pp. 669–674, 2000.

[16] D. Mohan, Pittman Charles U., and P. H. Steele, "Pyrolysis of Wood/Biomass for Bio-oil: A Critical Review," *Energy & Fuels*, vol. 20, no. 3, pp. 848–889, May 2006.

[17] C. Di Blasi, C. Branca, and A. Galgano, "Effects of Diammonium Phosphate on the Yields and Composition of Products from Wood Pyrolysis," *Ind. Eng. Chem. Res.*, vol. 46, no. 2, pp. 430–438, Jan. 2007.

[18] L. M. Ilharco, A. R. Garcia, J. Lopes da Silva, and L. F. Vieira Ferreira, "Infrared Approach to the Study of Adsorption on Cellulose: Influence of Cellulose Crystallinity on the Adsorption of Benzophenone," *Langmuir*, vol. 13, no. 15, pp. 4126–4132, Jul. 1997.

[19] J. Bouchard, N. Abatzoglou, E. Chornet, and R. P. Overend, "Characterization of depolymerized cellulosic residues," *Wood Sci. Technol.*, vol. 23, no. 4, pp. 343–355, 1989.

[20] A. Kumar and H. M. Jena, "Preparation and characterization of high surface area activated carbon from Fox nut (Euryale ferox) shell by chemical activation with H_3PO_4," *Results Phys.*, vol. 6, pp. 651–658, 2016.

[21] S. M. Yakout and G. Sharaf El-Deen, "Characterization of activated carbon prepared by phosphoric acid activation of olive stones," *Arab. J. Chem.*, vol. 9, no. Supplement 2, pp. S1155–S1162, 2016.

[22] F. X. L. Xamena and A. Zecchina, "FTIR spectroscopy of carbon dioxide adsorbed on sodium- and magnesium-exchanged ETS-10 molecular sieves," *Phys. Chem. Chem. Phys.*, vol. 4, no. 10, pp. 1978–1982, 2002.

[23] M. S. Solum, R. J. Pugmire, M. Jagtoyen, and F. Derbyshire, "Evolution of carbon structure in chemically activated wood," *Carbon N. Y.*, vol. 33, no. 9, pp. 1247–1254, 1995.

[24] M. Jagtoyen, M. Thwaites, J. Stencel, B. McEnaney, and F. Derbyshire, "Adsorbent carbon synthesis from coals by phosphoric acid activation," *Carbon N. Y.*, vol. 30, no. 7, pp. 1089–1096, 1992.

[25] M. Nahata, C. Y. Seo, P. Krishnakumar, and J. Schwank, "New approaches to water purification for resource-constrained settings: Production of activated biochar by chemical activation with diammonium hydrogenphosphate," *Front. Chem. Sci. Eng.*, 2017.

[26] F. Suárez-García, A. Martínez-Alonso, and J. M. D. Tascón, "Activated carbon fibers from Nomex by chemical activation with phosphoric acid," *Carbon N. Y.*, vol. 42, no. 8, pp. 1419–1426, 2004.

[27] C. Branca and C. Di Blasi, "Oxidation characteristics of chars generated from wood impregnated with $(NH_4)_2HPO_4$ and $(NH_4)_2SO_4$," *Thermochim. Acta*, vol. 456, no. 2, pp. 120–127, 2007.

[28] K. S. W. Sing, "Reporting physisorption data for gas/solid systems with special reference to the determination of surface area and porosity (Recommendations 1984)," *Pure Appl. Chem.*, vol. 57, no. 4, pp. 603–619, 1985.

[29] M. Molina-Sabio and F. Rodríguez-Reinoso, "Role of chemical activation in the development of carbon porosity," *Colloids Surfaces A Physicochem. Eng. Asp.*, vol. 241, no. 1, pp. 15–25, 2004.

[30] G. Sethia and A. Sayari, "Activated carbon with optimum pore size distribution for hydrogen storage," *Carbon N. Y.*, vol. 99, pp. 289–294, 2016.

[31] M. Açıkyıldız, A. Gürses, and S. Karaca, "Preparation and characterization of activated carbon from plant wastes with chemical activation," *Microporous Mesoporous Mater.*, vol. 198, pp. 45–49, 2014.

[32] H. Marsh and F. Rodríguez-Reinoso, *Activated carbon*. Elsevier, 2006.

[33] Y. Zhou, S. L. Candelaria, Q. Liu, E. Uchaker, and G. Cao, "Porous carbon with high capacitance and graphitization through controlled addition and removal of sulfur-containing compounds," *Nano Energy*, vol. 12, pp. 567–577, 2015.

[34] T. Jawhari, A. Roid, and J. Casado, "Raman spectroscopic characterization of some commercially available carbon black materials," *Carbon N. Y.*, vol. 33, no. 11, pp. 1561–1565, 1995.

[35] N. Shimodaira and A. Masui, "Raman spectroscopic investigations of activated carbon materials," *J. Appl. Phys.*, vol. 92, no. 2, pp. 902–909, 2002.

Chapter 3

Characterization of surface functional groups and evaluation of the effect of process variables on activated carbon properties

Introduction

The surface chemistry and adsorption behavior of activated carbons are primarily governed by the presence of heteroatoms (O, P, N, etc.) and their bonding state [1]–[4]. Phosphorus and oxygen, for instance, are known to affect the acidic and cation exchange properties of activated carbon [5], [6]. Studies focused on the chemical activation by H_3PO_4 have elucidated upon the nature of phosphorus bonding to carbon [5], [7], [8]. With the use of DAP as an activating agent, additional nitrogenous functionality stem from the interaction of ammonia with the pyrolyzing cellulose. A variety of techniques such as XPS, DRIFTS, elemental analysis, pH drift and zeta potential measurements have been employed in this chapter to characterize these functional groups. These methods often provide complementary data and when synthesized together give us substantial information about the nature of carbon surfaces.

In chapter 2, we demonstrated the synthesis of activated carbon under POX conditions at 450°C (holding time = 1 hr) and focused on the characterization of its porosity to estimate the properties under a fixed set of operating conditions. This chapter explains the rationale behind the selection of the proposed operating condition. Given that the intended application is for resource-

constrained settings, the exploration of various process variables is important to evaluate trade-offs between changed inputs and the resultant biochar quality. This approach further allows us to study the resilience of the synthesized material to a change in operating conditions and helps one envisage the trend in biochar properties as a response to change in process variables due to unforeseen circumstances. Charcoal is a preferred product of biomass pyrolysis at moderate temperatures: 350-500°C [9]. Higher temperatures aid the formation of gaseous products, as suggested by thermodynamic calculations. Despite promising yields estimated from thermodynamic calculations, charcoal production technologies, especially in the African continent are not well optimized. Efficiencies of ~10% have been achieved in the traditional industrial kilns of Rwanda and Madagascar [10]–[12]. If we envision community scale apparatus, proper design is necessary to optimize yields and reduce wasteful consumption of wood. It, therefore, becomes important to study the effect of different process parameters such as heat treatment temperature (HTT), gas environment, heating rate, flow rate of the sweeping gas, holding time, etc. Since porosity is intimately linked to the space between defective sheets of the graphene that constitute char, a simultaneous effect on porosity is examined as a function of the changing parameters. One important aspect this study aims to address is the effect of the gas environment on the yield and physical properties of the obtained carbon. Traditionally, charcoal synthesis is carried out under inert gas conditions, to eliminate undesirable effects of oxygen on diminishing yields due to the formation of CO and CO_2. The method of synthesis with DAP helps to counter the effect of oxygen to a large extent and is explored in detail in this chapter.

Experimental

Materials and methods

Microcrystalline cellulose (MCC) (≥99.9%) and diammonium hydrogenphosphate (DAP) (≥99%) were purchased from Sigma-Aldrich and used as received. Oakwood was obtained and milled to size (<80 mesh). The cellulose, hemicellulose and lignin content were determined using NREL Laboratory Analytical Procedures, based on the findings of several authors summarized by Fengel and Wegener [13]. The hemicellulose content was removed from the biomass by alkaline hydrolysis with KOH and the weight difference was noted. Acid hydrolysis of the remaining material with conc. sulfuric acid leaves only the acid insoluble lignin as residue whose dry mass can be measured. It was assumed that the acid soluble lignin was negligible relative to the acid soluble lignin. The ash content (inorganic constituents in wood) of the finely milled oak dust was estimated by combustion in a Thermogravimetric Analyzer (TGA) by heating it to 700 °C under dry air flow and holding it at that temperature for an hour. The material left on the TGA pan post this procedure gives the ash content of the sample. The natural ash content of the oakwood was found to be 0.2% by weight. This low ash oak dust was used as is for synthesis of the activated carbon.

Slow pyrolysis experiments under POX: The details of the semi-batch POX reactor have been described in chapter 2. A similar heat-treatment procedure was followed: ramping up at 5°C/min to the target temperature and holding for a desired time inside a Barnstead Thermolyne 48000 muffle furnace, where ambient air was freely accessible into the reactor system. Post heat-treatment the material was cooled down to room temperature.

Slow pyrolysis experiments under N_2 flow: The experimental setup used for slow pyrolysis experiments was a Thermolyne 21100 horizontal tube furnace. The construction and configuration have been described in chapter 2. At room temperature, the sample was purged with ultra-high purity nitrogen gas for 2 hours to minimize any residual oxygen in the system, followed by heating the sample at 5°C/min to a specific temperature. After the desired temperature was reached, the sample would be soaked at that temperature for a given time interval depending on the experiment and then cooled down back to room temperature.

Post pyrolysis in either the tube furnace or the POX reactor, the biochar was washed thoroughly (18-20) times with DI water in successive steps to extract the excess activating agent. The activated biochar was then dried at 110°C for 24 hours, cooled down to room temperature and stored in a glass vial. The porosity assessment was carried out by pretreating the material at 300°C to remove any adsorbed moisture. Hence for the sake of consistency, the dry charcoal yields have also been reported by heating the material to 300°C.

Fast pyrolysis experiment: After loading reactors with the appropriate substrate, it was vertically submerged in a Techne SBL-2 fluidized sandbath preheated to a desired temperature. The experiment was carried out for a given holding time. A Techne TC-8D temperature controller maintained the sandbath temperature to within ±2°C of the reaction temperature. After the desired reaction time, the material was allowed to cool down to room temperature. Due to the rapid pyrolysis, a lot of bio-crude was generated and condensed around the walls and within the char material. As a result, the bio-crude was first separated by methanol washing, followed by the regular procedure of successive DI water extractions of the activating agent.

Surface characterization

DRIFTS: The detailed procedure for collection of the DRIFTS spectra has been described in chapter 2. The surface elemental composition and the high-resolution elemental spectra were determined by X-ray Photoelectron Spectroscopy (XPS) on a Kratos Axis Ultra spectrometer. The carbon C 1s peak with a binding energy of 284.5 eV was used as a reference. Data processing was subsequently accomplished using CasaXPS software. The Point of Zero Charge (PZC) was estimated by the pH drift method developed for activated carbons [14]. Deionized water was sparged with N_2 for two hours to minimize dissolved CO_2, following which solutions were prepared in the range of pH 2 to 10. pH adjustment was carried out by using 0.1 M HCl or 0.1 M NaOH. 75 mg of carbon sample was added to 25 mL of a particular solution in a closed centrifuge tube. The mixture was then agitated for 24 hours to ensure equilibration and a plot of the final solution pH against the initial solution pH was constructed. The pH at which the curve crossed the line $pH_{initial} = pH_{final}$ was denoted as the point of zero charge. For estimating the Iso-Electric Point (IEP), the activated carbons were crushed to size < 10 microns using a mortar and pestle. Buffer solutions ranging from pH: 2 to 10 were used for this experiment. Approximately 1 mg of fine carbon powder was added to 1 mL of a buffer solution in a glass vial. The suspension was then dispersed by agitation inside a vortex shaker and 0.1 mL of the suspension was added to a fresh Eppendorf tube. The final volume was made to 1 mL by adding 0.9 mL of the same buffer (10X dilution). It was then tip sonicated 3 times and added to a DTS cell by a syringe, taking care that no air bubbles were formed during the transfer process. The zeta potential was measured on a Malvern zetasizer-nano device. The procedure was repeated for different pH values. The point at which the curve crossed the line of zero zeta potential was denoted as the Isoelectric Point (IEP). Total elemental compositions of the synthesized activated

carbons were carried out by sending the samples to Midwest Microlabs for analysis. C, H, N and P weight fractions were directly measured and the oxygen content was obtained as a difference upon mass balance. The results report the mean and standard deviation from a set of samples synthesized in three different batches. The error associated with each individual measurement was ± 0.3%.

Results and Discussion

Surface functional groups by DRIFTS

An important feature of activated carbon besides its porosity is the presence of surface functional groups, which largely governs adsorption behavior. From the DRIFTS spectra in Figure 3.1, we can observe various functional groups associated with the activated biochar. The DRIFTS spectra of all 3 activated biochar samples exhibit a broad asymmetric peak around (3100-3500) cm^{-1} which can be considered an overlap of various types of O-H (carboxylic, alcoholic) and N-H vibrations. Control experiments in N_2 flow revealed an absence of any detectable nitrogen in the biochar synthesized by pyrolysis of pure cellulose, indicating that N-H functionality present must have been a consequence of the reaction of ammonia (from DAP) with the pyrolyzing cellulose. The evidence of P-O-P and P-O-C vibrations at 1074 and 989 cm^{-1} [15] respectively, indicate that some fraction of phosphorus reacts and becomes a part of the biochar structure primarily as phosphates. This is also observed from XPS studies in the subsequent section. The vibration at 1570 cm^{-1} corresponds to the C=C aromatic stretch from the defective graphene layers. The C=O stretch around 1700-1710 cm^{-1} reveals the presence of carboxylic acids or lactones [16]. The presence of carboxylic acid functional groups can impart Brønsted acidity to

the material. The peak at 1385 cm^{-1} can be due to O-H or nitrates and the ones at 617, 2350 and 3715 cm^{-1} correspond to adsorbed CO_2 on the carbon surface [17].

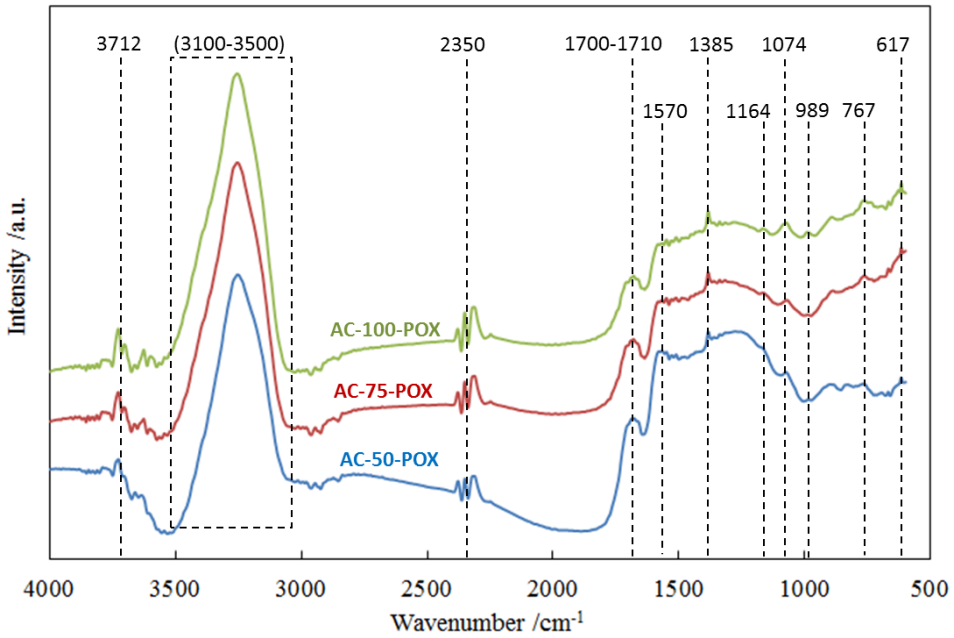

Figure 3.1: DRIFTS absorbance spectra of the activated biochars synthesized under POX conditions at 450°C and 1 hour holding time

A comparison of the activated carbon surfaces synthesized under POX conditions and N_2 flow is shown in Figure 3.2. Very similar structural features and functional groups were observed for both types of samples (N_2 and POX) bringing to light the role of H_3PO_4 in the entire process. During pyrolysis, a film of condensed phosphates and phosphoric acid prevents diffusion of oxygen into the bulk minimizing carbon oxidation and creating a very similar chemistry for activation; the consequence of which is reflected in Figure 3.2. Though similar functional groups were observed, their relative compositions might be different due to differences in reactor configuration and gas environment. Details are further assessed from XPS studies elaborated in the next section.

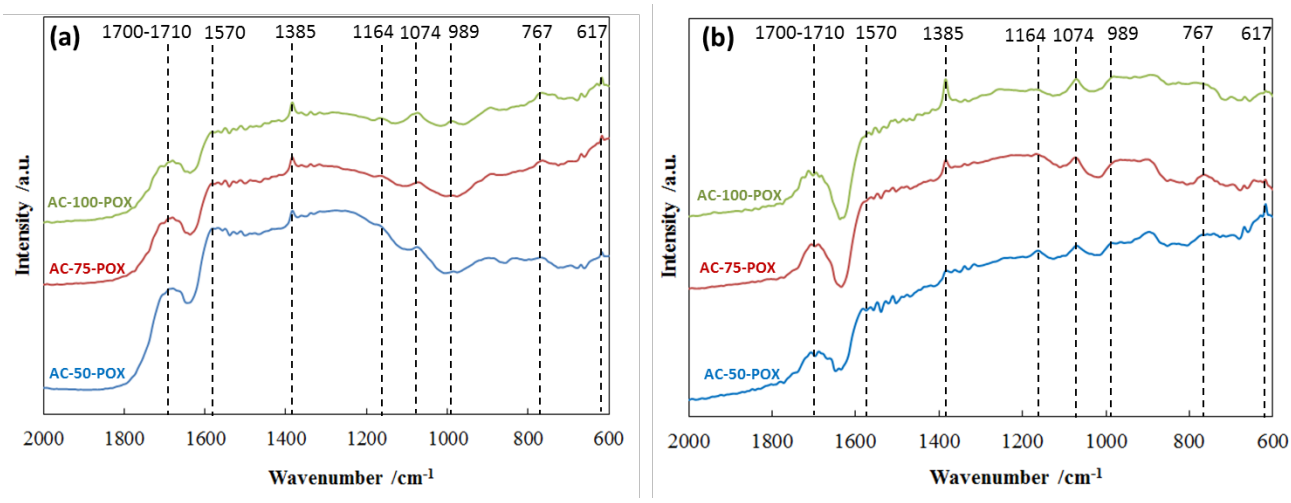

Figure 3.2: Comparison of the DRIFTS absorbance spectra of the activated biochar samples synthesized (HTT = 450°C, t_{hold} = 1 hr) under (a) POX conditions and (b) nitrogen flow

Surface study by X-ray Photoelectron Spectroscopy (XPS)

A survey scan revealed the presence of elements C, O, N, P as quantified in Table 3.1. From the surface elemental analysis by XPS (Table 3.1), one may expect significant functionalization, given the weight percentage of the heteroatoms. Any adsorption phenomenon entails an interaction of solute species with the carbon surface which makes this aspect of characterization vital and is thus addressed by XPS measurements.

Table 3.1: Surface elemental composition (H free) by XPS

Biochar sample	C /(wt. %)	O /(wt. %)	N /(wt. %)	P /(wt. %)
AC-50-N_2	80.87 ± 2.95	11.78 ± 2.66	4.79 ± 0.40	2.57 ± 1.91
AC-50-POX	79.40 ± 1.24	12.00 ± 0.62	7.17 ± 0.21	1.43 ± 0.48
AC-75-POX	78.62 ± 1.65	10.49 ± 1.10	8.74 ± 0.18	2.15 ± 0.70
AC-100-POX	73.69 ± 0.50	13.38 ± 1.66	10.07 ± 1.08	2.86 ± 0.35

From the elemental scan, a clear difference in the N content was observed when the surface composition of samples AC-50-N_2 and AC-50-POX were compared. This can be explained by the nature of the reactor configuration. In a typical flow-through setup as DAP decomposes, it liberates NH_3, some of which gets swept off immediately by an inert gas purge and the time of

contact with the pyrolyzing cellulose is short. However in the POX system, because of the nature of the design, the residence time of contact of NH_3 with the pyrolyzing cellulose is increased. Hence more of it can interact with the decomposing precursor and bond to the matrix. Now when we compare AC's 50, 75 and 100 under POX conditions, we see that the nitrogen content progressively increases with the increasing strength of activation. This is expected because more DAP was initially impregnated into the precursor and more NH_3 can interact with unit mass of cellulose. The carbon contents remain fairly constant except for the sample with activation strength as 100 (AC-100-POX). Simultaneously the mean oxygen content first decreases from 12.00 wt.% to 10.49 wt.% and then increases to 13.38 wt.% with increasing strengths of activation under POX conditions. As more nitrogen gets incorporated in the matrix, probably more carbon atoms are lost as CO and CO_2. A high-resolution XPS scan provided local bonding information about different elements. Fairly complex enclosures were obtained for each element, and the peaks were subsequently deconvoluted. The deconvolution of different elements for AC-50-POX is provided as an illustration in Figure 3.3. A similar procedure was followed for other samples, and their results are compiled in Table 3.2. Peak assignments to specific binding energies were obtained from the National Institute of Standards and Technology (NIST) database and other references in literature. The C 1s peak is majorly deconvoluted to its graphitic component (Peak A) because activated carbons are essentially sheets of defective graphene layers [18]. Peak B may include contributions from alcoholic, C-O-C and C-O-P groups. Puziy *et al*. [8] observed that the phosphate like structure bound to carbon is the most abundant and thermally stable P species in phosphoric acid activated carbons over a wide range of temperature. Peak C could include contributions from carbonyl compounds as well as compounds containing the C≡N group (which is also observed when the N-1s peak is deconvoluted) suggesting that it

may indeed be present. Similarly, at higher binding energies we get contributions from carboxylic acid groups, esters, and π-π* transitions in the aromatic sheet.

Table 3.2: XPS deconvolution results of various samples of activated biochar

Region	Peak	AC-50-N_2 /eV	AC-50-POX /eV	AC-75-POX /eV	AC-100-POX /eV	Assignment
C 1s	A	284.35	284.40	284.42	284.35	Graphite
	B	285.19	285.51	285.20	285.15	ROH , C-O-C, C-O-P
	C	286.84	286.78	286.48	286.38	RCOR´ , -C≡N
	D	288.83	288.36	288.59	288.38	RCOOH, RCOOR´
	E	-	290.12	-	290.43	π-π*
O 1s	A	530.73	530.88	530.78	530.67	=O in carbonyl, carboxyl and phosphates
	B	532.47	532.71	532.48	532.36	-O-
	C	535.95	536.17	536.00	535.69	Chemisorbed O
N 1s	A	398.27	398.25	398.28	398.23	Pyridinic-N
	B	400.21	400.22	400.29	400.05	Pyrrole, Pyridones, -C≡N
	C	-	404.11	403.46	403.40	-N-O #
P 2p	A	-	130.20	129.44	-	Elemental P
	B	132.88	132.91	133.26	133.11	Phosphates and pyrophosphates
	C	-	133.93	-	134.11	Metaphosphates
	D	135.86	136.19	135.55	135.53	P_2O_5

-N-O here has been used to represent oxidized nitrogenous functionalities of pyridines and other forms or nitrates

The O 1s peak when deconvoluted strongly suggests the presence of =O groups, encompassing carbonyl compounds, carboxylic acids (also noted from C 1s excitation) and non-bridging oxygen in the phosphate group [8], [19]. Peak B from the O 1s deconvolution can be assigned to oxygen atoms single-bonded across a variety of functional groups. Peak C, roughly at 536 eV, has been ascribed to the presence of chemisorbed oxygen. The N 1s peak is interesting and brings additional functionalities to the surface than what would have been possible with just phosphoric acid, because of the interaction of ammonia with decomposing cellulose. Pels [20]

after his seminal work on the studies of nitrogen functionalities in coals gave a strong indication that the major nitrogenous constituents are present in pyrrolic and pyridinic groups. Our deconvolution of the N 1s peak suggests similar a similar representation, with the major fraction (Peak B) around 400.2 eV which can be assigned to pyrroles and pyridones or a mixture of both [20], [21]. They are likely to exist as aromatic rings within the defective graphene sheets. However, there is also a possibility of the presence of compounds containing C≡N groups, whose existence was also suggested by C 1s deconvolution. The next largest fragment (Peak A) around 398.2 eV reflects the existence of primarily Pyridinic-N. Peak C, around (403.5-404) eV most likely corresponds to oxidized nitrogenous functionalities (represented here as -N-O), similar to N-oxides of pyridine and other forms or it may be attributed to the presence of nitrates [20]. However since the N-O component was not observed under N_2 flow, but is always observed in the POX reactor, it may imply that its formation is facilitated by the presence of atmospheric oxygen.

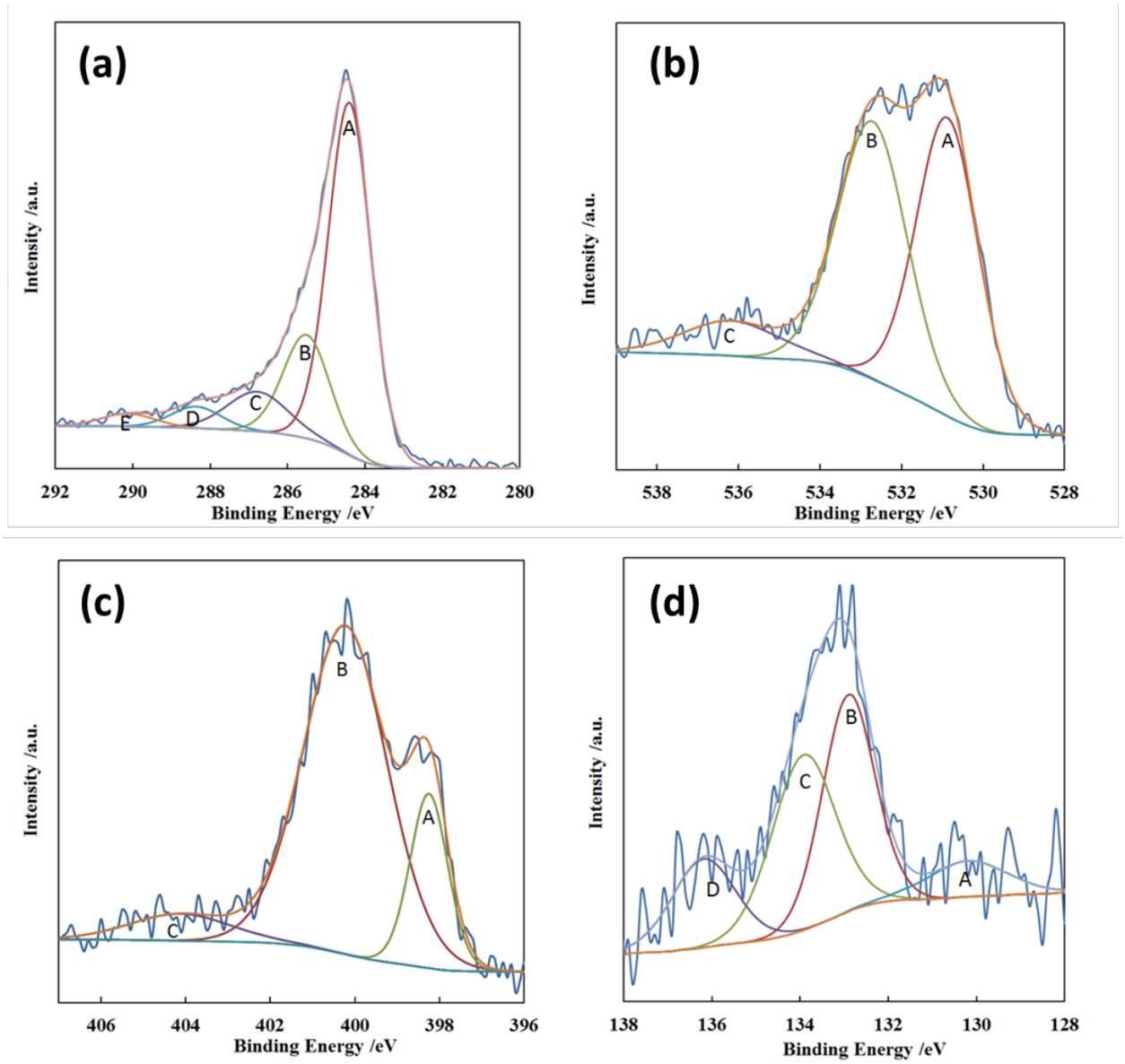

Figure 3.3: High-resolution XPS deconvolution spectra (sample: AC-50-POX) for (a) C 1s, (b) O 1s, (c) N 1s and (d) P 2p excitations

The P 2p spectrum is noisier because its concentration is relatively small (Table 3.1). Its deconvolution, however, provides interesting insights. The deconvolution suggests that the main contribution (Peak B) at a Binding Energy ~ 133 eV regularly observed across all samples is the pentavalent tetra-coordinated phosphorus (PO_4 tetrahedra) in condensed phosphates originating from a mixture of phosphoric and polyphosphoric acids, also observed in Puziy's study on phosphoric acid activation of polymer-based and fruit-stone carbons [8]. Metaphosphates (Peak

C) observed in some cases may arise from metaphosphoric acid which sometimes gets formed when several phosphoric acid units are bonded together in cyclic structures. Peak D, observed around 136 eV suggests the presence of P_2O_5 consistently across all samples tested. Although its contribution is small to the total P, it has important mechanistic implications. For a wide range of H_3PO_4 loading, Molina-Sabio and Reinoso observed that P_2O_5 acts as a template for microporosity generation in cellulosic biomass, the washing away of which eventually creates the porosity [22]. As H_3PO_4 is one of the products of DAP decomposition, one would likely expect that the mechanism of action of P_2O_5 should remain similar in the process of activation. This suggests that even with the use of DAP, P_2O_5 is playing an important role with respect to activation of cellulosic biochar. The presence of a very small Peak A which corresponds to elemental phosphorus [23] is debatable and at the individual's discretion, because as suggested in the Figure 3(d), it may be disregarded as noise. However, its likely presence was observed in two out of the four samples synthesized. Given our heat treatment temperature of 450°C, the physical properties of phosphorus (boiling point of white phosphorus = 280°C, red phosphorus sublimes at 416°C) [8], and that it may not survive the ultra-high vacuum in XPS, [8] phosphorus might exist in very fine pores that hinder evaporation. This explanation is consistent with that of Puziy *et al*. (8).

Total elemental analysis

The elemental analyses for the samples synthesized at 450°C at a holding time of 1 hour are reported in Table. 3.3. The oxygen content is associated with the acidic surface functional groups [24]. It is interesting to observe that there is a slight fall in the oxygen concentration of AC-75-POX relative to AC-50-POX and AC-100-POX. This may imply a reduction in the density of acid sites. A small fraction of the total P reacts and become permanently bound to the carbon

surface. The N concentration was found to increase with increasing DAP loadings of the precursor in (50, 75 and 100 POX) samples. This observation is consistent with the surface elemental analysis we observed from XPS (Table 3.1). XPS cannot measure hydrogen and surface compositions are thus hydrogen free. Since activated carbon is an assembly of layers of defective graphene, the notion of a macro-surface separate from the bulk may not be easily conceivable. Thus, surface compositions should not be significantly different compared to the bulk in activated carbons.

Table 3.3: Total/bulk elemental analysis for the samples synthesized at 450°C and 1 hour holding time

Sample	C /(wt.%)	H /(wt.%)	N /(wt.%)	P /(wt.%)	O /(wt.%)
AC-50-POX	73.36 ± 1.39	2.08 ± 0.34	7.81 ± 0.11	2.72 ± 0.69	14.03 ± 0.79
AC-75-POX	72.31 ± 2.86	2.03 ± 0.19	9.51 ± 0.48	2.75 ± 1.21	13.40 ± 2.15
AC-100-POX	68.45 ± 1.28	2.18 ± 0.12	10.44 ± 0.26	2.88 ± 0.48	16.05 ± 1.06

Note: The oxygen wt. % has been estimated from a difference upon mass balance

Surface charge measurement

Activated carbons are amphoteric in nature and behave corresponding to the pH of the environment they are exposed to. The point of zero charge and the isoelectric points are indicated in Figure 3.4(a,b). By the pH drift method, we get a measure of the total charge. For $pH < pH_{pzc}$, the carbon surface is positively charged and when $pH > pH_{pzc}$ the surface is negatively charged. Zeta potential gives us a measure of charge distribution more at an 'external' surface. From our results, we observe that all the 3 samples: AC-50-POX, AC-75-POX, and AC-100-POX exhibit a point of zero charge close to pH~2.5. The iso-electric point also occurs at a pH ~ 2.5. Based on this observation, we can come up with interesting insights. It appears that such behavior is largely a consequence of the dissociation of Brønsted acid sites. The nitrogen content though imparts Lewis basicity; it does not generate hydroxyl ions in solution and hence cannot significantly affect pH. It is interesting to note that in both forms of measurement, there is a substantial change in the slope of the curve around pH~ (4.0-4.2), which is very close to the pK_a

of Benzoic acid. (pK_a = 4.19). This probably corresponds to the dissociation of either benzoic or other carboxylic acid groups in the material. The presence of carboxylic acid functionality associated to aromatic rings is what we evinced from XPS and DRIFTS measurements. The close coincidence of the point of zero charge and the iso-electric point indicates that charge is homogeneously distributed in the material.

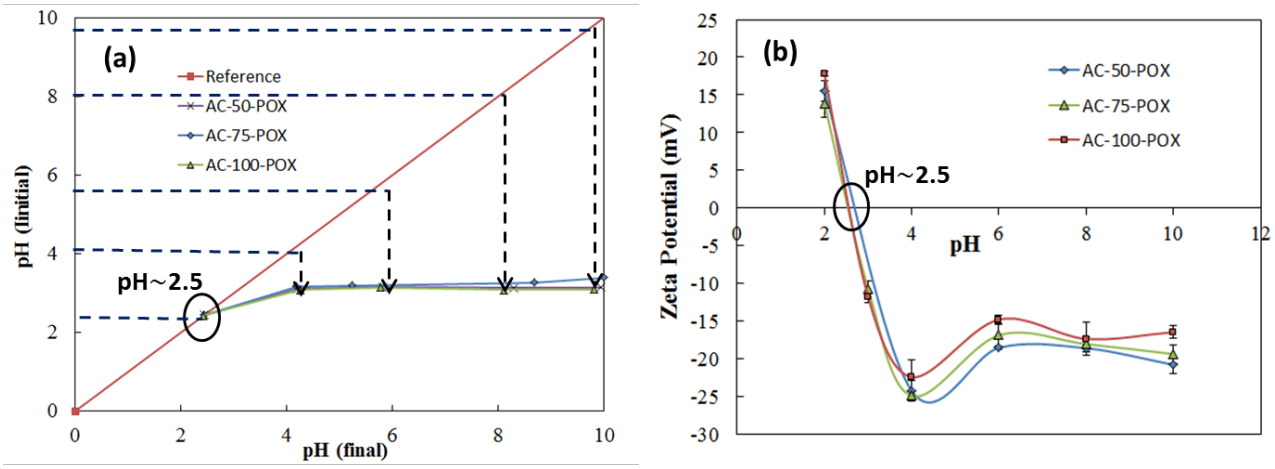

Figure 3.4: Surface charge measurement for activated carbons as a function of pH to calculate the (a) point of zero charge and (b) isoelectric point

Barton *et al*. [25] correlated the oxygen content (an indicator of acidic functional groups) in mmol/g to the point of zero charge for different types of activated carbon. A comparison of these values to the samples we have synthesized has been presented in Table 3.4.

Table 3.4: Comparison of $pH_{(pzc)}$ to the values of different activated carbon samples obtained from Barton *et al*. [25]

Carbon	[O] /(mmol.g^{-1})	pH(PZC)
BPL 900N2	0.61	10.40
AR	1.40	9.16
ECO 13	1.56	7.50
ECO 37	2.47	5.49
OX 25	3.91	4.52
OX 45	4.17	4.24
OX 65	5.99	3.91
OX 85	7.56	3.02
OX 95	10.00	2.50
AC-50-POX (This work)	8.77	~2.50
AC-75-POX (This work)	8.38	~2.50
AC-100-POX (This work)	10.03	~2.50

Effect of process variables

Effect of HTT: Heat treatment temperature (HTT) is the maximum temperature reached during the carbonization process. It is very important as it dictates the volatile matter content, pore volume and pore size distribution of charcoal. Charcoals synthesized below 400°C, without the use of an activating agent have negligible surface area and do not have useful commercial value [26]. They may be used for applications such as cooking fuels. In chapter 2, Figure 2.5 we had observed that the structural differences between the activated biochar at 300°C and 450°C were inappreciable. However, the volatile matter content was significant at 300°C (implying low porosity). Besides, previous work on H_3PO_4 activation suggested that the pore structure is well-developed post 400°C. This work thus examined the effect of temperature on porosity and yield at two temperatures 400°C and 450°C.

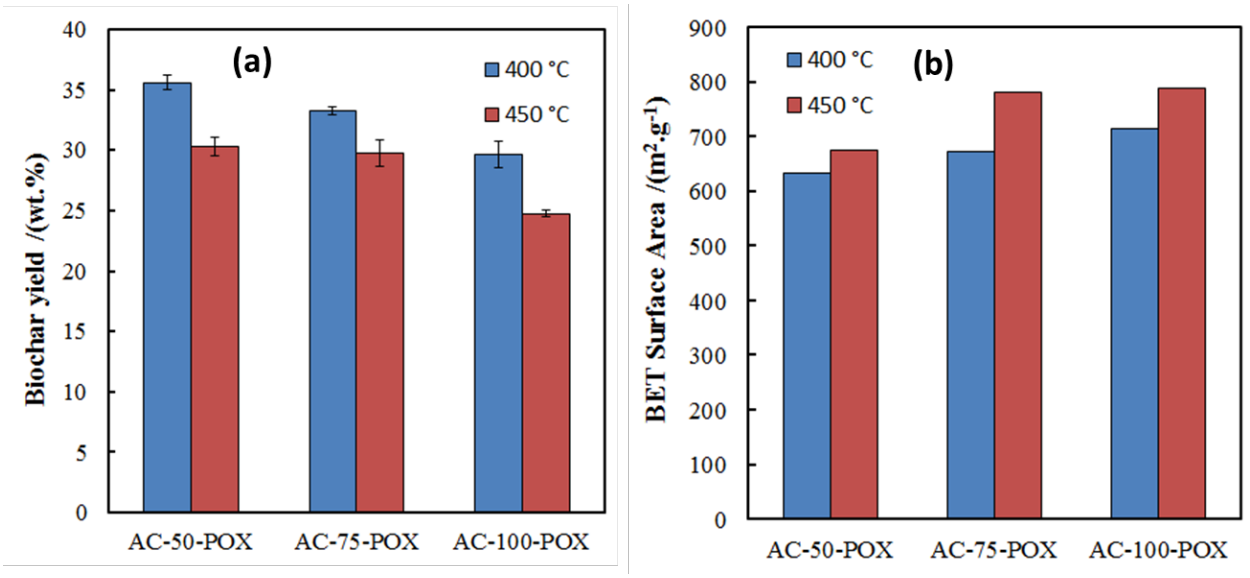

Figure 3.5: Effect of HTT on the (a) yield and (b) BET surface area of the synthesized activated biochars

To understand the effect of heat treatment temperature, it is useful to compare the BET surface area and yield as shown in Figure 3.5. Biochar is largely a product of solid phase carbonization reactions leading to the formation of primary char. The role of secondary vapor phase reactions

has been well established [27]. The pyrolyzing tars decompose and react on the surface of the primary char to yield more char, termed as 'secondary char' in the literature. The secondary char is more or less indistinguishable from primary char, has similar properties and gets intermingled with the bulk material. Total char yields were found to decrease with increasing temperature. Due to an increase in temperature, the higher molecular weight volatiles are lost, and the carbon has a more accessible pore structure. The loss in biochar yield was ~(3-6)wt.% , and the corresponding gain in BET surface area and micropore volume were ~(5-14)% and (8-15)% respectively due to the 50°C temperature differential. The peak temperature also has a strong influence on the surface functionalities and hence the adsorption properties. As oxygen-rich volatiles are lost, the biochar gets enriched in the percentage of fixed carbon with increasing heat treatment temperature.

Effect of gas environment: Carbonization experiments have been traditionally carried out under inert gas flows such as (N_2, Ar, He, etc.) to avoid undesirable loss of useful carbon by oxidation to CO and CO_2 in ambient air. Yields of the activated biochar synthesized at 450°C under nitrogen flow, (pre-and post-washing) are shown in Figure 3.6. The yield of the unwashed samples (containing the activating agent) tends to linearly increase with increasing mass loading of the activating agent. The unwashed samples include the weight of the char and the impregnated activating agent, which exists primarily as P_2O_5. The actual yield of the biochar post extraction of the activating agent with water is shown in Figure 3.6(b). With greater mass loading of the activant, a greater fraction of cellulose seems to react with the activating agent, creating higher porosity but lower yields. The gas environment (inert, air) also affects the relative proportions of various functional groups, which was discussed in the DRIFTS and XPS sections, explained earlier.

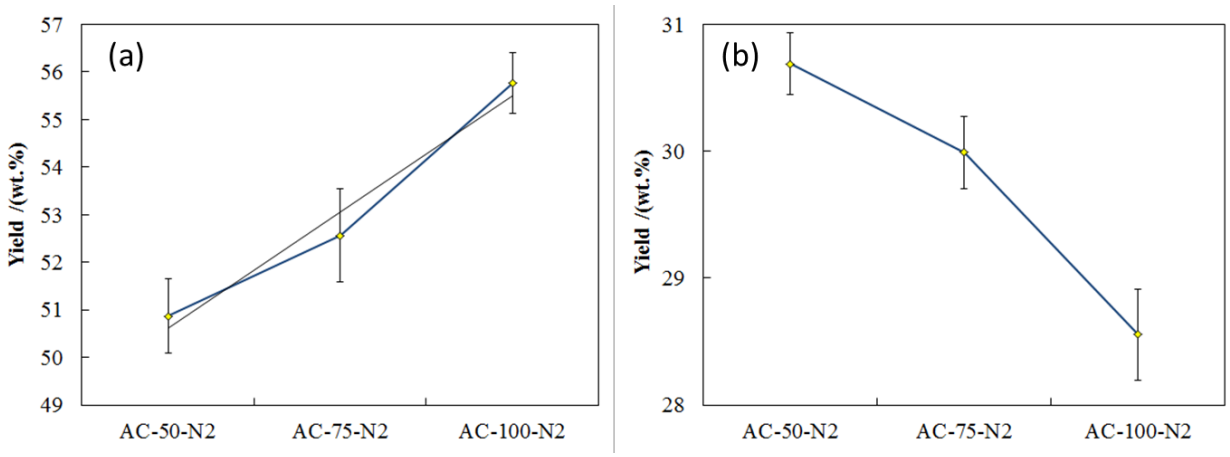

Figure 3.6: Plots showing the yield of (a) unwashed and (b) washed activated biochar synthesized under nitrogen flow of 100 mL/min

The results in Figure 3.6 correspond to synthesis conditions under a nitrogen flow rate of 100 mL/min. Similar experiments were carried out under N_2 flow rates of 50 mL/min and 10 mL/min. We observed that for a fixed temperature (450°C) and holding time (t_{hold}=1 hour), the mean biochar yield increased with a decrease in flow rate of the sweeping N_2 gas, as illustrated in Fig. 3.7. Standard deviation is reported based on triplicate measurements. The increased total char yield could be explained by the hypothesis that slower gas sweeping that allows more time for the volatiles to decompose on the surface of the primary char to generate secondary char.

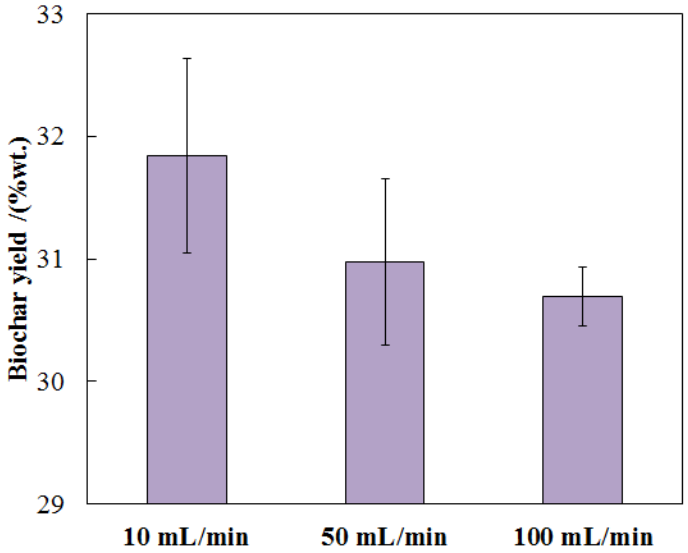

Figure 3.7: Effect of flow rate of the sweeping nitrogen gas on the yield of AC-50-N_2 at 450°C, t_{hold}=1 hr

Cellulose without any additive would completely burn away at (450-500) °C in air. The value of the activating agent DAP lies in the fact that besides activation, the film of condensed phosphates restricts the access of molecular oxygen into the system, preventing carbon loss. The design of the POX system permits a configuration where volatiles can react with primary char to generate more char (higher total char yields). Also, smaller specific volumes in such environments favorably enhance the rate of reaction due to increased fugacity of the volatiles. Thus the observed yields under POX conditions (Figure 3.8) are comparable in magnitude and trend to values under N_2 flow. The associated effect of the gas environment on the porosity of the carbons was previously elucidated in chapter 2.

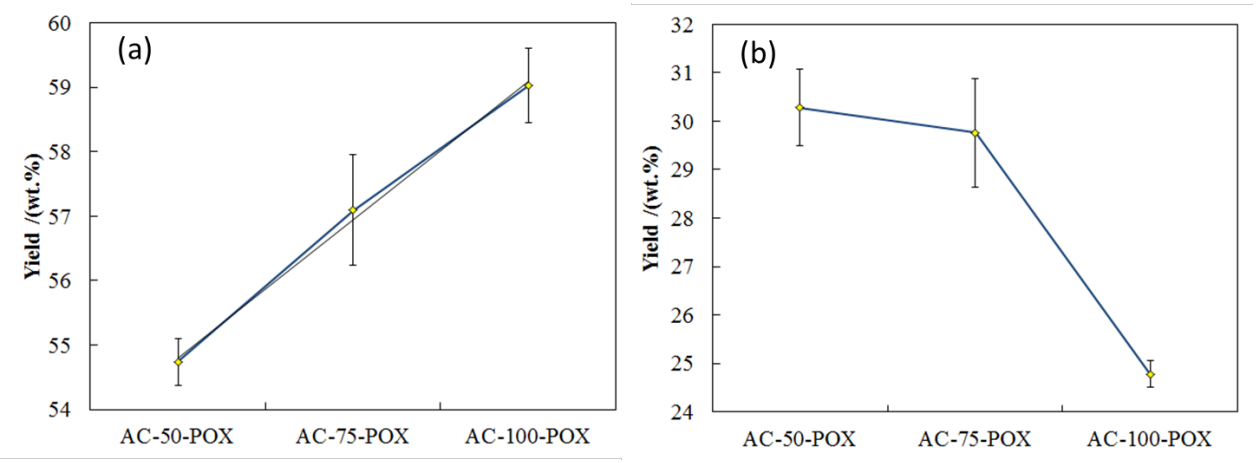

Figure 3.8: Plots showing the yield of (a) unwashed and (b) washed activated biochar synthesized under POX conditions at 450°C and t_{hold} = 1 hr

The effect of holding time on biochar porosity is illustrated by Figure 3.9. The sample synthesized with a one hour soak time is shown in solid color whereas the sample synthesized with a soak time of 5 hours is illustrated by dotted lines. Roughly a (5-10) % increase in micropore volume and BET surface area were observed with a corresponding decrease in biochar yield of ~ (3-5) wt.% for the samples held at 5 hours relative to the ones held for an hour at 450°C. At higher holding times, some of the unstable higher molecular weight aromatics

volatilize resulting in a more accessible pore space associated with a corresponding decrease in biochar yield. Since the improvement in surface area is meager compared to a 5X increase in holding time, the trade-off was regarded as unsuitable, especially when considering synthesis in low resource settings, where energy is a premium. Thus most of the characterization and application study in this dissertation has been done for samples synthesized at 450°C under a holding time of one hour.

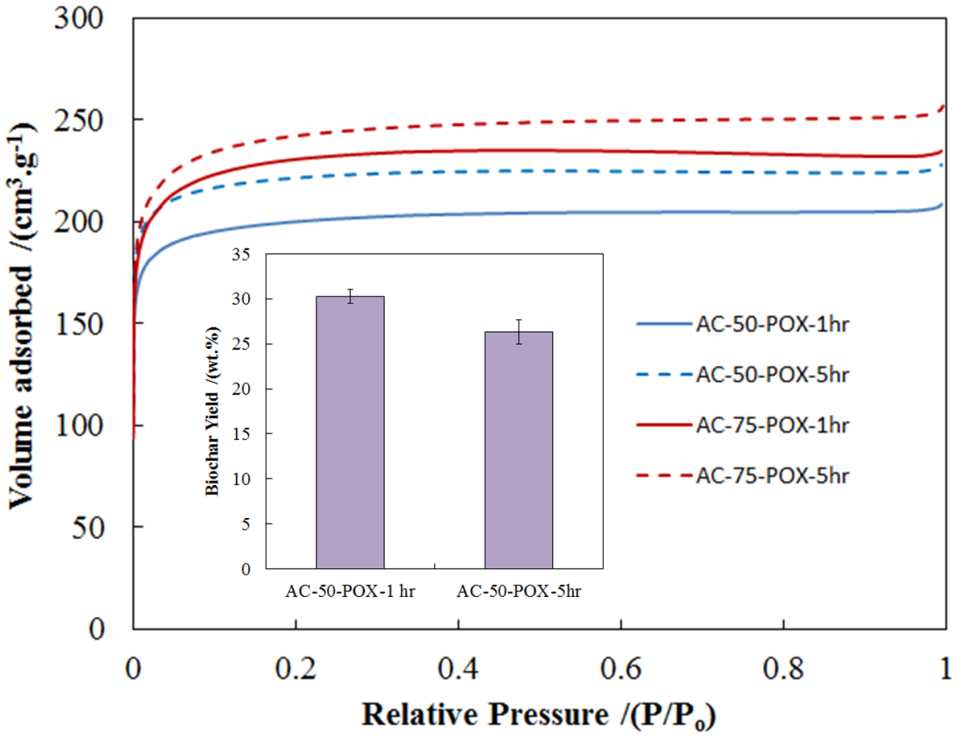

Figure 3.9: Comparison of nitrogen physisorption isotherms at 77 K for activated biochars synthesized at 450°C under holding times of 1 hour and 5 hours. Included as an inset is the associated biochar yield data for AC-50-POX

Reactor configuration: The reactor proposed in this study was constructed to have a 1/8 inch opening in a 3/4 inch internal diameter enclosure. This opening has an important role to play in ensuring sufficient vapor residence time for good char yields, access of air into the reactor and exit of oxidized volatiles by a natural pressure driven flow. If the reactors were to be operated in a strictly batch mode with a completely closed cap; the quality of biochar would expectedly

deteriorate. This, in fact, was experimentally observed as illustrated in Figure 3.10. A closed batch system does not allow volatiles to escape and they are recondensed back into the reactor, forming a tarry soup of charcoal. Due to the recondensation, an additional step of methanol washing is necessitated to separate the biocrude from the char. This is followed by the regular procedure of water washing to extract the activating agent. The micropore volumes and BET surface areas fall by ~43 and 33%, respectively, in the completely closed batch reactor mode, also requiring an additional step of tar separation. A completely closed batch system is thus not recommended as an operation mode.

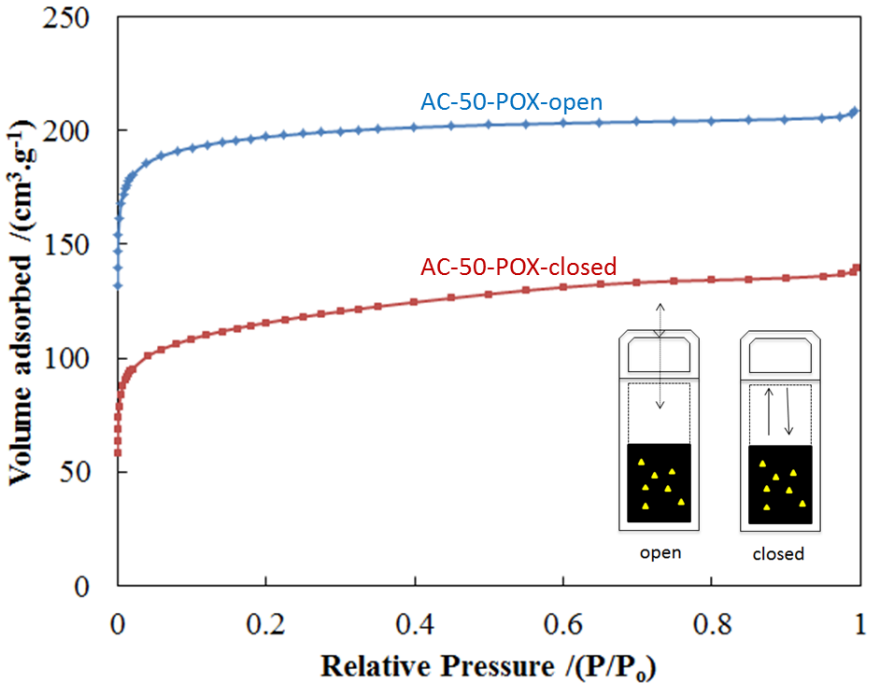

Figure 3.10: Comparison of nitrogen physisorption isotherms at 77 K for AC-50-POX synthesized under open and closed reactor configurations

Heating rate: Previous work dedicated to the study of charcoals as their primary product have examined the impact of heating rate on yields and elemental compositions, neglecting the effect on biochar porosity. Slow pyrolysis using a ramp of (2-10)°C/min has been known to affect reaction pathways that favor charcoal formation. This is because lower heating rates allow

enough time for the vapors to react and equilibrate with primary char to generate more char. The char yields, however, reach an asymptotic value at low heating rates [28].

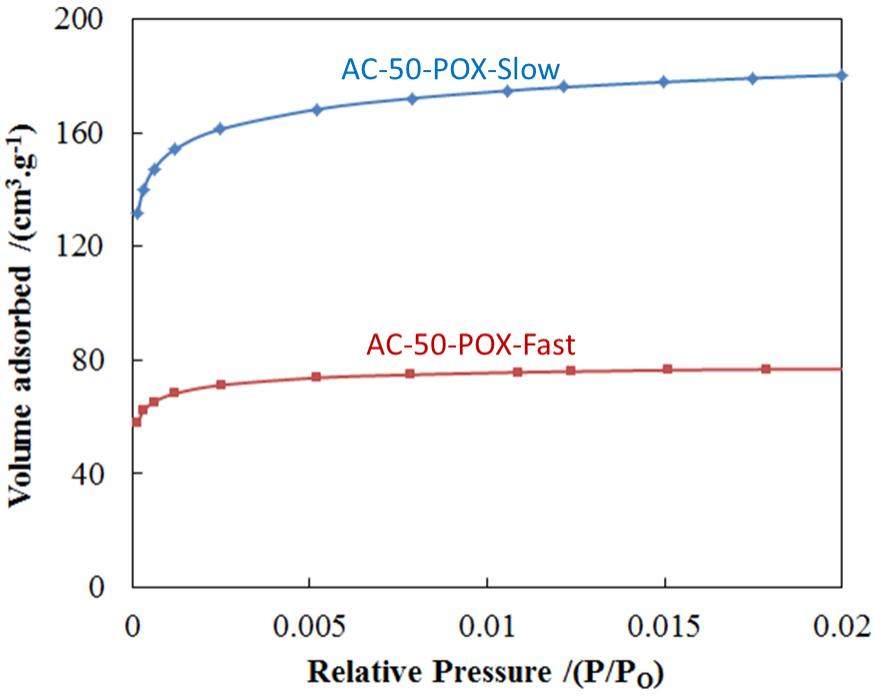

Figure 3.11: Comparison of nitrogen physisorption isotherms at 77 K for AC-50-POX synthesized under slow and fast pyrolysis conditions at 450°C

During fast pyrolysis, due to rapid breakdown of the cellulosic structure, different pathways are favored which accelerate the formation of levoglucosan, (the precursor to tars). Control experiments revealed that that thermal equilibrium was established fairly rapidly (~ 5 minutes) after the reactor was immersed in the hot sandbath at 450°C. We observed that a large fraction of the volatiles had condensed around the reactor to form biocrude, necessitating an additional step of methanol washing prior to DI water extraction of the activating agent. This was associated with a fall in porosity as illustrated in Figure 3.11. There is roughly a 60 % reduction in the micropore volume despite an additional step of methanol leaching. Concerning applications in

resource-constrained settings, future efforts can focus on the design of solar furnaces which can reliably and slowly heat the material to the desired temperature.

Applicability to real wood: Upon analysis, oakwood was found to have: (56.8 ± 2.3) % cellulose, (19.6 ± 3.5) % lignin and (23.6 ± 1.3) % hemicellulose. The compositional data are comparable to the results of oak and other hardwood tress grown in temperate zones [13], [29]. Cellulose being the bulk component largely controls the thermal response of oakwood and the structure of the final activated biochar created via the activation process. Biochar obtained from oakwood without any-pretreatment (control sample) was found to have a BET surface area ~350 m^2/g. We were able to synthesize activated biochar from oakwood using the DAP activation process in the same way as applied to pure cellulose. The N_2 adsorption isotherm for OAK-50-POX in Figure 3.12 is of IUPAC Type 1, conveying that the material is microporous. The pore properties are listed in Table 3.5. The nature of the OAK-50-POX isotherm is similar to that of AC-50-POX, suggesting that cellulose could be a good model compound to systematically track chemistry in such lignocellulosic materials. The cellulosic carbon (AC-50-POX) has higher micropore volume and BET surface area as compared to the carbon synthesized from oakwood (OAK-50-POX). DAP can easily depolymerize cellulose and hemicellulose by breaking down the glycosidic linkages; however, lignin which comprises ~20% of oakwood may be more resilient to its attack. The difference in predicted pore volumes between oakwood and cellulosic activated carbons is speculated to be largely due to the recalcitrance of lignin. The purpose here was just to demonstrate the applicability of the activation process to real biomass and a detailed investigation into modeling is beyond the scope of the present work.

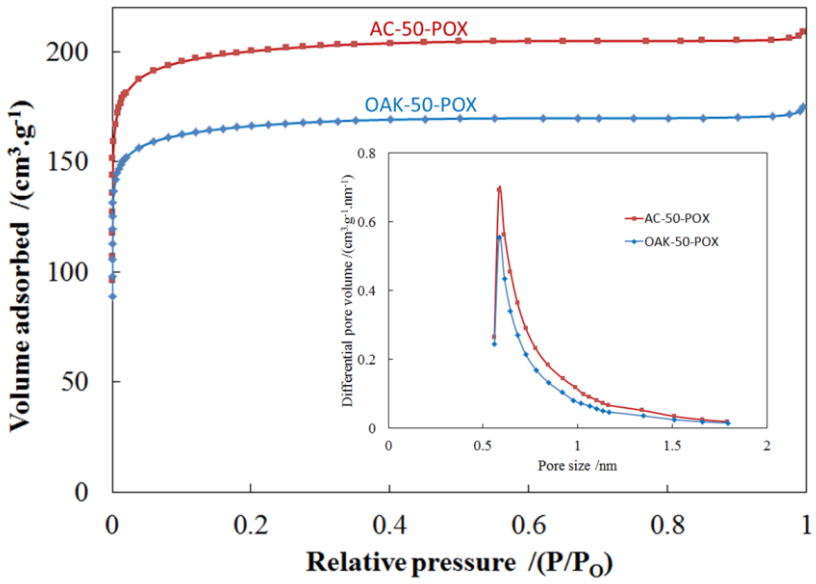

Figure 3.12: (a) Nitrogen adsorption isotherm for AC-50-POX, OAK-50-POX, and their associated pore size distribution

Table 3.5: Textural properties of the synthesized activated biochars

Biochar sample	Micropore volume /($cm^3.g^{-1}$)	BET Surface area /($m^2.g^{-1}$)	Total pore volume /($cm^3.g^{-1}$)
AC-50-POX	0.316	675	0.323
OAK-50-POX	0.261	562	0.271

Practical aspects

A stainless steel (SS-316) metallic reactor with a quartz insert was used for laboratory synthesis in this study to prevent corrosive effects during heat treatment. Modified oil barrels may be used instead in resource-constrained settings, but the cost of a glass interior would make it quite expensive. Ceramic reactors fabricated from clay or silica-based modified crucibles may be possible alternatives. Substantial energy is consumed during the drying step which can quite easily be substituted by solar thermal energy. Temperatures of ~80°C are easily achievable with a properly designed solar cooker vessel. However higher temperatures of (400-450)°C are required for pyrolysis, which poses a greater challenge. Crude solar concentrators constructed from scrap metal have been successful in achieving roughly 200°C but better designs have

achieved temperatures of ~450°C. Kaushika and Reddy [30] for instance demonstrated the design of a low-cost solar concentrator developed using the Aluminum frame of a satellite communication deep dish fitted with silvered polymer reflectors. The total cost associated with this device including the tracking system turned out to be ($120-140/m^2). This concentrator was able to achieve a stagnation temperature of (433-469)°C at insolation values of (940-980) W/m^2 in New Delhi, India. Admittedly the system performance would greatly depend upon the reliability of solar insolation at the particular location; however the possibility exists, if heating rates can be controlled. Alternatively, some of these limitations posed by solar can possibly be overcome by the design of well insulated wood fired stoves for heat up. During our site visits in Gabon for data collection and hands-on demonstrations, Prof. Joseph Trumpey (from the School of Arts & Design at the University of Michigan) and his cohort of undergraduate students built several cookstoves from locally available materials in Lambaréné. Students from USTM at Franceville built an Aluminum smelter on-site at Lambaréné, capable of reaching temperature of ~ 650°C (Figure 3.15). These furnaces can be modified and redesigned as a scaled-up partial oxidation reactor for activated biochar synthesis.

Figure 3.13 (a) A completed cookstove constructed on-site using locally available materials under demonstration (b) An aluminum smelter with an air-flow duct constructed on-site at Lambaréné

The reactor for current laboratory studies was roughly a 9 mL enclosure with reasonably uniform properties across the volume. However upon scale up, mass transfer limitations are expected to become quite important. One can imagine difficulty with the distribution of air flow and escape of oxidized volatiles upon scale-up. A configuration akin to Figure 3.13(b) with passive air-flow can be envisioned for a larger scaled-up reactor. The flow rate of air should be just enough to maintain minimal O_2 partial pressure which can provide benefits of increased porosity without significantly compromising the biochar yield. Besides, heat transfer with solar concentrators would get increasingly difficult with increasing size of the POX reactor. The question basically boils down to what would be the right scale (family scale, community scale for instance) for such an operation? Focused scale-up studies need to be carried out to answer these questions reliably in the context of the given scenarios. One advantage in our favor is that DI water used in the lab ought to find a convenient replacement in rain water collected in clean storage tanks for extracting out the activating agent. Due diligence to heat and mass transfer studies with temperature and heating rate control can make activated carbon synthesis possible in larger reactors in such settings.

Conclusions

The interaction of H_3PO_4 and NH_3 with cellulose imparts rich functionality to the resultant activated carbon as identified by DRIFTS and XPS. Phosphorus exists mainly as phosphates and nitrogen exists in heterocyclic rings (pyrrolic, pyridinic form) associated with the defective graphene layers. About 2-3 wt. % of the phosphorus was bound to the carbonaceous matrix; the remainder is largely recoverable as phosphoric acid in the water washing step (by mass balance).

The functional groups largely govern the adsorption behavior. The presence of carboxylic acid functional groups imparts Brønsted acidity to the activated biochar. Carbon materials being amphoteric in nature, the acidic or basic behavior is dependent on the environment condition (pH). The point of zero charge and the isoelectric point were found to be at pH~2.5, which indicated a homogeneous distribution of charges. The porosity of the activated carbons was tunable and it dependent upon a number of factors, the most important being the final heat treatment temperature and the DAP loading. Total pore volumes developed almost linearly with an increase in concentration of the activating agent. Temperature and holding time bring about a trade-off in total biochar yields and the pore volume. The synthesis conditions can be optimized depending upon a particular application and context. Slow pyrolysis facilitated higher biochar yields and was observed to be favorable for the development of porosity. Cellulose was useful as a model compound to study the activation process and systematically track pyrolysis chemistry.

References

[1] L. Caly and L.R. Radovic, "Interfacial Chemistry and electrochemistry of carbon surfaces," *Chem. Phys. Carbon*, vol. 24, pp. 213–310, 1994.

[2] B. R. Puri and R. C. Bansal, "Studies in surface chemistry of carbon blacks. Part I. High temperature evacuations," *Carbon N. Y.*, vol. 1, no. 4, pp. 451–455, 1964.

[3] H. P. Boehm, "Some aspects of the surface chemistry of carbon blacks and other carbons," *Carbon N. Y.*, vol. 32, no. 5, pp. 759–769, 1994.

[4] H. P. Boehm, D. D. Eley, H. Pines, and P. C. Weisz "Chemical Identification of Surface Groups,", Eds. Academic Press, vol. 16, pp. 179–274,1966

[5] A. M. Puziy, O. I. Poddubnaya, A. Martínez-Alonso, F. Suárez-García, and J. M. D. Tascón, "Surface chemistry of phosphorus-containing carbons of lignocellulosic origin," *Carbon N. Y.*, vol. 43, no. 14, pp. 2857–2868, 2005.

[6] A. M. Puziy, O. I. Poddubnaya, A. Martínez-Alonso, A. Castro-Muñiz, F. Suárez-García, and J. M. D. Tascón, "Oxygen and phosphorus enriched carbons from lignocellulosic material," *Carbon N. Y.*, vol. 45, no. 10, pp. 1941–1950, 2007.

[7] M. Jagtoyen and F. Derbyshire, "Activated carbons from yellow poplar and white oak by H_3PO_4 activation," *Carbon N. Y.*, vol. 36, no. 7, pp. 1085–1097, 1998.

[8] A. M. Puziy, O. I. Poddubnaya, R. P. Socha, J. Gurgul, and M. Wisniewski, "XPS and NMR studies of phosphoric acid activated carbons," *Carbon N. Y.*, vol. 46, no. 15, pp. 2113–2123, 2008.

[9] Antal Michael Jerry, S. G. Allen, X. Dai, B. Shimizu, M. S. Tam, and M. Grønli, "Attainment of the Theoretical Yield of Carbon from Biomass," *Ind. Eng. Chem. Res.*, vol. 39, no. 11, pp. 4024–4031, Nov. 2000.

[10] G. Foley, *Charcoal making in developing countries*, no. 5. Earthscan/James & James, 1986.

[11] J.-P. Lacaux, D. Brocard, C. Lacaux, R. Delmas, A. Brou, V. Yoboué, and M. Koffi, "Traditional charcoal making: an important source of atmospheric pollution in the African Tropics," *Atmos. Res.*, vol. 35, no. 1, pp. 71–76, 1994.

[12] D. M. Pennise, K. R. Smith, J. P. Kithinji, M. E. Rezende, T. J. Raad, J. Zhang, and C. Fan, "Emissions of greenhouse gases and other airborne pollutants from charcoal making in Kenya and Brazil," *J. Geophys. Res. Atmos.*, vol. 106, no. D20, pp. 24143–24155, Oct. 2001.

[13] D. Fengel and G. Wegener, "Wood: chemistry, ultrastructure, reactions," *Walter de Gruyter*, vol. 613, pp. 1960–1982, 1984.

[14] Y. Yang, Y. Chun, G. Sheng, and M. Huang, "pH-Dependence of Pesticide Adsorption by Wheat-Residue-Derived Black Carbon," *Langmuir*, vol. 20, no. 16, pp. 6736–6741, Aug. 2004.

[15] F. Suárez-García, A. Martínez-Alonso, and J. M. D. Tascón, "Activated carbon fibers from Nomex by chemical activation with phosphoric acid," *Carbon N. Y.*, vol. 42, no. 8, pp. 1419–1426, 2004.

[16] M. S. Solum, R. J. Pugmire, M. Jagtoyen, and F. Derbyshire, "Evolution of carbon structure in chemically activated wood," *Carbon N. Y.*, vol. 33, no. 9, pp. 1247–1254, 1995.

[17] F. X. L. Xamena and A. Zecchina, "FTIR spectroscopy of carbon dioxide adsorbed on sodium and magnesium-exchanged ETS-10 molecular sieves," *Phys. Chem. Chem. Phys.*, vol. 4, no. 10, pp. 1978–1982, 2002.

[18] K. Oshida, K. Kogiso, K. Matsubayashi, K. Takeuchi, S. Kobayashi, M. Endo, M. S. Dresselhaus, and G. Dresselhaus, "Analysis of pore structure of activated carbon fibers using high resolution transmission electron microscopy and image processing," *J. Mater. Res.*, vol. 10, no. 10, pp. 2507–2517, 1995.

[19] A. G. Kannan, N. R. Choudhury, and N. K. Dutta, "Synthesis and characterization of methacrylate phospho-silicate hybrid for thin film applications," *Polymer (Guildf).*, vol. 48, no. 24, pp. 7078–7086, 2007.

[20] J. R. Pels, F. Kapteijn, J. A. Moulijn, Q. Zhu, and K. M. Thomas, "Evolution of nitrogen functionalities in carbonaceous materials during pyrolysis," *Carbon N. Y.*, vol. 33, no. 11, pp. 1641–1653, 1995.

[21] G. Sethia and A. Sayari, "Comprehensive study of ultra-microporous nitrogen-doped activated carbon for CO_2 capture," *Carbon N. Y.*, vol. 93, pp. 68–80, 2015.

[22] M. Molina-Sabio and F. Rodríguez-Reinoso, "Role of chemical activation in the development of carbon porosity," *Colloids Surfaces A Physicochem. Eng. Asp.*, vol. 241, no. 1, pp. 15–25, 2004.

[23] M. Pelavin, D. N. Hendrickson, J. M. Hollander, and W. L. Jolly, "Phosphorus 2p electron binding energies. Correlation with extended Hueckel charges," *J. Phys. Chem.*, vol. 74, no. 5, pp. 1116–1121, Mar. 1970.

[24] F. Rodriguez-Reinoso, M. Molina-Sabio, and M. A. Munecas, "Effect of microporosity and oxygen surface groups of activated carbon in the adsorption of molecules of different polarity," *J. Phys. Chem.*, vol. 96, no. 6, pp. 2707–2713, Mar. 1992.

[25] S. S. Barton, M. J. B. Evans, E. Halliop, and J. A. F. MacDonald, "Acidic and basic sites on the surface of porous carbon," *Carbon N. Y.*, vol. 35, no. 9, pp. 1361–1366, 1997.

[26] M. J. Antal and M. Grønli, "The Art, Science, and Technology of Charcoal Production," *Ind. Eng. Chem. Res.*, vol. 42, no. 8, pp. 1619–1640, Apr. 2003.

[27] G. Várhegyi, P. Szabó, F. Till, B. Zelei, M. J. Antal, and X. Dai, "TG, TG-MS, and FTIR Characterization of High-Yield Biomass Charcoals," *Energy & Fuels*, vol. 12, no. 5, pp. 969–974, Sep. 1998.

[28] M. J. Antal, W. S. L. Mok, G. Varhegyi, and T. Szekely, "Review of methods for improving the yield of charcoal from biomass," *Energy & Fuels*, vol. 4, no. 3, pp. 221–225, May 1990.

[29] S. Parvathikar and J. W. Schwank, "Low-Temperature Gasification of Cellulosic Biomass,"*AIChE 2008 Annual Meeting*, 2008.

[30] N. D. Kaushika and K. S. Reddy, "Performance of a low cost solar paraboloidal dish steam generating system," *Energy Convers. Manag.*, vol. 41, no. 7, pp. 713–726, 2000.

Chapter 4

Application of activated carbon to recycle ammonia off-gassed from urine for soil amendment purposes

Introduction

Human urine holds vital agricultural nutrients in fairly concentrated form (~9000 mg/L N and ~700 mg/L P) [1]. Nutrient recovery is beneficial to protect the environment but is especially important in resource-constrained settings where fertilizer security is often low. For instance, in Ethiopia, the price of commercial fertilizers has been rising by 20% annually [2]. As efforts are accelerating to provide access to sanitation services, separation and collection of urine to produce beneficial products or recover nutrients are promising, and probably the only way source separation of urine can be sustainable (i.e., by providing a market for products and not just sanitation services). Given the limits to fertilizer security in many resource-constrained countries, methods are needed to recover nutrients and safely reuse them. Methods for P recovery via precipitation are well-established thanks to the low solubility of P salts, but recovery of N from urine is more challenging. About 85% of the nitrogen in fresh urine is fixed as urea, which is hydrolyzed over time by the enzyme urease to ammonia and CO_2 [1], [3]. This conversion results in an increase of pH from ~ 6 (at the body exit) to > 9 within a day to a few weeks, which further accelerates ammonia volatilization [4]. Post hydrolysis of urea, total

ammonia accounts for 90% of the nitrogen in stored urine [1]. Methods to recover nutrients are thus susceptible to ammonia off-gas, and in some cases, almost 50% of the nitrogen can be lost through volatilization [5]. Besides the loss of a valuable nutrient, accumulated ammonia has an unpleasant odor and at elevated concentration represents a health concern for human beings [6]. Ammonia loss occurs at different steps in urine handling: during storage, transport, application, treatment and especially during volume reduction [7]. Methods such as catalytic decomposition, reaction of ammonia with another gas, adsorption by solids, and stage combustion process, have been developed to remove ammonia from flue gas before it is released into the atmosphere [8]. Among these methods, removal and recovery of ammonia with low-cost adsorbents is a competitive and attractive approach, especially in low resource settings [9], [10]. Zeolites because of their inherent Lewis and Brønsted acidity have been well studied and optimized for ammonia capture in the chemical industry [11], [12]. Besides synthetic zeolites, activated carbon adsorbents have proven quite effective as well. Activated carbon is a well-known adsorbent which could serve as an NH_3 trap and simultaneously benefit by increasing the water holding capacity of soils. The goal of the work presented here is to synthesize and characterize cellulosic activated biochar, then use it to recover ammonia off-gassed from urine and release it back into the soil as a source of nitrogen for plants.

We [13] previously demonstrated a way to synthesize activated biochar at moderate temperatures via chemical activation using diammonium hydrogenphosphate (DAP) as the activating agent in the presence of air, which aimed at application in low resource rural settings. Design constraints under such circumstances require one to consider factors such as availability of carbon precursor, activating agents, safe storage and handling of the activants, relatively low operating temperature, etc. DAP is a very widely available fertilizer in rural settings. There are many

reasons to use it : distributed in bags and fairly convenient and safe to store, use and handle. More importantly, upon heating, it produces phosphoric acid which serves as an activating agent for biochar and is largely recoverable in the extraction step [14], [15]. Thermal decomposition of DAP also liberates NH_3. The simultaneous interaction of NH_3 with the pyrolyzing biomass at moderate temperatures imparts interesting surface functionality, an aspect which we had explored previously [13]. The implication of the physicochemical properties of the synthesized activated biochar on the adsorption and desorption of ammonia is explored in this chapter.

Experimental

Materials

Microcrystalline cellulose (MCC) (≥99.9%) and diammonium hydrogenphosphate (DAP) (≥99%) were purchased from Sigma-Aldrich and used as received. The Zeolite ZSM-5 (Si/Al =11.5) was obtained from Zeolyst, and commercial Beaded Activated Carbon (BAC) was obtained from Kureha.

Characterization

The preparation of the precursor was based on the method laid out by Nahata *et al*. [13]. Porosity assessment of the synthesized biochars was carried out by N_2 physisorption using an ASAP 2020 apparatus. Adsorbed moisture was eliminated by degassing the samples at 300°C under vacuum (~μm Hg), and physisorption was carried out at 77 K on the 'clean' surface obtained. The surface area was calculated by applying the BET equation to the isotherm data in the relative pressure (P/P_o) range from 0.05 to 0.20. The micropore volume was determined from the Dubinin-Astakhov equation, and the micropore size distribution was obtained from the Horvath-

Kawazoe (HK) model using slit pore geometry. The single point total pore volume was estimated from the amount adsorbed at a relative pressure (P/P_O) of ~0.99. For DRIFTS (Diffuse Reflectance Infrared Fourier Transform Spectroscopy) analysis, the sample was diluted with KBr and finely ground with a pestle and mortar. DRIFTS spectra were obtained on a Bruker Tensor 27 FTIR using a Harrick Praying Mantis diffuse reflectance system and OPUS data collection program. The background signal was collected using pure KBr. The resolution was 4 cm^{-1} and the number of scans was 256. The scanning range (cm^{-1}) was appropriately chosen depending upon the experiment performed and the region of interest under consideration. The surface elemental compositions (% dry weight) were assessed by XPS measurement on a Kratos Axis Ultra device. The bulk elemental compositions of the samples (% dry weight) were obtained by sending the samples to Midwest Microlabs. Before analysis, the samples were vacuum heated to 110 °C to remove any adsorbed moisture, and the materials were handled inside a glove box. C, H, N and P contents were directly measured, and the oxygen content was estimated as a difference upon mass balance. The errors for both surface and bulk compositions are reported as standard deviations from triplicate measurements of samples synthesized in different batches. The elemental composition of cellulose was determined directly from its molecular formula.

Thermogravimetric Analysis (TGA)

NH_3 adsorption isotherms were constructed by performing experiments on a Thermogravimetric Analyzer (TGA). Activated biochar samples ~(7-10) mg were loaded onto a TGA pan. The samples were pretreated to remove any adsorbed moisture by heating them to 300°C under pure nitrogen flow and holding them at the same temperature for an hour. The material was then cooled down under nitrogen flow to a temperature of 50°C. NH_3 diluted in nitrogen (~ppm) was then adsorbed on the dry material till saturation. Under constant temperature, the flow was

switched to pure N_2 resulting in desorption of the weakly bound NH_3. The balance of NH_3 left adsorbed on the biochar has been termed as strongly bound ammonia. This entire process is illustrated in Figure 4.1. In addition to these 50°C isotherms, isotherms at 35°C were obtained in a similar fashion. For experiments in the presence of moisture, following the pre-treatment at 300°C as described above, carrier gas N_2 was bubbled through a solution of 0.1 M NH_4OH and the sample was exposed to the vapor mix: H_2O (g) + NH_3 (g) till saturation. The flow was then switched to pure N_2 to remove the weakly bound ammonia and water. A control experiment was carried out with adsorption and desorption of pure water vapor. From the difference in these values, the total strongly bound ammonia was calculated.

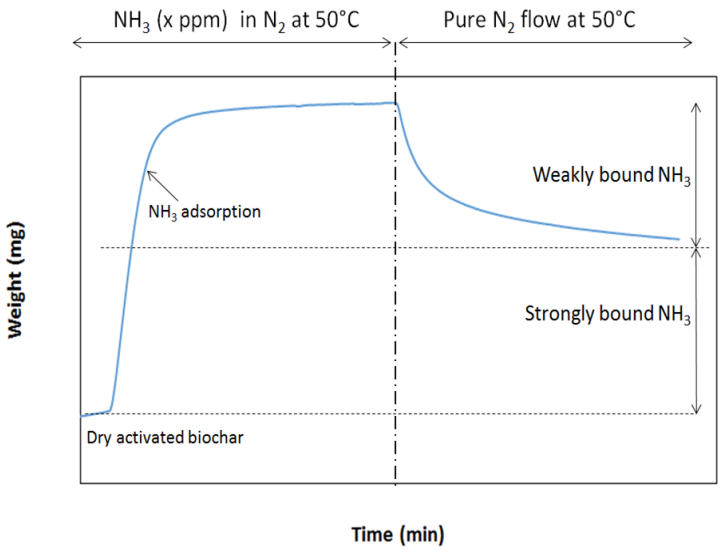

Figure 4.1: Schematic of TGA measurement showing the weakly and strongly bound ammonia

NH_3 Temperature Programmed Desorption (TPD)

TPD was used to assess the nature of the strongly bound ammonia. A packed bed comprising of ~60 mg of activated biochar was constructed by adding the sample in a ¼ inch quartz tube

supported over quartz wool. The sample was pretreated at 300°C under Argon flow for an hour and then cooled down to 50°C. Following the pretreatment ~700 ppm of NH_3 was passed over the activated biochar until saturation. The sample was then purged by pure Argon to remove the weakly bound NH_3. The samples were heated at a rate of 5°C/min to 550°C and the concentration of NH_3 in the effluent gas stream was measured by an MKS Multigas 2030 FTIR spectrometer with 0.5 cm^{-1} resolution. The FTIR cell volume was 200 mL and the Argon flow rate was 100 mL/min. Under these conditions (Ramp : 5°C/min) the peak temperature data of the TPD spectrum are associated with an error of ± 10°C.

Aqueous ammonia analysis

Post experiments on the TGA, the biochar samples with the strongly bound ammonia were mixed and agitated in 25 mL of deionized water for 24 hours to obtain the equilibrium recovery of ammonia in water. Ammonia in the aqueous phase was analyzed by the ammonia-phenate method. Solutions of aqueous ammonia were reacted with phenol, sodium nitroprusside, and bleach oxidant and left in the dark for two hours to develop a blue coloration. The intensity of the blue coloration proportional to the concentration of NH_3, was estimated by a BioTek μQuant spectrophotometer at a wavelength of 640 nm.

Results and Discussion

Figure 4.2 displays the isotherms for adsorbed ammonia on activated biochar at 50°C and 35°C under dry conditions. Unactivated biochar refers to the charcoal formed by pyrolysis of cellulose only, without the use of any activating agent and serves as a control sample. From the isotherms, it is clear that chemical activation via DAP helps to increase the ammonia uptake capacity. This

is due to the enhancement of the total pore volume and incorporation of acidic surface functionalities. The weakly bound ammonia is one which is bound by Van-der-Waals forces over the surface and is a function of the partial pressure of the adsorbing gas. This weakly bound ammonia gets released when the flow is switched to pure nitrogen. The amount of strongly bound ammonia, on the other hand, remains nearly constant when the flow is switched to nitrogen and appears to be a function of the number of adsorbing sites within the micropores of the material. The data for ammonia uptake on ZSM-5 zeolite is provided as a reference for comparison. These zeolites are known microporous materials having high ammonia adsorption capacity. The total capacity (sum of weakly and strongly bound ammonia) of the zeolite is higher than activated carbons due to much larger amounts of strongly bound NH_3, as the zeolite has many sites for chemisorption. A capacity comparison of the strongly bound ammonia for the synthesized activated carbons under dry and moist conditions is shown in Figure 4.3. Our data show a slight fall in the capacity of strongly bound ammonia under moist conditions for all the samples of activated biochar synthesized, probably due to the competition between water and ammonia for adsorption sites. It is well known that the oxygen content in activated carbon is an indicator of the acidic functional groups [16]. From the elemental analysis (Figure 4.5), a high percentage of oxygen indicates significant acidic functionality. Apart from the favorable interaction with acidic surface functionality, water can form hydrogen bonds with O as well as N in the biochar. The water holding capacities of the samples are listed in Table 4.1. The activated carbons are quite hygroscopic with a water holding capacity of ~ 215 mg/g at 35°C. The control sample without activation has a meagre water holding capacity of 24 mg/g at 35°C (our samples exhibit a 9 fold increase relative to control). There is also nearly a 3 fold increase water holding capacity in a 15°C temperature differential (50°C to 35°C) probably due to the formation of

multilayers of water at lower temperatures. Since our samples are already rich in oxygen, and those being potential acidic sites for NH_3 adsorption, the presence of water may mildly inhibit the adsorption of strongly bound ammonia due to occupation of potential adsorption sites by water. It is to be noted that the quantification in Figure 4.3 is with respect to the strongly bound ammonia. The weakly bound ammonia is unstable in nature and cannot be accurately compared with this method.

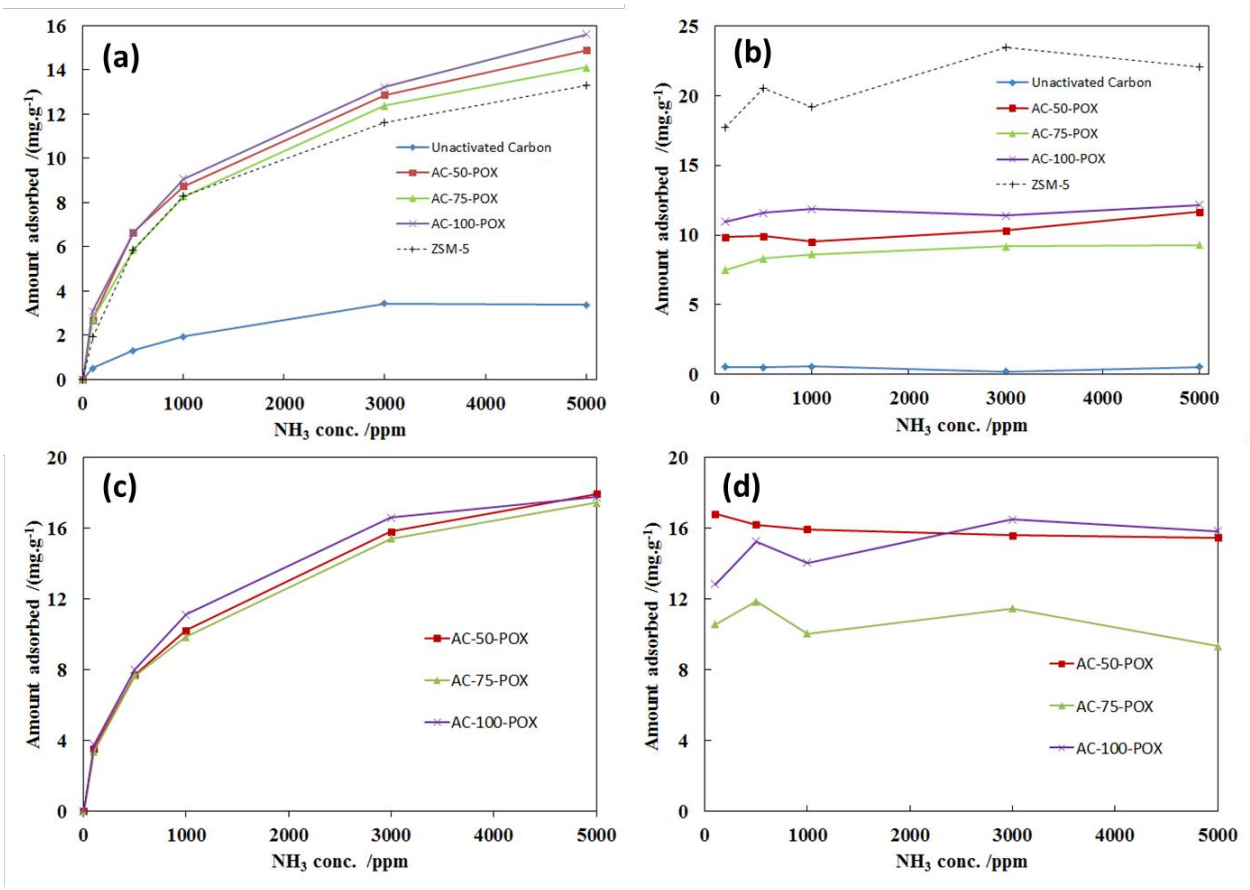

Figure 4.2: Adsorption isotherms at temperatures of (a,b) 50°C and (c,d) 35°C for different adsorbents displaying (a,c) weakly bound ammonia and (b,d) strongly bound ammonia

Table 4.1: Water holding capacity of the activated carbons at 50°C and 35°C (std. dev reported from triplicates)

Sample	Water capacity at 50°C /($mg.g^{-1}$)	Water capacity at 35°C /($mg.g^{-1}$)
AC-50-POX	84.64 ± 2.98	215.09 ± 6.07
AC-75-POX	80.88 ± 4.13	217.04 ± 5.15
AC-100-POX	82.36 ± 3.63	206.61 ± 3.87

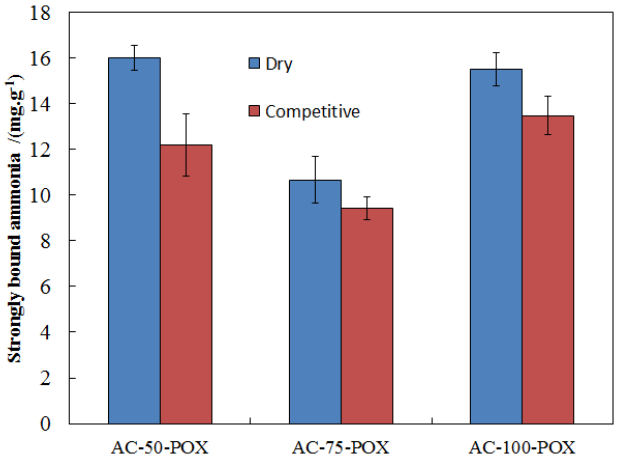

Figure 4.3: Capacity comparison of strongly bound ammonia at 35°C under dry and moist (competitive) conditions

The fractional occupancy of the strongly bound ammonia inside the micropore was found to be 4.5-7% of the total micropore volume, indicating that ammonia adsorption is a strong function of the density of acid sites within the micropore as opposed to the total micropore volume. From the equilibrium data in Figure 4.2, we observe that AC-75-POX apparently has a lower capacity for ammonia adsorption relative to AC-50-POX despite having higher BET surface area and micropore volume. NH_3 breakthrough experiments were conducted in an independent packed bed setup, and a similar trend was observed as shown in Figure 4.4. This trend can probably be explained by the reduction in density of acid sites for AC-75-POX relative to the other samples as shown in Figure 4.5. We had observed in chapter 3 that the oxygen content was a good estimator of acid surface functional groups. If the oxygen content is normalized by BET surface area or micropore volume, the reduction in density of acid sites for AC-75-POX becomes even more apparent, which perhaps reflects in a decreased ammonia capacity.

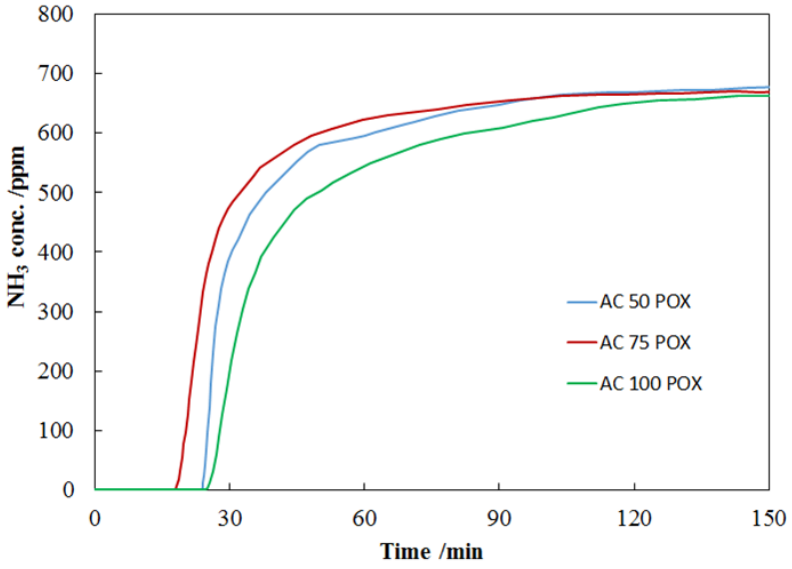

Figure 4.4: Ammonia breakthrough curves at 50°C for different activated carbons

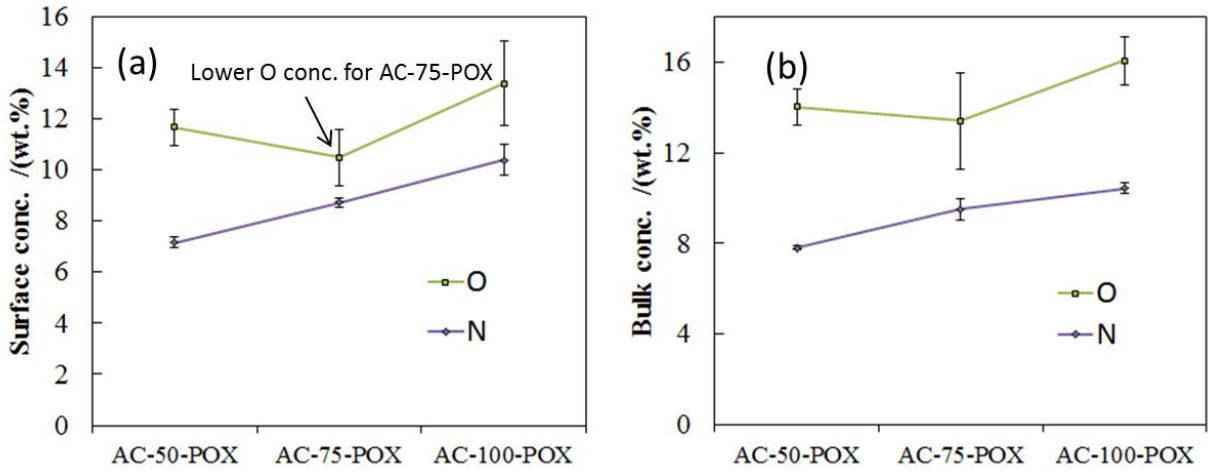

Figure 4.5: (a) surface and (b) bulk oxygen and nitrogen composition of the synthesized activated carbons

Figure 4.6 shows the N_2 physisorption isotherms for microporous AC-50-POX, ZSM-5 and commercial Beaded Activated Carbon (BAC). Their respective total ammonia adsorption capacities are also provided. BAC is manufactured from petroleum pitch and is generally utilized for VOC adsorption in the automobile and paints industry. It has a high BET surface area of ~1150 m^2/g. However, compared to other samples its ammonia adsorption capacity is the least.

The microporous zeolite ZSM-5 though has a BET surface area of (~350 m^2/g), which is nearly half the value of the surface area of AC-50-POX; it has a much greater capacity for strongly bound ammonia. This observation reiterates the importance of the density of relevant acid sites inside the micropore as opposed to the total micropore volume for ammonia adsorption, especially with respect to activated carbon. It also emphasizes the point that activated carbons are optimized for a particular operation (VOC, H_2S or NH_3 removal for instance). Each such operation would require carbons with different properties. High surface areas though are generally desirable. However, relevant surface functional groups are equally (if not more) important and dictate what application the materials may fit into.

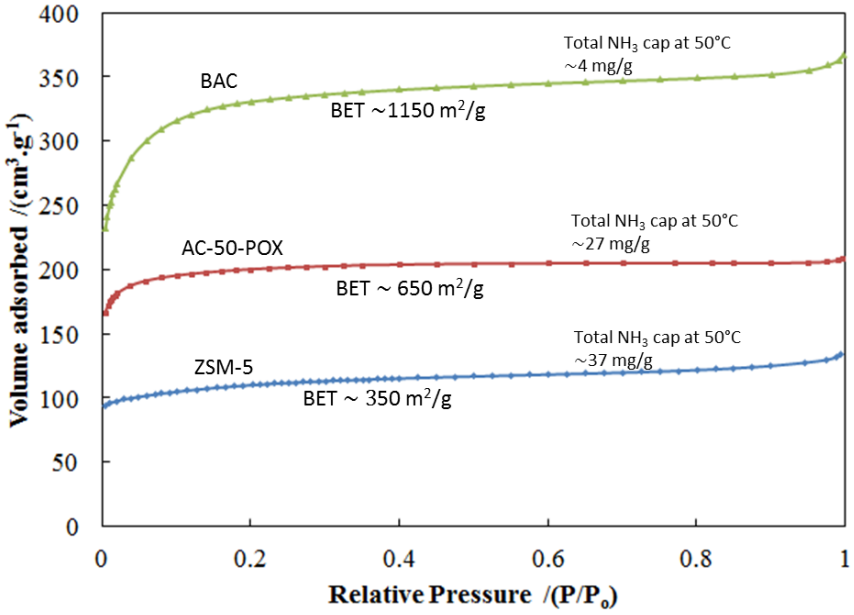

Figure 4.6: Nitrogen physisorption isotherms at 77 K for BAC, AC-50-POX and ZSM-5 along with their associated BET surface areas and total ammonia adsorption capacity at 50°C

The TPD spectrum of the strongly bound NH_3 as a function of temperature is shown in Figure 4.7. No ammonia was evolved from the control sample (freshly synthesized activated carbon), which indicates that the NH_3 TPD spectra resulted from desorption of the adsorbed ammonia.

The asymmetry of the peak indicates that there might be a distribution of different types of strongly bound ammonia. These different types can be assessed by deconvoluting the TPD spectra into individual peaks. Peaks (1,2) at ~150 and ~200°C have been assigned to strongly physisorbed NH_3 molecules, probably due to hydrogen bonding within the micropores [12]. These peaks might correspond to different hydrogen bonded interactions (NH_3---N) and (NH_3---O) or one might view them as a continuum of interactions across the spectrum of the pore size distribution. The peaks (3, 4) at ~300°C and 450°C are most likely a consequence of reactive retention of ammonia in the biochar, the likely cause of which is discussed later.

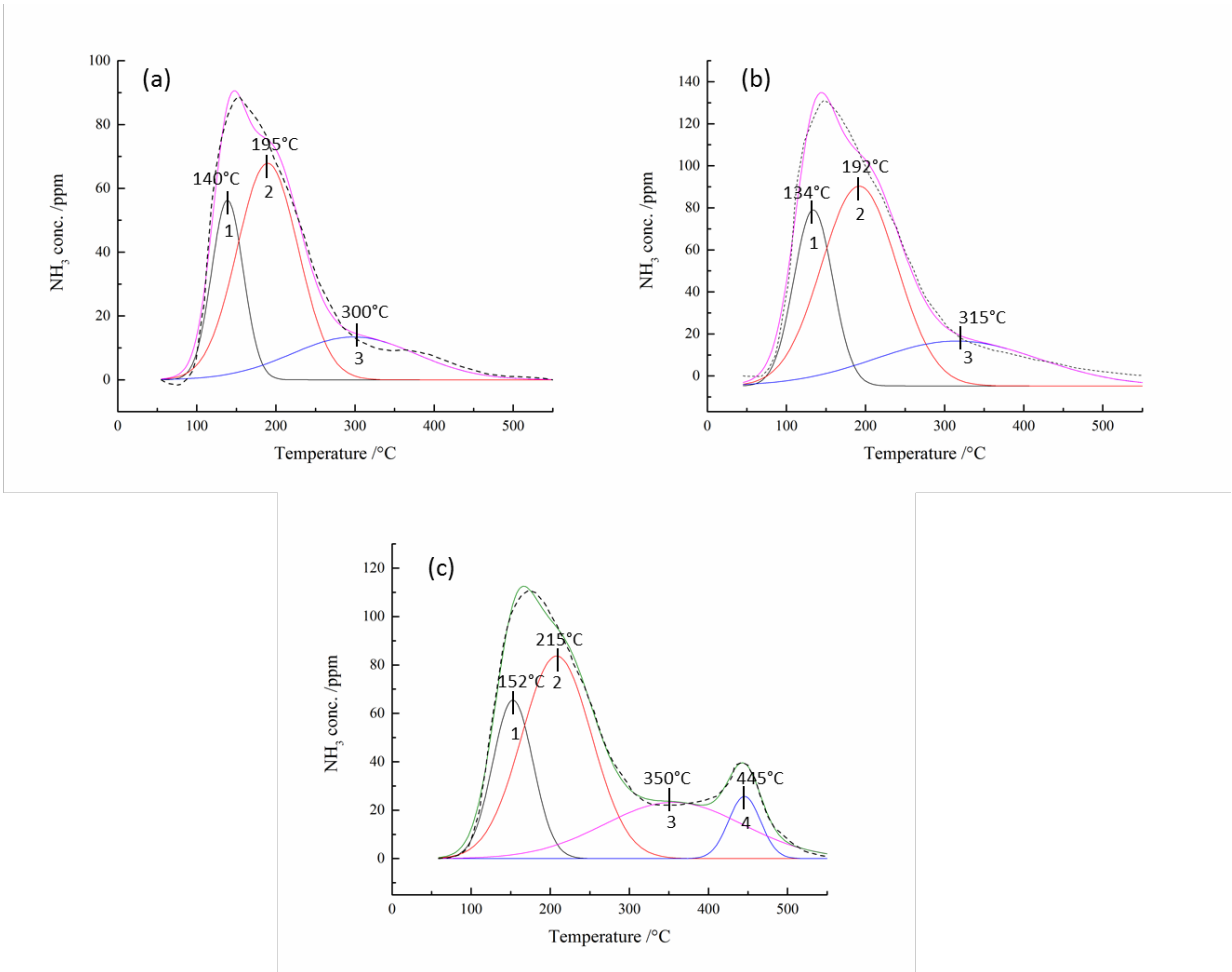

Figure 4.7: TPD spectra of the strongly bound ammonia for (a) AC-50-POX, (b) AC-75-POX and (c) AC-100-POX. The spectra were baseline corrected and rescaled

The biochar material is largely made up of defective graphene sheets surrounded by oxygen-rich functional groups at the edges, such as carboxylic acids and lactones. Because of the electron withdrawing nature of these oxygen groups, there exists a partial positive charge throughout the graphene layer, which facilitates the creation of potential sites for interaction of ammonia. The weakly bound NH_3 held only by Van-der-Waals forces can be swept off by a nitrogen gas purge. However, the strongly bound NH_3 is assumed to be distributed in the micropores between the defective graphene sheets. Based on the TPD spectra most of the NH_3 is assumed to be hydrogen bonded inside the micropores and is recoverable by agitation in water (Figure 4.9). It is speculated that reactive retentions may arise by pathways given in Eq. 4.1 and 4.2. When exposed to biochar, NH_3 is more likely to interact as stated in Eq. 4.1 forming $RCOO^-NH_4^+$. The ammonia can thus be recovered in water (Eq. 4.3). A direct amide formation (Eq. 4.2) is also possible when ammonia attacks the carbon center of RCOOH as opposed to hydrogen. The probability of such an event (Eq. 4.2) directly occurring is lower, because a relatively stronger carbon-oxygen bond needs to be broken to form an amide.

$$RCOOH + NH_3(g) \rightarrow RCOO^-NH_4^+ \quad (4.1)$$

$$RCOOH + NH_3(g) \rightarrow RCONH_2 + H_2O \quad (4.2)$$

$$RCOO^-NH_4^+ + H_2O\ (l) \rightarrow RCOOH + NH_3(aq) + H_2O \quad (4.3)$$

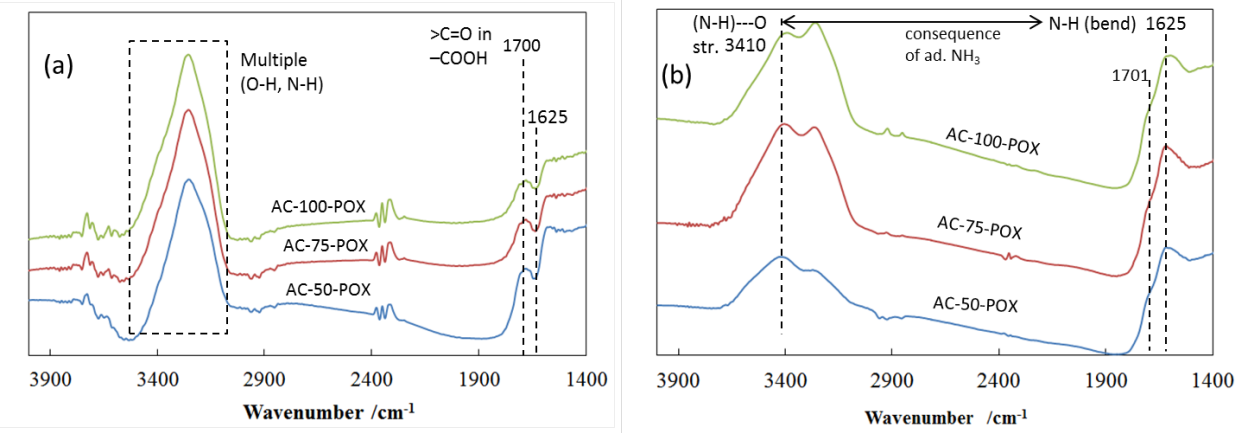

Figure 4.8: DRIFTS spectra showing (a) the freshly synthesized samples and (b) samples with strongly bound NH_3

The DRIFTS spectra of the samples are shown in Figure 4.8. The freshly synthesized samples exhibit a broad, asymmetric peak around 3000-3500 cm^{-1}, which is due to an overlap of various types of O-H and N-H vibrations. Because of the innate nitrogenous functionality present in the fresh biochar samples, there are some N-H stretches present in the matrix, existing primarily as pyrrolic structures associated with the aromatic sheet [13]. The C=O stretch of carboxylic acids is visible around 1700 cm^{-1} in the fresh samples. Besides, C=C aromatic stretch of the defective graphene appears at 1570 cm^{-1} [17], [18]. When we observe the DRIFTS spectrum of the biochars with the strongly bound NH_3 (Figure 4.8b), two features are striking. The first one is the change in shape of the broad peak in the range (3000-3600) cm^{-1} and the shift of the peak centered at 1700 to 1625 cm^{-1}. Post ammonia adsorption, the major vibration, at ~3410 cm^{-1} (absent in the fresh sample) is assigned to the N-H stretch of the adsorbed ammonia. This is a reflection of the state of the strongly bound ammonia in the vicinity of oxygen-rich groups [19]. It is also interesting to compare the region 1800 to 1600 cm^{-1} of the fresh sample and the sample with strongly bound ammonia. The fresh samples have a peak centered around 1700 cm^{-1} corresponding to C=O stretches of carboxylic acids and other carbonyl compounds. However, when the biochar samples with strongly bound ammonia are observed, the peak shifts to 1625 cm^{-1}. The peak at ~1625 cm^{-1} is believed to be due to an N-H bend and the original C=O vibration at ~1700 cm^{-1} is visible as a faint shoulder.

As stated earlier, our goal was to capture ammonia and then release it back into the soil. Therefore, ammonia release experiments were carried out in water at room temperature. As shown in Figure 4.9, more than 90% of the adsorbed ammonia was recovered in water. Some NH_3 may have reacted with the biochar and remains permanently bound to the surface and thus cannot be recovered by water washing. One such possibility is through the pathway of Eq. 4.2.

The zeolite (ZSM-5) has considerable amounts of chemisorbed ammonia which cannot be recovered by room temperature water washing and must be heated to high temperature for ammonia recovery. The peak at 3400 cm^{-1} dwindles upon water washing, and so does the N-H bend at 1625 cm^{-1} (water regenerated surfaces), and the original structure begins to recuperate, further reaffirming the rationale of the mode of interaction of ammonia with biochar. About (85-90) % of the original BET surface area of the activated biochar samples could be regenerated post-water-washing. We have thus attempted to demonstrate a method to synthesize activated biochar from cellulose in a semi-batch setup in the presence of ambient air. The activated biochar exhibits good potential to trap ammonia off-gassed from sanitary installations and recycle it back to wet soil. The simple mechanism of NH_3 release from the biochar is expected to facilitate soil amendment applications as envisioned and the nitrogen should be readily available to plants. Ammonia recovery by a method of simple water washing reduces the need for energy-intensive thermal regenerations and also fits well into the proposed application as a soil amendment.

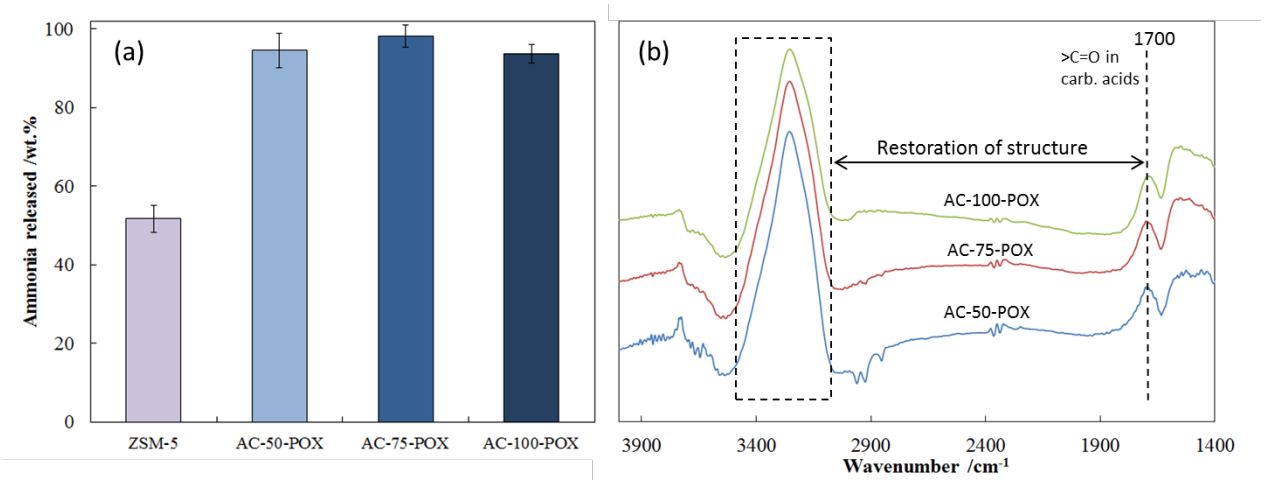

Figure 4.9: (a) Equilibrium recovery of the strongly bound ammonia in water and (b) DRIFTS absorbance spectra revealing the restoration of original structure of the activated biochar post water washing

Practical aspects

During the synthesis of activated biochar, the first step involved drying of the cellulose-DAP

mixture at 80°C to form the precursor. This process transforms DAP to MAP and off-gasses ammonia, as observed in chapter 2. Cellulose itself has no nitrogen, so the entire contribution of Nitrogen is from the DAP loaded initially (which is defined as: initial total N). This ammonia is recoverable by bubbling through DI water. Post the drying step, the precursor is pyrolyzed to biochar. During pyrolysis, the residual nitrogen in the precursor either reacts with cellulose (to become a part of the aromatic ring in the activated biochar) or escapes in the gas phase as N_2, NH_3 and NO_x. The functional form in which N exists in the aromatic ring was covered in chapter 3. The fraction of N in the biochar was calculated by elemental analysis and the remainder lost during pyrolysis has been estimated by mass balance. The resultant mass distribution of N across various steps involved in the synthesis is summarized below in Table 4.2.

Table 4.2: Mass distribution of Nitrogen during the synthesis steps of activated carbon

Material	% of initial N recoverable during drying step	% of initial N incorporated in biochar	% of initial N lost during pyrolysis (by mass balance)
AC-50-POX	41	30	29
AC-75-POX	49	27	23
AC-100-POX	49	21	30

From the results observed thus far, AC-50-POX appears to be the best trade-off (relative to AC-75-POX and AC-100-POX) in terms of the mass loading of the activating agent used for synthesis, quality of the resultant biochar in terms of yield, ammonia adsorption capacity and desorption ease. The Nitrogen lost during pyrolysis is difficult to recover, however a substantial portion of N is also incorporated in the activated biochar. Depending upon viewpoint and the time scale in question, the fraction of N in the biochar may or may not be considered 'lost'. We have thus defined the terms 'N lost during pyrolysis' and 'total N lost' separately. The 'total N lost' is defined as the sum of the nitrogen lost during pyrolysis and the nitrogen incorporated in the biochar.

The application envisioned is adsorbing ammonia off-gassed from urine and recycling it back

into the soil. The ammonia component of DAP does not really contribute to activation, but the interaction of ammonia with cellulose cannot be avoided. With the proposed application in mind, one may consider the net balance as: utilizing N from DAP during activated biochar synthesis and then replacing it back by the adsorption of ammonia off-gassed from urine. Taking into account the effect of moisture on the capacity of strongly bound ammonia and temperature fluctuations, two reasonable estimates of capacity for AC-50-POX along with the number of adsorption-desorption cycles it takes to replace the nitrogen lost during pyrolysis and the total lost nitrogen are reported in Table 4.3. This calculation is based on the premise that there is no loss in ammonia adsorption capacity on successive cycling. A cycle is defined as one run of complete saturation of the carbon surface with ammonia followed by its complete desorption. This is a fair assumption based on our data where we demonstrated that about 90-95% of the adsorbed ammonia could be desorbed in the first cycle. Since most of the ammonia was found to be physisorbed, the capacity is not expected to significantly decline over multiple cycles. The calculation is conservative in the sense that it does not factor weakly bound ammonia (a significant fraction in the total ammonia), but it does assume no loss in capacity on successive cycling. These two factors may compensate for one another providing a realistic estimate in Table 4.3, however experiments however need to be performed to test this hypothesis for more than 1 cycle.

Table 4.3: Number of cycles required to replace different types of lost N for AC-50-POX

Capacity of strongly bound NH_3 (mg/g)	# of cycles to replace total lost N	# of cycles to replace N lost during pyrolysis
12	12-13	6-7
15	9-10	5

Irrespective of N balance, the material undoubtedly can address the problem of unpleasant odors in toilets, simultaneously providing numerous benefits. The justification of DAP for this

application relative to N balance needs to be assessed over numerous cycles. Once added to soil, it can better hold nutrients from inorganic fertilizers added in the future. In the vast array of implications, the perspective of N balance is just one of the trade-offs. The main activating agent phosphoric acid is largely recoverable (~85-90%) and can be used again to activate carbon, which in principle may be used to capture more ammonia. Along with ammonia capture, the activated biochar greatly improves the water holding capacity of soils, which can result in improved crop yields especially in the dry season. The long term benefits of activated biochar (e.g. Terra-preta in the amazon) needs to be accounted as well [20], [21]. On a different tangent, the synthesized activated carbon may also be used as a component of drinking water treatment systems. The time dependent and diverse set of implications makes the question of economic viability difficult to reconcile with, in terms of a net present $ value. A focused long–term effort is required to assess the various scenarios posed in this situation. However, in absence of other reagents, DAP activation in presence of air is definitely one way to address the synthesis of activated biochar in resource-constrained settings. The idea was to develop a method to synthesize activated biochar locally with relative ease, and provide communities with flexibility of application depending upon need. The utilization of activated biochar in sanitary installations to recycle ammonia was just one of the applications explored.

Conclusions

Finally to conclude, the synthesized activated carbons exhibit good capacity to adsorb ammonia from the gas phase. The work brings out of the importance of acidic surface functional groups over the net micropore volume and BET surface area for ammonia adsorption, given that the

pore size distributions were quite similar for the synthesized activated biochars (AC-50-POX, AC-75-POX and AC-100-POX). There is a spectrum of adsorbed ammonia with different strengths of adsorption: from weakly physisorbed to hydrogen bonded to reactively bound ammonia as indicated by DRIFTS and TPD measurements. The carboxylic acid sites were speculated to be important in the process. It was shown that most of the ammonia was physisorbed and could be recovered by simple water washing at room temperature, preventing the need for high temperature thermal regeneration. The present study demonstrated fairly high regeneration ability of the activated biochar for one cycle of adsorption and desorption. However multiple cycles of measurement should be carried out in future to assess the scope of its practical applicability.

Acknowledgements: The contribution of Prof. Nancy Love with intellectual discussions throughout this work and the involvement of Zerihun Getaneh with TGA experimental work are gratefully acknowledged. Adriana Arcelay helped by providing training for aqueous phase ammonia analysis and Amin Reihani generously contributed towards TPD experiments.

References

[1] K. M. Udert, T. A. Larsen, and W. Gujer, "Fate of major compounds in source-separated urine," *Water Sci. Technol.*, vol. 54, no. 11–12, pp. 413-420, Dec. 2006.

[2] W. I. Robinson, A. T. Lieberg, and L. Trebbi, "FAO/WFP Crop and Food Supply Assessment Mission to Ethiopia, Special Report," Rome, 2006.

[3] K. M. Udert, T. A. Larsen, M. Biebow, and W. Gujer, "Urea hydrolysis and precipitation dynamics in a urine-collecting system," *Water Res.*, vol. 37, no. 11, pp. 2571–2582, Jun. 2003.

[4] A. Chandran, S. K. Pradhan, and H. Heinonen-Tanski, "Survival of enteric bacteria and coliphage MS2 in pure human urine," *J. Appl. Microbiol.*, vol. 107, no. 5, pp. 1651–1657, Nov. 2009.

[5] K. S. Warren, "Ammonia Toxicity and pH," *Nature*, vol. 195, p. 47, Jul. 1962.

[6] Z. Bai, Y. Dong, Z. Wang, and T. Zhu, "Emission of ammonia from indoor concrete wall and assessment of human exposure," *Environ. Int.*, vol. 32, no. 3, pp. 303–311, 2006.

[7] Z. S. Ban and G. Dave, "Laboratory studies on recovery of N and P from human urine through struvite crystallisation and zeolite adsorption," *Environ. Technol.*, vol. 25, no. 1, pp. 111–121, Jan. 2004.

[8] B. Dou, M. Zhang, J. Gao, W. Shen, and X. Sha, "High-Temperature Removal of NH_3, Organic Sulfur, HCl, and Tar Component from Coal-Derived Gas," *Ind. Eng. Chem. Res.*, vol. 41, no. 17, pp. 4195–4200, Aug. 2002.

[9] S. E. Jorgensen, O. Libor, K. Lea Graber, and K. Barkacs, "Ammonia removal by use of clinoptilolite," *Water Res.*, vol. 10, no. 3, pp. 213–224, 1976.

[10] G. Busca and C. Pistarino, "Abatement of ammonia and amines from waste gases: a summary," *J. Loss Prev. Process Ind.*, vol. 16, no. 2, pp. 157–163, Mar. 2003.

[11] M. Sawa, M. Niwa, and Y. Murakami, "Relationship between acid amount and framework aluminum content in mordenite," *Zeolites*, vol. 10, no. 6, pp. 532–538, 1990.

[12] N. Katada, H. Igi, and J.-H. Kim, "Determination of the Acidic Properties of Zeolite by Theoretical Analysis of Temperature-Programmed Desorption of Ammonia Based on Adsorption Equilibrium," *J. Phys. Chem. B*, vol. 101, no. 31, pp. 5969–5977, Jul. 1997.

[13] M. Nahata, C. Y. Seo, P. Krishnakumar, and J. Schwank, "New approaches to water purification for resource-constrained settings: Production of activated biochar by chemical activation with diammonium hydrogenphosphate," *Front. Chem. Sci. Eng.*, 2017.

[14] M. Jagtoyen and F. Derbyshire, "Activated carbons from yellow poplar and white oak by H_3PO_4 activation," *Carbon N. Y.*, vol. 36, no. 7, pp. 1085–1097, 1998.

[15] M. Molina-Sabio, F. Rodríguez-Reinoso, F. Caturla, and M. J. Sellés, "Porosity in

granular carbons activated with phosphoric acid," *Carbon N. Y.*, vol. 33, no. 8, pp. 1105–1113, 1995.

[16] S. S. Barton, M. J. B. Evans, E. Halliop, and J. A. F. MacDonald, "Acidic and basic sites on the surface of porous carbon," *Carbon N. Y.*, vol. 35, no. 9, pp. 1361–1366, 1997.

[17] A. Puziy, O. Poddubnaya, A. Martínez-Alonso, F. Suárez-García, and J.M.Tascón, "Synthetic carbons activated with phosphoric acid: I. Surface chemistry and ion binding properties," *Carbon N. Y.*, vol. 40, no. 9, pp. 1493–1505, 2002.

[18] M. S. Solum, R. J. Pugmire, M. Jagtoyen, and F. Derbyshire, "Evolution of carbon structure in chemically activated wood," *Carbon N. Y.*, vol. 33, no. 9, pp. 1247–1254, 1995.

[19] A. A. Tsyganenko, D. V Pozdnyakov, and V. N. Filimonov, "Infrared study of surface species arising from ammonia adsorption on oxide surfaces," *J. Mol. Struct.*, vol. 29, no. 2, pp. 299–318, 1975.

[20] B. Glaser, L. Haumaier, G. Guggenberger, and W. Zech, "The 'Terra Preta' phenomenon: a model for sustainable agriculture in the humid tropics," *Naturwissenschaften*, vol. 88, no. 1, pp. 37–41, 2001.

[21] B. Glaser, J. Lehmann, and W. Zech, "Ameliorating physical and chemical properties of highly weathered soils in the tropics with charcoal – a review," *Biol. Fertil. Soils*, vol. 35, no. 4, pp. 219–230, 2002.

Chapter 5

Future Directions

Introduction

The capability of activated carbons to address a particular application largely depends on its surface chemistry which is inextricably interwoven into the method of synthesis. Activated carbons have high pore volumes which make them versatile adsorbents. It is being increasingly demonstrated how they can be engineered to have specific functional groups to drive particular needs. They are easy to produce commercially and are quite inexpensive ($1-10) per kg. Though inexpensive, the importance of regeneration is quite significant especially in low resource contexts. Nitrogen is one of the most vital nutrients for plant growth. An understanding of how plants respond to N is key to maintaining and improving crop growth and yield [1]. It was demonstrated that ammonia adsorbed on activated biochar could be easily desorbed in water. This implies theoretical availability of N to plants once ammonia augmented biochar is exposed to wet soil. However, there are complex pathways in the soil N-cycle from the point of release, its transformation to nitrates and other species before it is finally absorbed by plant roots. Once activated biochar is added to soil, owing to its microstructure and demonstrations from previous literature [2]–[4]; wasteful loss of N as nitrates and off-gassed ammonia are expected to be minimized. This would result in better retention of nutrients if inorganic fertilizers are externally

added in the future, implying more efficient utilization of nutrients as opposed to them being washed off. A detailed mass balance of the desorbed ammonia and its effect on the soil N-cycle is the next logical step in this study. ^{15}N markers can be used for this purpose. This would help to quantitatively assess plant growth, changes in off-gassed ammonia and leached nitrates.

Future work in the synthesis and characterization aspects

Several avenues open up naturally following the work done in this dissertation which is suggested for future pursuit:

- Carrying out synthesis of activated carbon with pure phosphoric acid under equivalent concentration of DAP used in this study and comparing the porosity and nature of the surface functional groups.
- It is speculated that though activation with phosphoric acid may result in activated carbons with higher ammonia adsorption capacities from the gas phase; its (ammonia) desorption might be more difficult. The density of Brønsted acid sites in DAP activation are relatively diluted by the incorporation of Nitrogen in the carbon matrix during DAP activation.
- This work evaluated the use of cellulose as a model biomass and tested the efficacy of synthesis on hardwood sawdust. Moving ahead, it would be important to assess different types of biomass and their mixtures which are not necessarily woody in nature. Wheat straw, rice husk etc. are also cellulosic but with very different textural properties and may not respond in the same way to DAP activation as hardwood sawdust. Compositional and structural analysis of the parent biomass can be carried out in more detail to assess how it may respond during heat treatment.

- Powdered activated carbon, with a mean particle size of ~80 microns was synthesized in this study. As shown in chapter 3, the method of synthesis would work well for finely ground sawdust. However, if one has access to larger biomass particles (~ mm), the impregnation method should likely change to ensure close contact of the activating agent with the raw material. A systematic study on working with larger millimeter sized particles to synthesize granular activated carbon would be an interesting and important direction to pursue.
- Modeling efforts on possible heat and mass transfer limitations in a scaled up reactor should be carried out to identify bottlenecks for the synthesis of a larger batch. This can be followed by verifying results for a larger reactor (~100 mL) before moving on towards synthesis in an actual expected scale (~ litres). Substantial work can be done in reactor design itself. For instance, exploring the effect of the size of the opening relative to the diameter of the reactor and assess how it alters the yield and porosity of the activated carbon. It would be useful to assess the effect of air to fuel ratio in the POX reactor on the distribution of evolved gases. A complete study can be focused on trying out methods to heat the material to (400-450)°C in absence of electric heating. This can include a combination of modeling efforts and experimental validation.

Exploring an alternative application (for drinking water treatment)

Besides soil amendment, the material can also be used for a more conventional application such as a component for drinking water treatment in resource-constrained settings. The need for clean drinking water in rural regions of the developing world is one of the biggest challenges today. Everyday nearly 1500 children under the age of 5 die as a result of drinking unsafe water and the

acquired diarrheal diseases [5] . There exists a vast body of literature on the use of ordinary biochar synthesized from locally available biomass without any pretreatment to remove various contaminants in water [6]–[9]. However, demonstrations of activated carbon have been fewer. Activated carbons have been used to remove a wide range of contaminants in water from natural organic matter to heavy metals. Mohan for instance provides a comprehensive review for low cost adsorbents including activated carbons for Cr remediation in water, which gives a good insight into the current state-of-the-art [10]. Gabon with its rich biodiversity is a major freshwater repository for equatorial Africa. Despite being classified as an 'upper-middle income' country by the World-Bank , about 38% of the rural population lacks access to improved water sources and 69% of the rural population lacks access to improved sanitation [11]. As a part of the REFRESCH project at the University of Michigan, a workshop was organized in the summer of 2016 at Lambaréné, Gabon to collaboratively participate and discuss issues at the Food-Energy-Water (FEW) nexus. Participants included people from the neighboring villages, personnel from the national park service, non-profit organizations and students from local universities and vocational schools. This workshop provided an opportunity to carry out preliminary water-testing around the villages of Lambaréné to identify elements of concern for their subsequent treatment. The local population expressed active interest in gaining access to low-cost water treatment methods, of which activated carbon was envisioned as one of the components/steps of a more complex unit/process. The work done here provides insights into what one may expect to observe in such locations as efforts for detailed water quality surveys are initiated.

Summary of methods

14 different villages around Lambaréné (7 accessible by road and 7 accessible by the Ogooué river) were identified for preliminary water-testing. Villages were selected based on the number of inhabitants, proximity to the city of Lambaréné, and the inhabitants' willingness to engage in discussions about water quality. The village chief, or a representative in the chief's absence, reported which water source was used for drinking by the largest number of people; this source was tested, along with a major secondary source when identified. Most of the water testing was executed in the villages using a Del-Agua field testing kit. The Del-Agua kit provides portable equipment designed to test for critical parameters specified in the World Health Organization (WHO) guidelines for drinking water quality. Experimental details and protocol can be found in the Del-Agua manual [12]. The temperature, turbidity, pH, conductivity, and total dissolved solids (TDS) were measured using appropriate calibrated meters. Chemical reagents and a portable spectrophotometer were used to measure nitrite, nitrate and dissolved oxygen, post filtration of water samples through a 0.2 micron filter. For testing coliforms, water samples were collected in sterile vessels, stored in an ice-water bath, and analyzed within four hours of collection. Additional samples were brought back to U-M for analysis of heavy metals (Fe, Mn, Pb, Cr, Cd, As, Zn, Cu) using Inductively Coupled Plasma Mass Spectroscopy (ICP-MS). Preliminary identification of parameters of concern would help to initiate focused long-term studies on water quality and design appropriate treatment methods.

Key Findings

Water quality appeared to differ primarily based on source. A total of 15 out of 19 water sources tested in 14 different villages contained high bacterial contamination, indicated by fecal coliforms (generally > 50% of the total coliform count). The tested quality of self-reported stored rainwater tended to more closely align with EPA (Environmental Protection Agency) targets than other sources for parameters such as pH, TDS, turbidity, and metal content, but in some cases bacterial contamination was high, as well. Based on testing, informal discussions, and on-site observations, it is likely that contamination is due to a combination of factors that includes source water quality as well as sanitation and hygiene practices. However, at least one personal source may also point toward successful existing practices of rainwater collection, storage, and adequate hygiene. Some metals were found in relatively significant concentrations in various water sources, concentrations that exceeded primary or secondary water standards of the US's EPA. Iron, manganese, and zinc are associated with EPA secondary water standards based on negative aesthetic (taste and odor), cosmetic, or technical effects. Primary water standards are set for compounds that negatively affect public health; lead is the only type of primary contaminant that the water tests in Gabon identified. High iron levels (~800 ppb, compared to the US secondary water standard maximum of 300 ppb) were consistently found in river water sources from communities situated along the Ogooué River. According to local residents, most people directly consumed raw river water, whereas some used techniques such as settling and cloth filtration prior to consumption. Other metals were generally not a concern except for scattered cases of relatively high manganese and zinc concentrations, of which the potential causes would require more extensive future data collection. A plastic tank containing stored

water was the only source of elevated lead contamination ~ 18 ppb, but the cause again is unknown. Though this current evaluation does not recognize a deleterious effect on health by these elements, there has been some literature that suggests that there may be negative health effects caused by elevated levels of manganese in water [13]. Some of the summarized results of preliminary water-testing are presented in Figures 5.2, 5.3 and 5.4. Figure 5.2 provides pictures of actual water sources from villages in Gabon so that the reader may have a better understanding of the points of data collection and possible origins of contamination. Figures 5.3 and 5.4 represent the distribution of Iron and Fecal (thermotolerant) coliform across different villages around Lambaréné.

Figure 5.1 (a) Participants in the workshop held at the Albert Schweitzer hospital in Lambaréné (b) Students (left to right) Anna Hayden and Mohit Nahata preparing to carry out water testing in a village

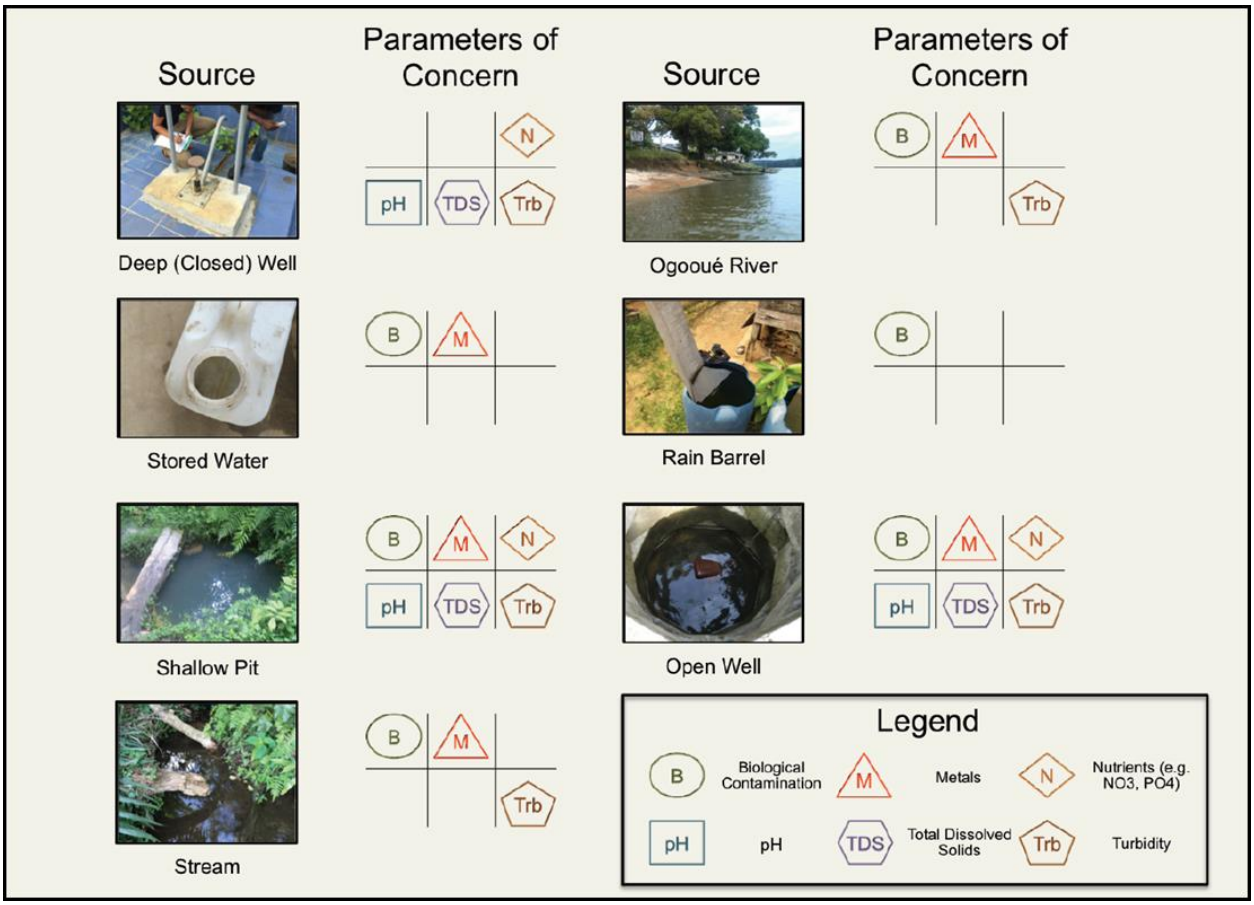

Figure 5.2: Summary of contaminants per water source across different villages tested

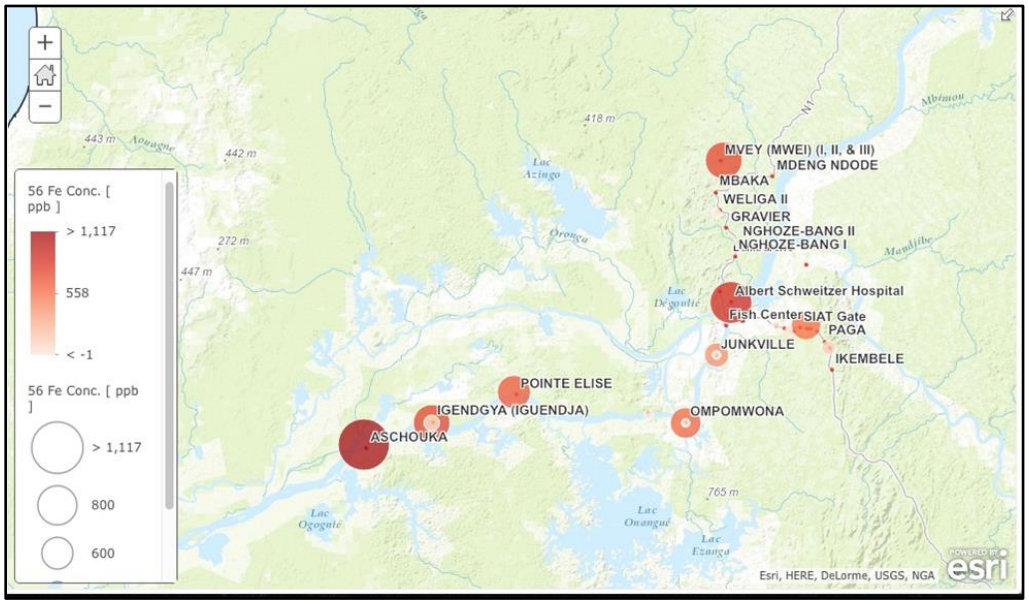

Figure 5.3: Distribution of [Fe] in ppb across various water sources in different villages around Lambaréné. Multiple circles at a location indicate multiple sources

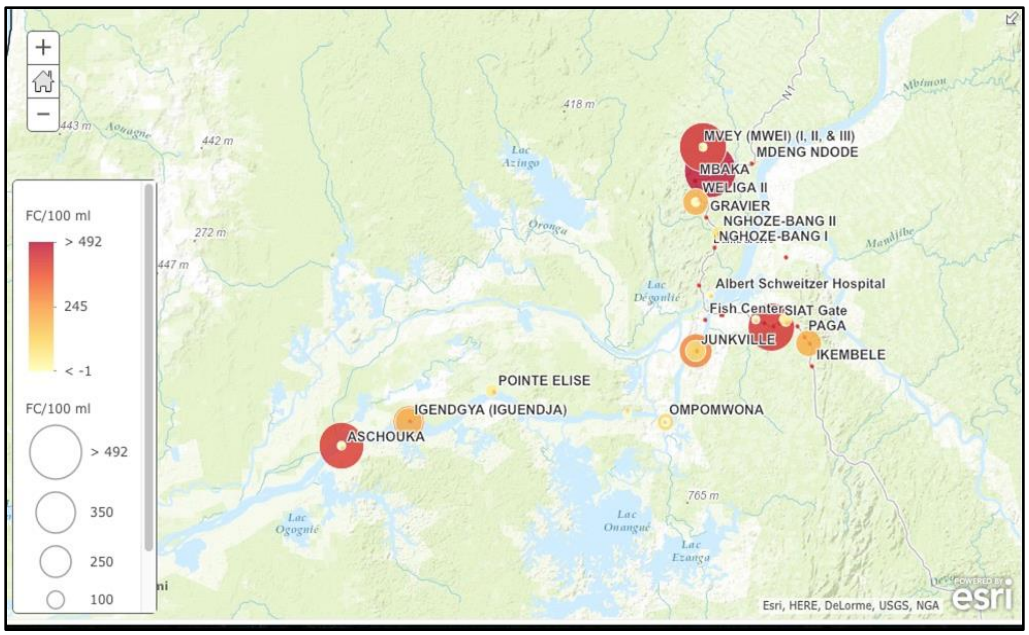

Figure 5.4: Distribution of Fecal coliform expressed as colony forming unit per 100 mL (CFU/100 mL) in water sources across different villages around Lambaréné. Multiple circles at a location indicate multiple sources

Conclusions

Based on observation and initial data, sanitation and hygiene seems be an aspect which if improved could lead to significant improvements in drinking water quality. Care has been taken to identify points of concern, abstaining from drawing immediate correlations relating to possible causative factors as the data provided only a snapshot of several water sources (lack of frequency of data collection and knowledge of seasonal variance). However a general picture of the water quality was obtained. The results of the water testing were provided to each village in the form of simple handouts which included basic WASH (Water and Sanitation Hygiene) principles approachable for varying levels of literacy and education. It is desired to work with village residents in future studies to understand reasons for current behavior and determine mechanisms

to induce safer WASH behaviors. The synthesized activated carbons are quite versatile in the range of contaminants they can adsorb and as more focused work develops; they may be employed at different stages of the water treatment process. We are currently looking at the use of ceramic filters and activated biochar to address some of the problems associated with drinking water.

Acknowledgments: The water testing in Gabon was possible due to help of numerous people. The contribution of Anna Hayden and Matthew Vedrin was important to carry out experiments on-site. Mike Burbidge, Fredéric Ongonwou, Gislhain Djessi Tchouty, Franck Binze Bi-Kumbe and Katie Browne helped in establishing relations with community members in villages and communicating with the village chief prior to water testing. Prof. Lutgarde Raskin and Prof. Krista Wigginton helped with the purchase of the field-testing kits and answering questions about doing experiments on-site. Tom Yavaraski helped with the training on the ICP-MS.

References

[1] D. W. Lawlor, G. Lemaire, and F. Gastal, "Nitrogen, Plant Growth and Crop Yield BT - Plant Nitrogen," Springer Berlin Heidelberg, 2001, pp. 343–367.

[2] K. A. Spokas, J. M. Novak, and R. T. Venterea, "Biochar's role as an alternative N-fertilizer: ammonia capture," *Plant Soil*, vol. 350, no. 1–2, pp. 35–42, 2012.

[3] A. Taghizadeh-Toosi, T. J. Clough, R. R. Sherlock, and L. M. Condron, "A wood based low-temperature biochar captures NH_3-N generated from ruminant urine-N, retaining its bioavailability," *Plant Soil*, vol. 353, no. 1–2, pp. 73–84, 2012.

[4] H. Zheng, Z. Wang, X. Deng, S. Herbert, and B. Xing, "Impacts of adding biochar on nitrogen retention and bioavailability in agricultural soil," *Geoderma*, vol. 206, pp. 32–39, 2013.

[5] WHO, "Diarrhoeal disease fact sheet," 2017.

[6] H. Lu, W. Zhang, Y. Yang, X. Huang, S. Wang, and R. Qiu, "Relative distribution of Pb^{2+} sorption mechanisms by sludge-derived biochar," *Water Res.*, vol. 46, no. 3, pp. 854–862, 2012.

[7] D. Mohan, A. Sarswat, Y. S. Ok, and C. U. Pittman, "Organic and inorganic contaminants removal from water with biochar, a renewable, low cost and sustainable adsorbent – A critical review," *Bioresour. Technol.*, vol. 160, pp. 191–202, 2014.

[8] Y. Yao, B. Gao, M. Inyang, A. R. Zimmerman, X. Cao, P. Pullammanappallil, and L. Yang, "Removal of phosphate from aqueous solution by biochar derived from anaerobically digested sugar beet tailings," *J. Hazard. Mater.*, vol. 190, no. 1, pp. 501–507, 2011.

[9] M. K. Hossain, V. Strezov, K. Y. Chan, A. Ziolkowski, and P. F. Nelson, "Influence of pyrolysis temperature on production and nutrient properties of wastewater sludge biochar," *J. Environ. Manage.*, vol. 92, no. 1, pp. 223–228, 2011.

[10] D. Mohan and C. U. Pittman, "Activated carbons and low cost adsorbents for remediation of tri- and hexavalent chromium from water," *J. Hazard. Mater.*, vol. 137, no. 2, pp. 762–811, 2006.

[11] WHO/UNICEF, "Knoema water supply statistics," 2015.

[12] Del-Agua, "Portable water testing kit user manual," Marlborough, Wiltshire, 2015.

[13] ASTDR, "Public Health Statement : Manganese (CAS # 7439-96-5)," 2012.

Appendix A

TGA-DSC studies

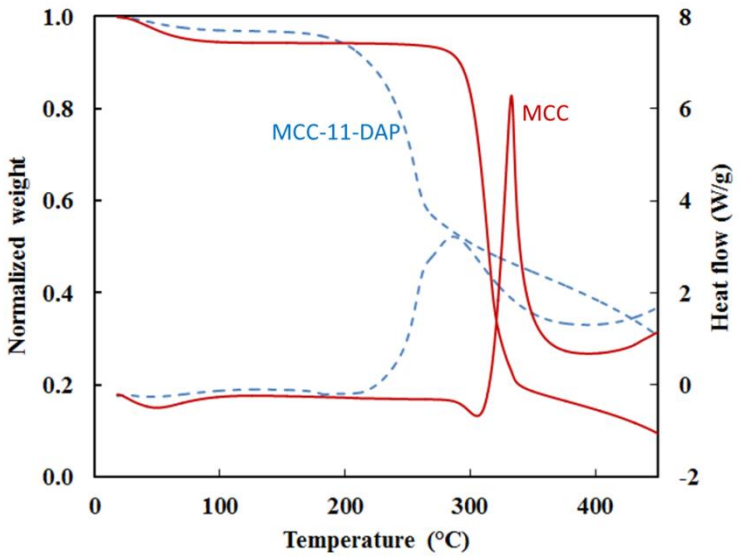

Figure A1: TGA-DSC profiles in air flow for MCC and MCC-11-DAP showing the mass loss and the associated heat changes upon heat treatment. Positive heat flows are exothermic.

The presence of oxygen brings important changes in the product distribution and reaction energetics of decomposition of cellulose and cellulose impregnated with DAP. It was observed in chapter 2 (Fig. 2.8c), that in the presence of oxygen in the Thermogravimetric analyzer, the volatiles evolved from MCC-11-DAP were largely oxidized to CO_2. The data in Fig. A1 shows the decomposition of MCC and MCC-11-DAP in air flow and the associated heat changes as analyzed from a TGA-DSC. Cellulose has high volatile matter content and breaks down sharply at temperatures > 300°C to generate volatiles and char which are subsequently oxidized. The sharp exotherm associated with MCC is a consequence of this oxidation. Cellulose impregnated with DAP on the other hand shows resistance to oxidation. Due to an onset of pyrolysis at lower

temperatures, the exotherm appears earlier, but its magnitude is decreased and is broadly spread. This is because the condensed phosphates generated during heat treatment prevent the access of oxygen into the carbonaceous matrix. The magnitude of this exotherm is expected to drop when more concentrated precursors are used (MCC-50-DAP), indicating preservation of useful carbon and making synthesis of activated carbon feasible in environment of air.

Supplementary figures

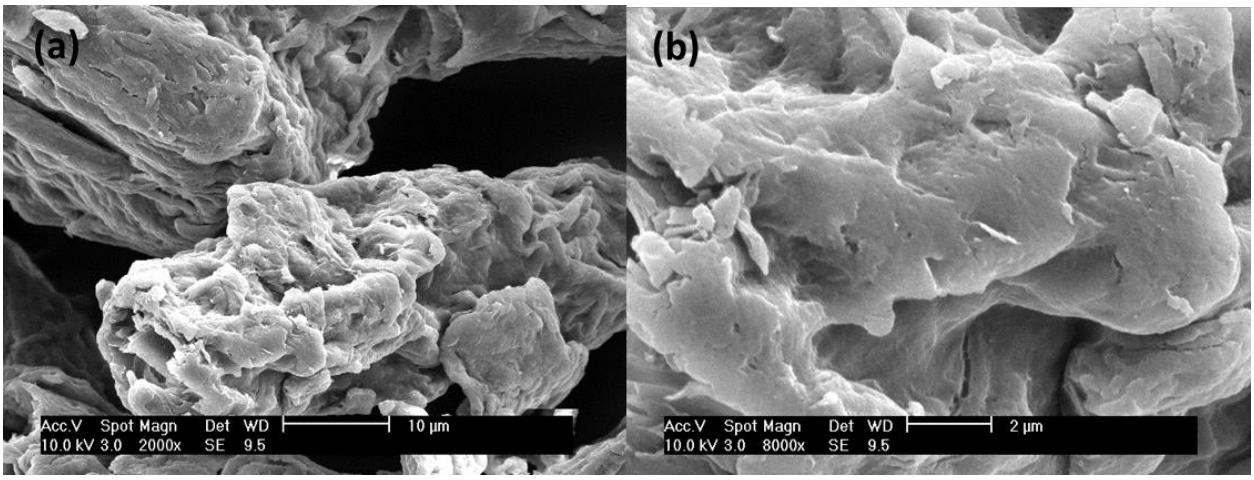

Figure A2: SEM images of pure microcrystalline cellulose (MCC)

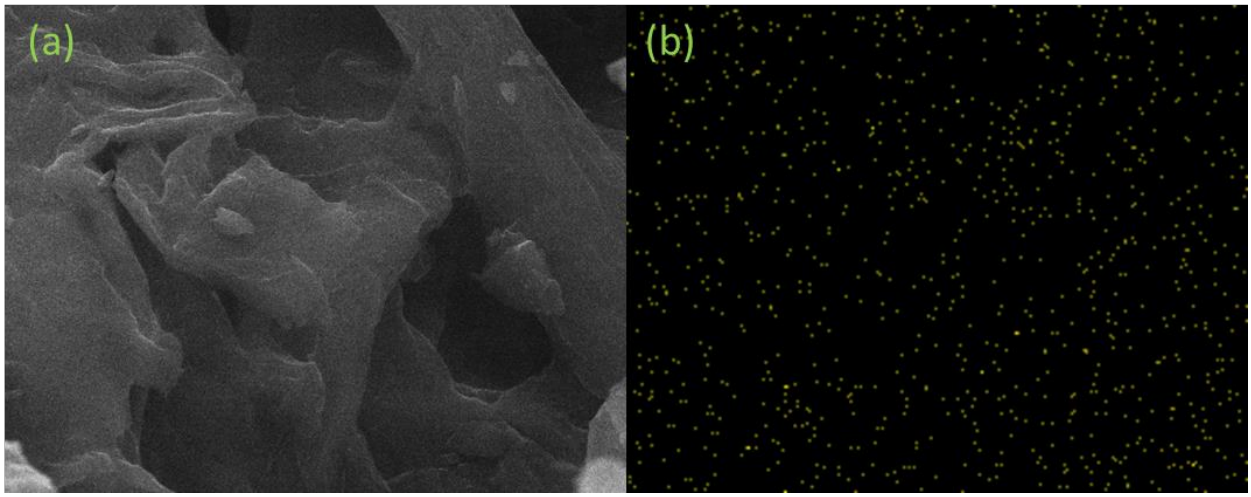

Figure A3: (a) MCC-50-DAP capture zone and (b) the associated EDS mapping of Phosphorus